Summer 2020

Mesh networking and full-duplex communication for wireless networks

Arul Mathi Maran Chandran

Department: Electrical and Computer Engineering

MESH NETWORKING AND FULL-DUPLEX COMMUNICATION FOR WIRELESS NETWORKS

by

ARUL MATHI MARAN CHANDRAN

A DISSERTATION

Presented to the Graduate Faculty of the

MISSOURI UNIVERSITY OF SCIENCE AND TECHNOLOGY

In Partial Fulfillment of the Requirements for the Degree

DOCTOR OF PHILOSOPHY

in

ELECTRICAL ENGINEERING

2020

Approved by

Dr. Maciej Zawodniok, Advisor
Dr. Minsu Choi
Dr. Jiangfan Zhang
Dr. Akim Adekpedjou

PUBLICATION DISSERTATION OPTION

This dissertation consists of the following six articles which have been accepted for publication, or submitted for publication as follows:

Paper I: Pages 5 - 19 have been accepted by the IEEE International Telemetering Conference (ITC).

Paper II: Pages 20 - 32 have been accepted by the IEEE Consumer Communications and Networking Conference (CCNC).

Paper III: Pages 33 - 52 have been accepted by the IEEE International Instrumentation and Measurement technology Conference (I2MTC).

Paper IV: Pages 53 - 72 have been accepted by the IEEE International Instrumentation and Measurement technology Conference (I2MTC).

Paper V: Pages 73 - 96 have been accepted by the IEEE Access Journal.

Paper VI: Pages 97 - 113 have been submitted to the IEEE International Conference on Smart Computing (SMARTCOMP).

ABSTRACT

Connectivity with large coverage area; and an increase in spectral efficiency of communications are highly desired features for any wireless network. The presented research work addresses these two feature improvements. First, the work analyzed mesh networks to enhance connectivity for wireless networks. The work analyzed both homogeneous and heterogeneous mesh networks. The work includes the development of an Android application to enable smartphones with multiple interfaces, such as Wi-Fi, Bluetooth, and cellular services, to become convergence devices. These convergence devices are then used to build a heterogeneous mesh network improving connectivity and coverage area. Second, the work explored full-duplex communications, which can achieve twice the spectral efficiency achieved by existing half-duplex communications. A novel method was proposed to address the estimation of self-interference, besides the estimation of the communication channel. A system model was proposed and the performance limits of the estimators was determined. Both flat fading and frequency selective channels are used in this analysis. An experimental analysis was performed on the USRP family of devices in full-duplex communication. The internal leakage which manifests as internal self-interference in full-duplex operation was characterized across the operating frequencies of each device. Finally, the work analyzed the usage of learning techniques to improve channel estimations. The work explored two potential applications. First, the selection of a channel model from a poll of existing models; to match the dynamic channel conditions. The target learner was proposed for this dynamic selection. Second, to estimate the data which are missed not at random at the reception, and proposed to estimate these missed data using simple random imputation.

ACKNOWLEDGMENTS

I am very thankful to my advisor, Dr. Maciej Zawodniok for his unwavering support guiding throughout my master's and doctoral program. He provided a friendly and professional environment to work. I gained valuable knowledge from him to perform research, present the work both in publications and practical implementations.

I am also thankful to my doctoral research committee members, Dr. Levent Acar, Dr. Minsu Choi, Dr. Jiangfan Zhang, Dr. Akim Adekpedjou, and also former members members of the committee Dr. Egemen Çetinkaya and Dr. Ivan Guardiola.

I wanted to extend my gratitude to all the members of the department of electrical and computer engineering. I want to thank Intelligent Science Center (ISC) and Intelligent Maintenance System (IMS) for supporting my research.

Special thanks to the Office of Graduate Studies and the Office of International Affairs for their support throughout the program and acknowledge everyone who helped me during the years of my graduate studies at Missouri S&T.

I would like to thank Dr. E. Srinivasan, Mr. K. Tamijoli, Mr. B. Padmakishore, Mrs. D. Maheswari, Mr. G. Vengadessane Anand, Mr. Niranjan Dasappa, and to all my friends across the globe.

My special thanks to Dr. Angel Ricardo Morales for his support and guidance throughout my stay in Rolla.

I am also thankful to my lovely fiancée, RyeoEun Kim for her constant encouragement and her moral support.

I am always grateful to my awesome mother, Valliammai Chandran supporting all my dreams and I am thankful to my family.

Finally, I am grateful to the Divine blessings guiding me every step in my life.

TABLE OF CONTENTS

Page

LIST OF ILLUSTRATIONS

SECTION

LIST OF TABLES

SECTION

1. INTRODUCTION

1.1. MOTIVATION

In the present digital way of living, wireless devices play an integral role in connecting us with others in and around the world. Their penetration in our life extends to our home, office, transportation, etc. shows how much we are dependent to these devices. They help us connect with each other, navigate us to our destination, property surveillance, and effectively managing different systems in our home improving power efficiency. One key attribute of these devices' success is their ability to connect to each other and form a network. Earlier these networks are wired with a physical link between them, but these days more and more devices connect to each other wirelessly with no need for a physical link between them. This migration to wireless networking brings many advantages and challenges. Since there is no need for a physical link, there is less infrastructure required to establish these networks. Thus, enabling the network to scale rapidly. The wireless network plays a key role in bringing high-speed Internet connections to rural areas where the investment in physical infrastructure is not economical. With the ease in scalability, the network faces a challenge in reliability and resilience. The physical link provides reliability and resilience to the network under multiple adverse conditions such as weather, cyber-attack. In contrast, the wireless network communicates in the open environment vulnerable to all kinds of attacks from outside such as a denial of service, man in the middle attacks.

The scalability of the network puts forth a key challenge which is supporting all the devices with enough bandwidth with no interruption. A network successfully scales when no device in the network waits for more than a standard time to communicate with others. The wait duration is dictated by the protocol standard of the interface used by these devices.

1.2. OBJECTIVE

The presented research work focuses on these challenges, to build a scalable network with the efficient use of the limited spectrum available across devices in the network. Most existing networks or homogeneous where all the devices in the network using a single interface to communicate with each other such as Wi-Fi, Bluetooth, Zigbee, cellular data service (LTE). These interfaces operate independently, and most commonly they are proprietary. For example, the home and office network uses Wi-Fi or Bluetooth, the most personal network uses Wi-Fi or cellular data service. Since they operate independently, communication across these devices does not occur, limiting only to the devices with the common interface. Mesh networking is one of the solutions to improve the scalability of the wireless network. The present home and office network is scalable using mesh networking. Most existing mesh networks are all also homogeneous using a single interface such as Wi-Fi, Bluetooth, Zigbee, cellular data services (LTE). As the number of devices increases in a homogeneous mesh network, the scalability is limited by the protocol standard of the interface used. A heterogeneous mesh network can address this hard limit with multiple interfaces seamlessly interacting with others across the network. The convergence devices are key to a heterogeneous mesh network. These convergence devices have multiple interfaces capable of transferring information from one interface to another.

In the presented research work, the analysis was performed on a homogeneous Wi-Fi mesh network and the development of convergence devices to build a heterogeneous mesh network. These analyses are useful in building a desired wireless network. A mesh network on itself does not address all the desired properties. In a mesh network, the nodes

split the bandwidth over multiple devices and hops, and suffers interference, such as a hidden terminal, among the nodes while operating on a longer range. The deployment of full-duplex communication which potentially doubles the available bandwidth and also addressing interference among the nodes in the network. The performance of the proposed full-duplex method depends on the particular channel model and not effective for a more dynamic channel. The last sections of the present works explored the usage of the target learner as a middle ground between a fixed channel model and a deep neural network.

Connectivity

Wireless Mesh Networking

Paper 1: Performance of IEEE 802.11s for Wireless Mesh Telemetry Network
Paper 2: Convergence Communication over Heterogeneous Mesh Network for Disaster and Underserved Areas

Spectral Efficiency

Full-Duplex Communication

Paper 3: Measurement of Internal Self-Interference of USRP Family of Devices in Full-Duplex Operations
Paper 4: Transmitter Leakage Analysis When Operating USRP (N210) in Duplex mode
Paper 5: Channel Estimators for Full-Duplex Communication using Orthogonal Pilot Sequences

Learning

Channel Estimation Improvement

Paper 6: Targeted Learning for the Dynamic Selection of Channel Estimation Methodology

Figure 1.1. Categories and organization of the publications presented.

The target learner samples the incoming signal and chooses a channel model from a pool of channel models to match the dynamic channel. Besides, the presented work modeled the targeted interference channel as a response to missing data not at random. Thus, combing a mesh network with full-duplex communication aided by the target learner yields a most desirable wireless network.

The publications are categorized and organized as shown in the Figure 1.1 for the presented work. The works in each contributes to different features such as connectivity, coverage area, scalability and high bandwidth for the envisioned wireless network.

PAPER

I. PERFORMANCE OF IEEE 802.11S FOR WIRELESS MESH TELEMETRY NETWORKS

I. Nathan D. Price, II. Arul Mathi Maran Chandran, III. Kurt Kosbar, IV. Maciej Zawodniok

Department of Electrical & Computer Engineering

Missouri University of Science and Technology

Rolla, Missouri 65409

Email: ndp43@mst.edu, ac62f@mst.edu, kosbar@mst.edu, mjzx9c@mst.edu

ABSTRACT

Wide area sensor networks have numerous agricultural, industrial, scientific, medical, and military applications. For many years now, such networks have been implemented through wireless mesh networks. As wireless mesh networks have come to maturity, several network standards have become readily available. The WiFi mesh extension 802.11s was finalized in 2008 and officially adopted into the 802.11 standard in 2012, is extremely interesting thanks to the wide spread adoption of WiFi and low cost. In this paper, we evaluate the performance of a small 802.11s network implemented on low-cost, off-the-shelf single board computers for the purpose of building a telemetry sensor network.

Keywords: IEEE 802.11s

1. INTRODUCTION

A number of developments have lead to the realization of cost effective wireless mesh networks. A tremendous amount of wireless mesh research Sarangapani (2007) over the last 20 years has culminated in a number of standardized wireless mesh protocols. The cost of computing has declined to the pint that requirements required for this project can be had for as little as $5. The widespread adoption of wireless computing such as WiFi has allowed for commodity pricing of the necessary wireless hardware. Additionally, the open source community generously provided an implementation built into the Linux operating system.

Despite those advancements, the adoption of mesh networking is slow. The main challenge is the understanding of limitations and practical constraints that a multi-hop, mesh network faces in realistic deployment. Some researchers Alam *et al.* (2012); Elahi *et al.* (2012); Imboden *et al.* (2012); Rethfeldt *et al.* (2016); Wang *et al.* (2010) have evaluated WiFi based mesh test beds and identified some weaknesses including effects of TCP algorithms, network topology, and payload length. However, many of these findings are limited in that the performance data is only applicable to that test environment. For example, a loss of 1 Mbps in performance is significant if the maximum throughput of the channel is 11 Mbps but is insignificant if the maximum throughput is 300 Mbps. In contrast, this paper presents analysis of the performance from an experimental setup and compares them to benchmarks made in the same environment. Wireless mesh networks (WMNs) have several advantages over traditional infrastructure based 1 wireless networks. The most notable advantage that a WMN has over a traditional wireless network like a cellular network or traditional infrastructure-mode WiFi is that it requires no central infrastructure to manage and relay communications. Each wireless device communicates directly in an ad-hoc or peer-to-peer fashion and can forward traffic on behalf of another device when

no direct route is present. This makes WMNs cheap to operate as they don't require extra infrastructure beyond the client devices themselves. Should an individual route or neighbor device fail.

WMNs generally possess the ability to re-route traffic. This makes WMNs extremely robust as they generally don't have a single point of failure.

2. BACKGROUND

One of the distinguishing features of WMNs is the ability to relay and route traffic. WMN routing schemes fall somewhere between two paradigms of routing: proactive routing and reactive routing Sarangapani (2007). In proactive routing each STA proactively creates and maintains routes. The benefit of proactive routing is that there is no time wasted setting up a route prior to its use, however there is the constant overhead of maintaining routes that scales with the size of the network. On the other hand, reactive (on-demand) routing creates routes as required. By contrast, reactive routing has the benefit of low overhead, but incurs a setup time penalty before a route is used.

3. IEEE 802.11S

802.11s adds new type of network, a Mesh Basic Service Set (MBSS), to the WiFi standard. Both the MBSS and Basic Service Set (BSS) commonly referred to as an ad-hoc mode WiFi network posses no central access point unlike traditional infrastructure-BSS networks. STAs in a BSS can communicate only with other STAs in range of direct communication. An MBSS network distinguishes itself from a BSS network in that its STAs posses the ability to route and forward traffic in the data link layer (i.e. layer 2 of the OSI model) 802.11s (2011); Carrano *et al.* (2011). In the past, multi-hop routing schemes such as AODV, OLSR, DSDV, DSR, B.A.T.M.A.N., etc BATMAN (2017); RFC3561 (2017);

RFC3626 (2017); RFC4728 (2017). have been designed and implemented for BSS networks though only through the use of network layer (i.e. layer 3 of the OSI model) routing and by violating the principal of strict layer separation Kawadia *et al.* (2002).

MBSS networks contain three different types of STAs: mesh stations (mesh STAs), mesh access points (MAPs), and mesh gates. A mesh STA differs from a normal STA in that it has the ability to forward traffic to and from other STAs and perform path discovery. A MAP is a mesh STA and acts as a WiFi access point that can bridge standard STAs into the mesh network. A mesh gate is an STA that provides access to an external network (i.e. Internet access). None of the three new types of STAs are mutually exclusive meaning a mesh STA can serve multiple roles simultaneously.

3.1. MAC LAYER

Like traditional WiFi, 802.11s uses the distributed coordination function (DCF) mechanism for channel contention but adds a its own unique extension called mesh coordination function (MCF).Recall from 802.11 that DCF is a carrier sense multiple access with collision avoidance (CSMA/CA) based MAC layer. The MCF extension to DCF can operate operate in both a contention mode using the enhanced distributed channel access (EDCA) and a contention free mode called MCF controlled channel access (MCCA). In this contention free mode, mesh STAs use EDCA to bid for time slots. Then the mesh STAs can operate in a contention free mode similar to an infrastructure BSS.

3.2. HYBRID WIRELESS MESH PROTOCOL

For routing, 802.11s uses a routing scheme that is a combination of proactive and reactive routing techniques aptly named the hybrid wireless mesh protocol (HWMP). HWMP is most similar to the reactive routing scheme called the ad-hoc distance vector (AODV) protocol 802.11s (2011); Carrano *et al.* (2011); RFC3561 (2017), however it also

incorporates proactive techniques. The process of path discovery in AODV takes place via path requests (PREQ) and path replies (PREP) messages. To establish a route from a source STA to a destination STA, a source begins by broadcasting a PREQ. This PREQ contains the address of the original source and destination as well as a hop counter. When a PREQ is received by an STA that a is not the destination the hop count is incremented and the PREQ is rebroadcasted. Each forwarding STA records a reverse route (destination to original source) via the previous, PREQ-forwarding STA. In this way, a reverse route is created in steps from the destination to the original source as the PREQ is relayed forward.

Once the PREQ is received by the destination a reply process begins. The destination first responds with a path reply (PREP) message. The PREP gets relayed along the reverse route established by the PREQ. As the PREP propagates back toward the original source, a forward route (original source to destination) is established via the previous, PREP-forwarding STA. In an identical fashion to the PREQ, each STA increments a hop counter contained in the PREP message until it reaches the original source. Since a PREQ is broadcasted, it is likely that a destination STA will receive multiple copies of the PREQ each having traveled a different route to the destination. The destination STA replies to the PREQ with the lowest hop count. Each STA tracks its routes via a timer to detect breaks. When a route is used the timer is reset. Should a route timer expire (a route break), a path error (PERR) message is sent backward to all STAs on the route before break. Path discovery must take place again before further communication with the destination STA of a broken route. HWMP differs from AODV in the use of the Airtime Link Metric (ALM). The ALM takes the place of the hop counter in PREQ and PREP messages. The ALM is an estimation of amount of time required to send one frame between two STAs. Before forwarding a PREQ or a PREP, an STA will calculate the ALM between itself and the previous STA and add this number to accumulated sum in PREQ or PREP. The destination STA is likely to receive several copies of the same PREQ hence it will reply only to PREQs with the lowest accumulated ALM.

HWMP introduces three proactive routing modes and three types of proactive routing messages respectively. The new types of routing messages are the root announcement (RANN) message, the gateway announcement message (GANN), and proactive PREQ. STAs serving as a gateway can be configured to send a GANN on a periodic basis. The GANN is processed like a PREQ to create a route from a STAs to the mesh gate, but GANNs are not replied to. This allows STAs in the mesh to maintain an active route to external networks via gateway STAs and keep ALMs up to date. Alternatively, STAs (including gateways) can be configured as a root. Root STAs periodically broadcast RANNs to all STAs to maintain an active routes between themselves and all other STAs in the mesh. If an STA receives a RANN and the ALM contained in a received RANN is better than its stored metric, the STA will initiate path discovery with RANN-sending, root STA. Any STA, for example an STA with an important network resource, can be made a root STA. Finally, root nodes can be configured to send proactive PREQs periodically. Proactive PREQs are the same as PREQs except the destination address is set to all ones. STAs may optionally reply with a PREP, or they may be compelled to reply depending on configurable flags in the proactive PREQ.

3.3. AIRTIME LINK METRIC

The ALM uses frame error rate ef to weight the estimated time needed to transmit each frame. If the success or failure of each transmission is thought of as a sequence of Bernoulli trials, Equation (1) resembles the expected value for a geometric distribution.

$$\frac{1}{1-e_f} = \frac{1}{1-q} = \frac{1}{p} \tag{1}$$

$$c_a = \left[O + \frac{B_t}{r}\right] \frac{1}{1-e_f} \tag{2}$$

Thus the ALM seen in Equation (2) is simply the expected number of transmissions times the time needed for each transmission. The value O is the overhead time generated from frame headers, error checking, etc. relative the current configuration of the physical layer (e.g. bits per symbol, coding rate, etc.). The second term $\frac{B_t}{r}$ is simply the maximum frame size B_t (i.e. 8192 bits) divided by the current data rate r.

$$MIN\_i \in I, j \in J c_a\left(i,j\right) x_{ij} \tag{3}$$

Equation (3) represents the total ALM seen by an STA for a particular route. The x_{ij} is a boolean value indicating if the route made a single hop from from STA i to STA j thus the final ALM is the of the summation of ALMs across all single hops taken. HWMP keeps the route with lowest ALM for any particular destination. Since the ALM is calculated in units of time and since HWMP uses the route with the total ALM, ALM is therefore an attempt at a latency optimized routing.

4. TESTING METHODOLOGY AND EXPERIMENTAL SETUP

Our network consisted of inexpensive single board computers (SBC) and inexpensiveWiFi adapters. Our single board computers consisted of 4 Raspberry Pi 2s and 2 Raspberry Pi 1s running the Raspbian Linux distribution (kernel version 4.4). Our WiFi adapters were USB connected and based on the Atheros AR9271 chipset. Choice of WiFi adapter was made carefully as not all adapters currently support 802.11s mode. The adapters were configured for 20 MHz channels in high throughput mode allowing for up to 75 Mbps of throughput theorpacetically. A summary can be found in Table 1.

The presented work focuses on experimental performance evaluation ofWiFi-based mesh networking. A set of end-to-end metrics were gathered on our demo network for TCP and UDP performance using the open-source tool IPerf3.

Table 1. Hardware and software configurations.

Hardware	Setup
SBC	Raspberry Pi 1 & 2
WiFi Adapter	Atheros AR9271 chipset
Channel	Ch1 - 2.412 GHz
Bandwidth	20 MHz
Mode	High Throughput (802.11n)
MIMO Configuration	1×1
Distribution	Raspbian Jessie
Kernel Version	v4.4
IPerf3	v3.0.7

For TCP, throughput and retry count were recorded, and for UDP, throughput, jitter, and packet loss were recorded.

Figure 1. Mesh network in the campus.

A random cluster topology was used for the primary experiment. The cluster features 5 data generating STAs running the IPerf3 client that were placed placed at various angles and distances relative to a gateway STA running the IPerf3 server. Depending on the application each STA potentially could contain a sensor platform gathering multiple channels of data. In this scenario, multiple flows of data (i.e. one per STA) were relayed to the gateway STA that could represent a local server, a connection to a cloud-server, etc. This experiment was conducted on our campus green with STAs placed directly on the ground.

Figure 2. Placement of nodes in the park to test individual hop metrics.

A secondary, linear topology was used to gather performance figures that could be used as a benchmark. STAs were arranged in a line with equal spacings. Routing was set statically so that each node could communicate only with its one-hop neighbor(s). A

single data flow was generated and relayed across varying numbers of hops. Testing was repeated with 10 m, 15 m, 20 m spacing. Results from this test can be used a relative ceiling for performance. This experiment was run once on the same campus green and once in a nearby park both with STAs placed directly on the ground.

5. RESULTS

This section presents the results of the experiments namely the cluster topography and the staticrouting, multi-hop benchmark at both locations. Table 2 and Figures 3 through 6 show the results from the mentioned experiments.

Table 2. Iperf3 TCP results.

STA	Distance from the Gateway (m)	Throughput (bits/s)	Retries
2	27.5	1.10 M	202
3	25	966 K	159
4	15	902 K	141
5	19	756 K	142
6	12	748 K	179

The performance observed in the cluster topography are reasonable despite low numbers. Figure 3a shows the maximum single-hop single-flow performance to be about 4.1 Mbps. After review routing tables on each STA, we observed that all STAs were using a single hop route to connect to the gateway. With that in mind the best expected performance for each STA is roughly $1/5^{th}$ of the maximum single-hop, single-flow speed (i.e. 0.82 Mbps). The throughput values in Table 2 are near 0.82 Mbps.

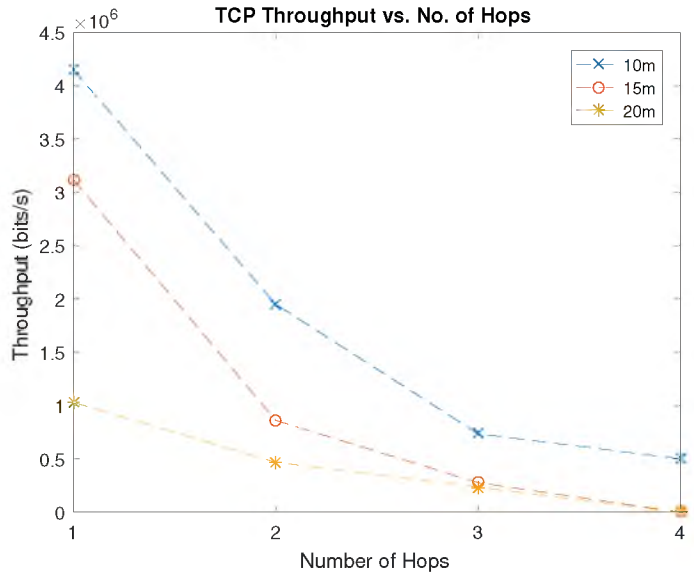

Figure 3. TCP results when operated the network with interference from other network (Throughput vs Number of hops).

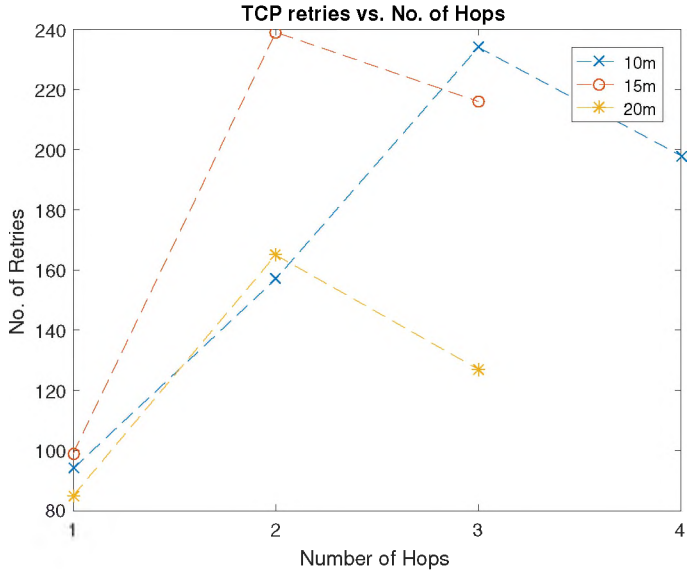

Figure 4. TCP results when operated the network with interference from other network (Number of retries vs Number of hops).

Plots from Figures 3 through 6 show similar trends across multiple hops. Maximum throughput was achieved in the park scenario in contrast to the campus scenario. The primary difference between these two scenarios was that there was noWiFi activity on

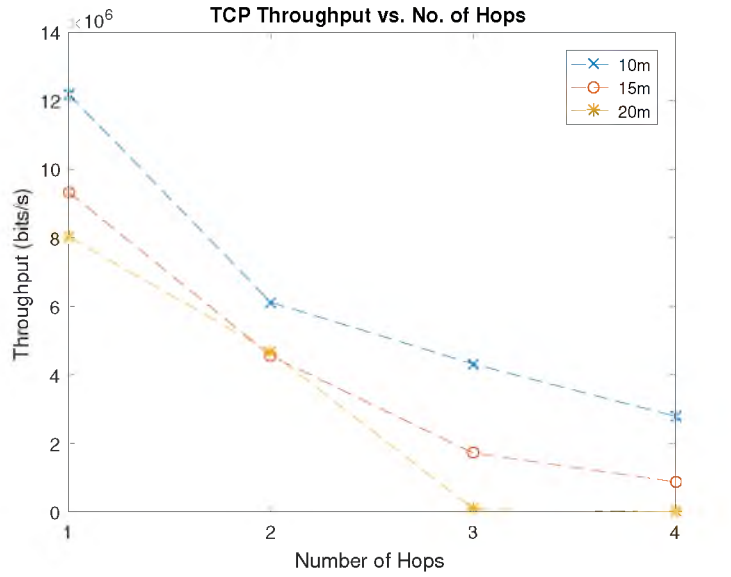

Figure 5. TCP results when operated the network with no interference from other network (Throughput vs Number of hops).

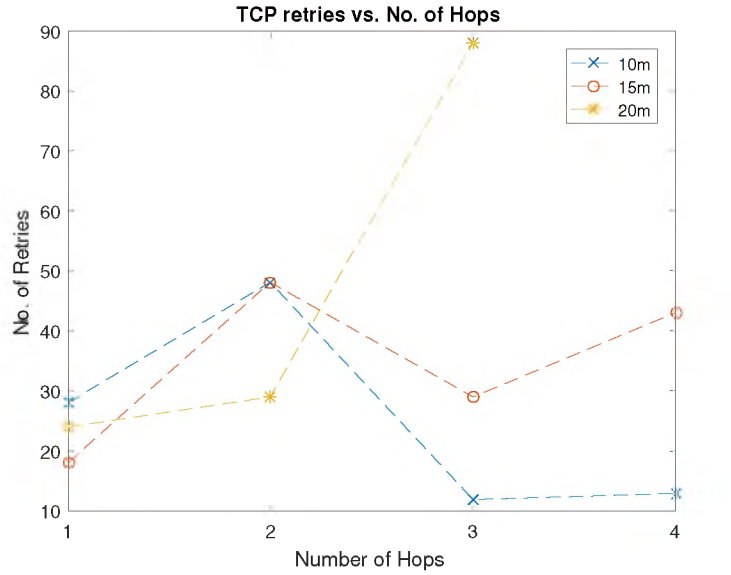

Figure 6. TCP results when operated the network with no interference from other network (Number of retries vs Number of hops).

channel 1 in the park whereas there was a campus network active on channel 1. The campus network likely introduced additional channel contention that reduced performance of the

mesh. The number of retires in both scenarios show a peak at two hops. There are multiple factors that may have contributed to this trend including but no limited to the distance covered, the hop number, the topography, and/or WiFi's physical layer configuration.

During our testing, we found IPerf3 to be an unreliable tool for measuring UDP performance in a wireless mesh network. IPerf3 does not throttle UDP data generation automatically like TCP. This would require the user to manually identify the throughput maximum throughput by trialand-error. An overestimation resulted in IPerf3 crashing whereas a underestimated value did not result in the maximum throughput. The trial-and-error result was not reliable across multiple trials. Additionally, IPerf3 failed to establish a link with the server when throughputs dipped below approximately 200 Kbps which is why in Figure 4 there are data points missing.

6. CONCLUSION

In this paper we evaluated the performance of a small demo mesh network built using 802.11s. Our goal for this paper was to provide context for such performance figures. The maximum throughput in our multi-flow scenario comprised of five flows of data was 1.10 Mbps and the minimum was 745 Kbps. The maximum throughput achieved in a single-flow, single-hop, activity-free, WiFi channel was 12.2 Mbps whereas 4.2 Mbps was achieved in an active WiFi channel. When compared against our single flow metric we found the multi-flow results to be reasonable. We believe 802.11s a network has place in telemetry systems.

In our paper we found IPerf3 to be an inadequate tool for measuring UDP performance in a mesh network. In future work, we hope to incorporate better tools. Due to the small size of our network, we did not observe any multi-hop routing. We would also like to increase the scale of the network so that we may make observations related to routing and routing techniques.

REFERENCES

802.11s, 'IEEE Standard for Information Technology–Telecommunications and information exchange between systems–Local and metropolitan area networks–Specific requirements Part 11: Wireless LAN Medium Access Control (MAC) and Physical Layer (PHY) specifications Amendment 10: Mesh Networking,' 2011 pp. 1–372, doi:10.1109/IEEESTD.2011.6018236.

Alam, M. N., Jntti, R., Kneckt, J., and Nieminen, J., 'Performance Study of IEEE 802.11s PSM in FTP-TCP,' in '2012 IEEE Vehicular Technology Conference (VTC Fall),' 2012 pp. 1–5, doi:10.1109/VTCFall.2012.6398931.

BATMAN, 'Better approach to mobile ad-hoc networking,' https://www.open-mesh.org/projects/open-mesh/wiki, 2017.

Carrano, R. C., Magalhaes, L. C. S., Saade, D. C. M., and Albuquerque, C. V. N., 'IEEE 802.11s Multihop MAC: A Tutorial,' volume 13, ISSN 1553-877X, 2011 pp. 52–67, doi:10.1109/SURV.2011.040210.00037.

Elahi, E., Qayyum, A., and Naz, S., 'The effect of payload length on QoS in IEEE 802.11s Wireless Mesh Networks,' in '2012 18th IEEE International Conference on Networks (ICON),' 2012 pp. 70–73, doi:10.1109/ICON.2012.6506536.

Imboden, T., Akkaya, K., and Moore, Z., 'Performance evaluation of wireless mesh networks using IEEE 802.11s and IEEE 802.11n,' in '2012 IEEE International Conference on Communications (ICC),' 2012 pp. 5675–5679, doi:10.1109/ICC.2012.6364932.

Kawadia, V., Zhang, Y., and Gupta, B., 'System services for implementing ad-hoc routing protocols,' in 'Proceedings. International Conference on Parallel Processing Workshop,' 2002 pp. 135–142, doi:10.1109/ICPPW.2002.1039723.

Rethfeldt, M., Danielis, P., Beichler, B., Konieczek, B., Uster, F., and Timmermann, D., 'Evaluating Cross-Layer Cooperation of Congestion and Flow Control in IEEE 802.11s Networks,' in '2016 IEEE 30th International Conference on Advanced Information Networking and Applications (AINA),' 2016 pp. 181–188, doi:10.1109/AINA.2016.12.

RFC3561, 'Ad hoc On-Demand Distance Vector (AODV) Routing,' https://datatracker.ietf.org/doc/rfc3561/, 2017.

RFC3626, 'Optimized Link State Routing Protocol (OLSR),' https://datatracker.ietf.org/doc/rfc3626/, 2017.

RFC4728, 'The Dynamic Source Routing Protocol (DSR) for Mobile Ad Hoc Networks for IPv4,' https://datatracker.ietf.org/doc/rfc4728/, 2017.

Sarangapani, J., *Wireless Ad Hoc and Sensor Networks: Protocols, Performance, and Control*, Control Engineering Series, CRC Press Taylor & Francis Group, LLC, Boca Raton, FL, 2007, ISBN 0-8247-2675-8.

Wang, J. C. P., Hagelstein, B., and Abolhasan, M., 'Experimental evaluation of IEEE 802.11s path selection protocols in a mesh testbed,' in '2010 4th International Conference on Signal Processing and Communication Systems,' 2010 pp. 1–3, doi:10.1109/ICSPCS.2010.5709664.

II. CONVERGENCE COMMUNICATION OVER HETEROGENEOUS MESH NETWORK FOR DISASTER AND UNDERSERVED AREAS

I. Arul Mathi Maran Chandran, II. Maciej Zawodniok

Department of Electrical & Computer Engineering

Missouri University of Science and Technology

Rolla, Missouri 65409

Email: ac62f@mst.edu, mjzx9c@mst.edu

III. Aaron Phillips

SitePro Inc.

Lubbock, TX, USA

Email: aphillips@sitepro.com

ABSTRACT

The existing data service providers have gaps in their connectivity, especially in disaster and remote underserved areas. A mesh network can address this shortcoming by providing Internet access to devices outside the coverage area with the help of other nearby devices. Mesh networks are homogeneous using a single interface across the network and require large-scale deployment of proprietary devices. We propose to build a heterogeneous mesh network using various interfaces such as Wi-Fi, Bluetooth, and cellular data services to connect devices. These interfaces are available in devices such as smartphones, laptops, and home automation devices and have the potential to be a convergence device. We present an Android application enabling devices with various interfaces to become convergence devices and build heterogeneous mesh networks to address the shortcoming of the existing wireless ISP services. We target this prototype implementation to provide a tactical communication

link in disaster zones, enabling the public to build the network and send a life-critical distress signal calling for help. The proposed implementation achieved an average throughput of 1 Mbps with multiple hops and through Wi-Fi, Bluetooth, and cellular data service.

Keywords: Heterogeneous Mesh Network, Wi-Fi, Bluetooth, Cellular data services, Convergence devices, Tactical communication

1. INTRODUCTION

The Internet has become a part of our daily lives, providing the latest news, weather forecast, commute information, and keeping people connected. The public accesses the Internet through Internet service providers (ISPs) either by a physical link or a wireless connection. In general, people use a physical link when they are in home and a wireless cellular link when they are out. The deployment of cellular data services is not uniform across any given geographical area. There are gaps in the network where there is no connectivity to the Internet. These shortcomings are due to the lack of infrastructure, which requires the deployment of base stations to provide data services. In urban areas, the lack of infrastructure can be due to commercial interests and strategies by the data service provider(s). In contrast, in rural areas, it is due to economic feasibility to build the infrastructure and get returns from it. Despite an area being urban or rural, during emergency events such as natural calamities, power outages can cripple existing infrastructure leaving the affected area disconnected from relief efforts. A mesh network can address this shortcoming by restoring connectivity across the disaster area.

A mesh network establishes a link to the Internet through multiple hops/links using nearby devices. These multi-hops use a single interface and form a homogeneous mesh network. However, it is difficult to find nearby devices with a common interface to establish a link to the Internet. The realistic approach in finding nearby devices and getting access to the Internet is by using different interfaces across the network. It requires a framework

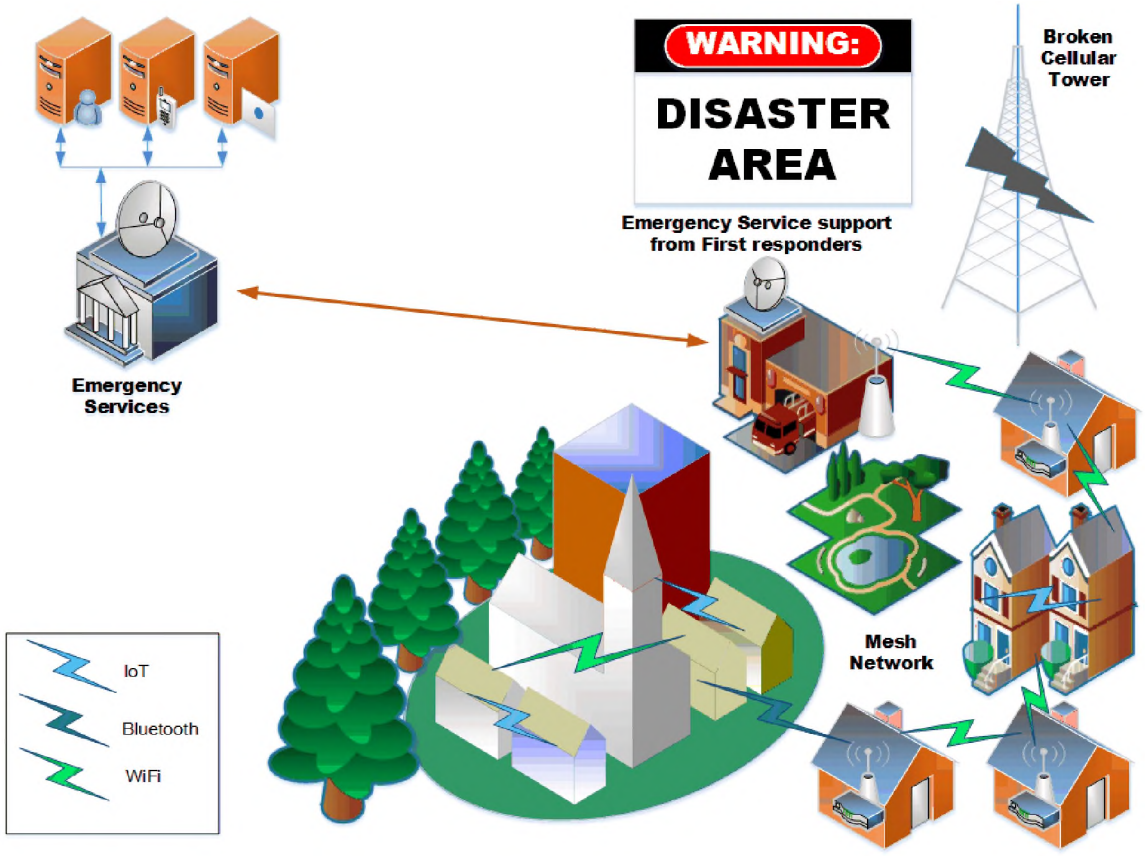

Figure 1. Heterogeneous mesh network connecting the disaster zone to emergency services.

to integrate different interfaces and communicate with each other becoming a convergence device. Convergence devices are important in building the proposed heterogeneous mesh network.

A convergence device has different interfaces that seamlessly communicate with each other passing the messages from one to other(s). Most devices have different interfaces which operate independently and do not interact with each other. For example, Bluetooth streaming music to headphones or transfer files while Wi-Fi and cellular data service providing Internet access. These devices have the potential to become a convergence device to harness their capability to build a heterogeneous mesh network and bridge connectivity to gain Internet access. For example, Figure 1 shows a disaster zone where cellular data

service is down. The devices in the disaster zone communicate through different interfaces and do not have access to the Internet since the data service has been knocked down. They built a heterogeneous mesh network using these devices to reach the first responder's station to call for help. The data traffic from different users in the disaster zone reached the destination (emergency services) by hopping through different interfaces in the network. Other application sites suitable for heterogeneous mesh networks are campsites, RV parks where Internet access is available at one spot, typically in the visitor center.

The proposed implementation is an application developed in the Android platform that enables smartphones to become convergence devices and use them to build a heterogeneous mesh network. The server receives the messages from different users that hops across the network through multiple different interfaces.

2. RELATED WORKS

There are various proposals and demonstrations available to provide and extend coverage to remote underserved areas using high-altitude balloons, solar-powered drone, satellite, power lines, high range Wi-Fi antennas, mesh network. Project Loon flies high-altitude balloons to create a network in the sky and provides access to anyone on the ground by establishing a connection to anyone of their balloons Loon LLC. (2017). Similarly, project Aquila uses a fleet of solar-powered drones and provides communication within a 60-mile diameter under each drone Mark Zuckerberg (2016). Broadband over Power Line (BPL) uses the existing power line to provide broadband services to remote areas Mahmood *et al.* (2019). All these proposals require the deployment of proprietary equipment and require investment for both initial deployment and maintenance of the infrastructure supporting the network.

Recently, mesh network has gained interest in both research and commercial areas, due to its ease in bridging network gaps in terms of connectivity. There are different methods proposed to build a temporary mesh network and evaluate their performance for disaster

area Dey *et al.* (2017); Ferranti *et al.* (2019); Miura *et al.* (2013); Ngo *et al.* (2013); Sugita *et al.* (2015). IBM/Weather Channel partnership demonstrating a weather alert system using a homogeneous mesh network built using smartphones The Weather Company - IBM (2017). Meanwhile, proprietary consumer products are available, which builds a proprietary mesh network providing connectivity goTennaMESH (2008). In contrast, the presented application does not require any new devices and not limited to a single interface for transmission. It can be installed to existing smartphones and harness the benefits of their various interfaces to build a heterogeneous mesh network.

3. OVERVIEW

The objective of the presented application/implementation is to enable the devices with different interfaces to become a convergence device, and aid in the formation of a heterogeneous mesh network to establish access to the Internet. The current prototype is limited to sending messages with other critical information of the user, such as name, location coordinates, and timestamp. The application is tailored to aid victims in a disaster zone, enabling the victims to call for help even when all data services are down. The network built by the application is called "NEED" (Network for Emergencies, Evacuation, and Disaster). The NEED consists of smartphones with our application and a web server. The web server is the destination for all the messages sent by the users. The message packets hop across the network through multiple different interfaces until it finds the devices with Internet access and then sent to the server. In case there is no Internet access to any device in the network, the application acts as a chat application allowing users connected to the network to communicate by text.

The first step of the application is to enable the smartphone to become a convergence device such that it can communicate through different interfaces. The application uses Android APIs to access Wi-Fi and Bluetooth adapters. The Wi-Fi connections can be operated in both infrastructure mode and Wi-Fi direct.

The design and implementation of the application to build a heterogeneous mesh network posed several challenges. First is enabling smartphones to be convergence devices. To achieve convergence, different interfaces should be able to seamlessly relay their packets. Each interface has its wireless protocol posing a unique challenge since these protocols are not designed to interact across different interfaces. The application acts as a middleman to route messages across different interfaces available as shown in Figure 2 and maintains compliance with different wireless protocols.

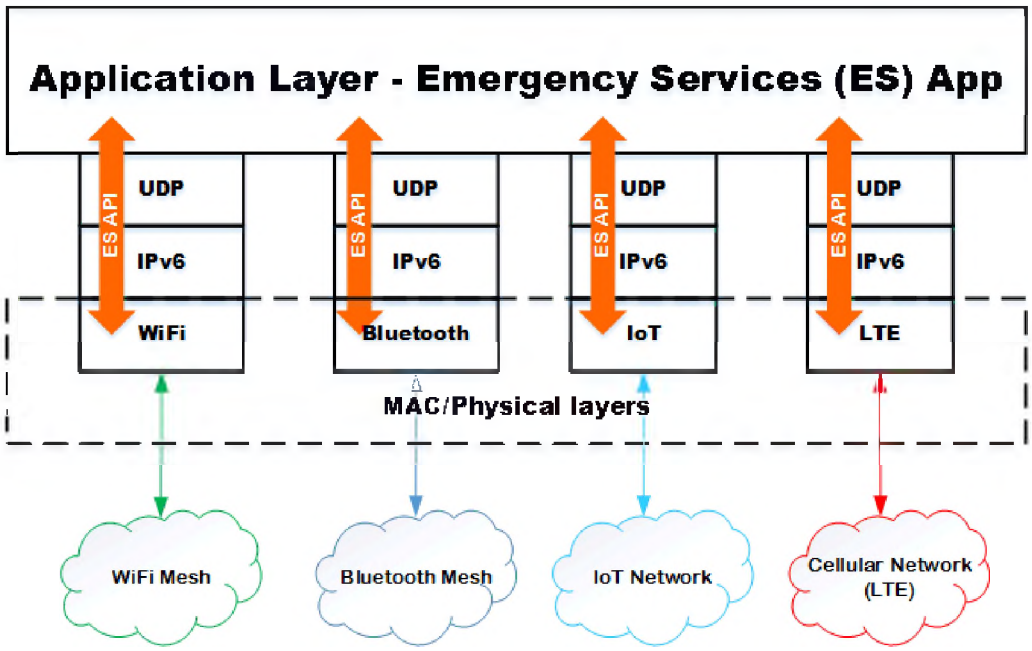

Figure 2. Interaction of different interfaces at the application layer.

Second is the bottleneck created due to the nature of the mesh network. For example, consider the heterogeneous mesh network shown in Figure 1. The capacity of each link in the network is not the same. For example, the capacity of Bluetooth and IoT links is less than the capacity of the Wi-Fi, and this can create a bottleneck affecting data traffic. Routing algorithms can address this bottleneck by finding alternative routes without affecting existing traffic. In disaster scenarios, communication is more tactical where the delivery of the message is more valued than the size of the message.

Finally, the implementation of the envisioned application in the Android operating system as its challenges. APIs of different interfaces, services should work fully compliant with each other. The restriction from the existing APIs limited the application feature and the mode of its operation. For example, the Bluetooth APIs from the Android library does not allow the application to establish a secure connection with other devices without the user's approval each time when it finds a peer which is not compatible with the feature of the application. The application should not continuously be prompting the user's approval while establishing the connections, which inhibits the flow of the process and potentially annoy the user who is already in distress. The trade-off was achieved by configuring the Bluetooth adapter to the insecure mode, which does not prompt user approval for each link established. The user data can be protected from being compromised due to the insecure mode by adding encryption to the user data.

4. RESULTS

In this section, we discuss briefly the application usage and different interfaces, in addition to the test environment and results.

The application begins with the registration. During registration, the application prompts the user's information, which is stored for identification when they are connected to the network. After successful registration, the user can start the service anytime to join and assist the traffic through the network. The users are not obligated to run service, and there is an option available to turn on and off the service to participate in the network whenever he/she desires.

Figure 3 shows the home page from which messages are sent. All the messages from the users in the network are sent to the server. The messages from different users are displayed on a map pinned to their location through a web interface. This comes handy

for the first responders to locate the victims and have more knowledge about the victim's condition from their distress messages. Figure 4 AmpliSine Labs LLC (2018) shows the web interface indicating the user's location with his/her distress message.

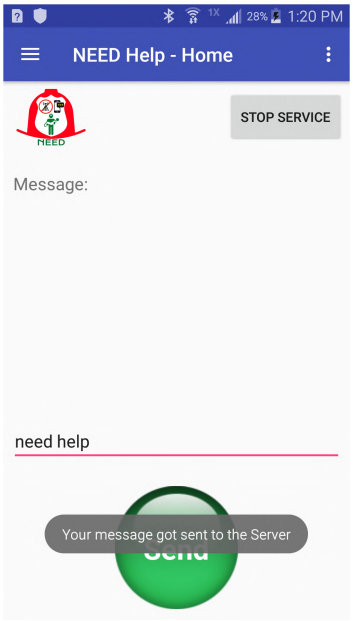

Figure 3. Message sent to server in device with the Internet access.

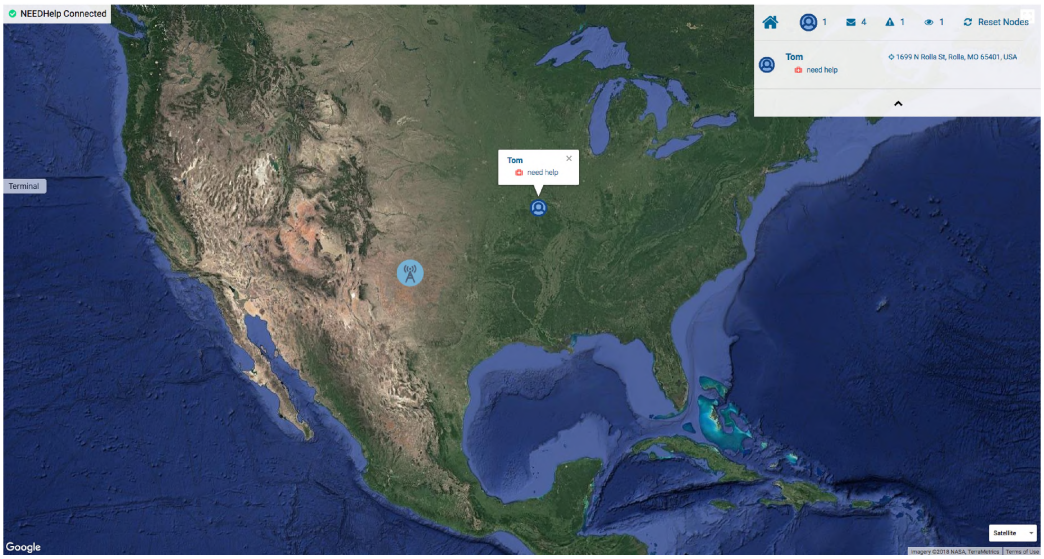

Figure 4. Received message displayed by NEED website AmpliSine Labs LLC (2018).

The messages from the network reach the server when at least one user in the network has Internet access. When none of the users has a connection to the Internet, the messages do not reach the server and the web interface does not help in the relief mission. However, the first responders can connect to the network and receive the messages which are being relayed and start communicating similar to a chat application. Figure 5 shows how two users, Tom and Ryan (First responder) can communicate without the Internet.

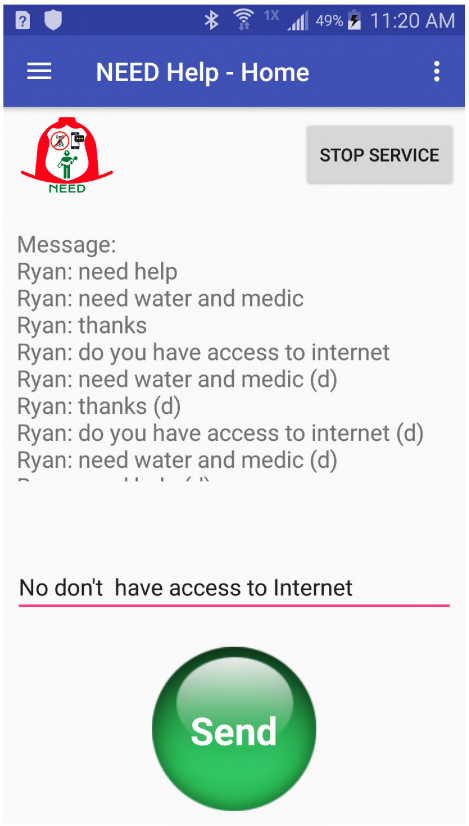

(a) User Tom Page.

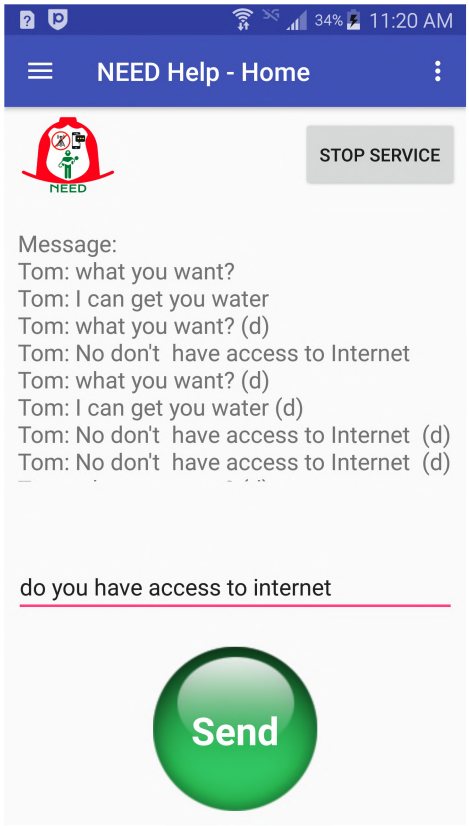

(b) User Ryan Page.

Figure 5. NEED chat between users when there is no Internet available.

The selection of various interfaces is performed without any notification to the user. The application turns on all available interfaces (Wi-Fi, Bluetooth) with initial approval from the user when launched.

The messages are sent to the interface with Internet access. If none of the interfaces have Internet access, then the messages are sent through both Wi-Fi and Bluetooth.

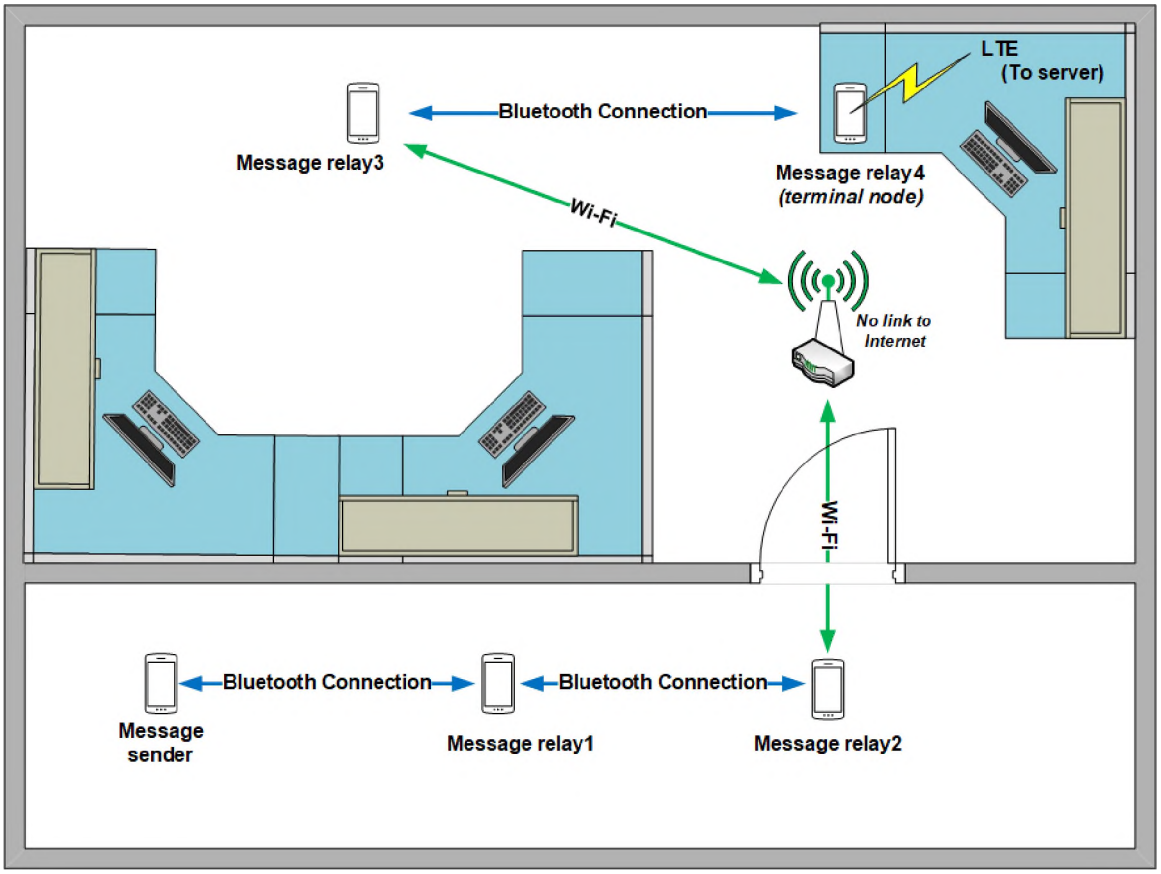

Figure 6. Topology of the test environment (placement of devices are not to the scale).

Figure 6 shows the topology of the test environment comprising five smartphones and a Wi-Fi router (IEEE 802.11g, AP mode, 2.4 GHz - channel 6) without Internet access. The smartphones used are from different manufactures with varying specifications (low-end to high-end). The devices form a heterogeneous mesh network where the messages are relayed to the server through Wi-Fi, Bluetooth, and cellular data service.

Table 1 lists the performance metrics measured at the terminal node of the network for the considered topology. The network traffic is measured when relaying to the server. The network traffic was measured using the Profiler from Android Studio. The traffic was

Table 1. Performance metrics measured for the considered topology.

Number of hops *(tested)*	5
Average distance between the devices	30 feet
Network traffic at the terminal device	1 Mbps

monitored at the final link, which has the link to the Internet. The maximum length of the message is 120 characters. The network achieved a throughput of 1 Mbps on average over different trials. The network bottleneck was observed at smartphones with low specifications and Bluetooth links.

Table 2. Comparison of average throughput achieved by homogeneous and heterogeneous links in the network.

Only Wi-Fi links	1.24 Mbps
a Wi-Fi and a Bluetooth link	1.53 Mbps

The average network traffic was measured with only Wi-Fi links and a combination of Wi-Fi and Bluetooth across two hops involving three devices. Table 2 shows the average throughput achieved by both the configurations and shows that the heterogeneous links achieve throughput greater than the homogeneous links in the network. The results from Price and Chandran (2017) show that in a Wi-Fi mesh network, throughput decreases as the number of hops increases since the bandwidth is split equally among the devices. Both Wi-Fi infrastructure and peer-to-peer modes require an access point or a group owner, which limits the number of hops. This limitation inhibits a homogeneous Wi-Fi mesh network to expand and provide coverage to more devices. A heterogeneous mesh network addresses this by allowing multiple Wi-Fi mesh networks connected by Bluetooth or Zigbee and also allowing the devices to operate in different Wi-Fi channels.

5. CONCLUSION

We implemented an Android application enabling smartphones to become convergence devices to build a heterogeneous mesh network. The messages from different devices hopped through Wi-Fi, and Bluetooth across the network. The network achieved an average throughput of 1 Mbps. We also developed a web server application to collect the messages and plotted on the map based on the location coordinates from the messages. Any device with access to the Internet could forward the messages from the network to the server. The app provides a chat functionality among members of the mesh when there is no Internet access. We planned to add more features such as caching, routing, and authentication to improve the performance and security of the network.

REFERENCES

Al-Saadi, A., Setchi, R., Hicks, Y., and Allen, S. M., 'Routing protocol for heterogeneous wireless mesh networks,' IEEE Transactions on Vehicular Technology, 2016, **65**(12), pp. 9773–9786, ISSN 00189545, doi:10.1109/TVT.2016.2518931.

AmpliSine Labs LLC, 'NEED Help website,' http://amplisinelabs.com/, 2018.

Dey, S., Kamal, M. N., Dutta, S., Tiwari, A., Ray, S., Moatasimbillah, M. J., Saha, N., Adhikary, N., Mukherjee, D., Nayak, S., Dey, R., and Saha, S., 'Ad-hoc networked UAVs as Aerial Mesh Network for disaster management application and remote sensing: An approach,' in '2017 8th IEEE Annual Information Technology, Electronics and Mobile Communication Conference (IEMCON),' 2017 pp. 301–304, doi:10.1109/IEMCON.2017.8117231.

Ferranti, L., D'Oro, S., Bonati, L., Demirors, E., Cuomo, F., and Melodia, T., 'Hiro-net: Self-organized robotic mesh networking for internet sharing in disaster scenarios,' in '2019 IEEE 20th International Symposium on "A World of Wireless, Mobile and Multimedia Networks" (WoWMoM),' 2019 pp. 1–9, doi:10.1109/WoWMoM.2019.8793029.

goTennaMESH, 'Gotennamesh,' https://gotennamesh.com/, 2008.

Loon LLC., 'Project loon,' https://loon.com/technology/, 2017.

Mahmood, S. H., Salih, A. M., and Khalil, M. I., 'Broadband services on power line communication systems: A review,' in '2019 22nd International Conference on Control Systems and Computer Science (CSCS),' ISSN 2379-0482, 2019 pp. 465–470, doi:10.1109/CSCS.2019.00085.

Mark Zuckerberg, 'The technology behind aquila,' https://www.facebook.com/notes/mark-zuckerberg/the-technology-behind-aquila/10153916136506634/, 2016.

Miura, R., Inoue, M., Owada, Y., Takizawa, K., Ono, F., Suzuki, M., Tsuji, H., and Hamaguchi, K., 'Disaster-resilient wireless mesh network - experimental test-bed and demonstration,' in '2013 16th International Symposium on Wireless Personal Multimedia Communications (WPMC),' 2013 pp. 1–4.

Ngo, T., Nishiyama, H., Kato, N., Shimizu, Y., Mizuno, K., and Kumagai, T., 'On the throughput evaluation of wireless mesh network deployed in disaster areas,' in '2013 International Conference on Computing, Networking and Communications (ICNC),' 2013 pp. 413–417, doi:10.1109/ICCNC.2013.6504119.

Price, N. D. and Chandran, A. M. M., 'Performance of ieee 802.11s for wireless mesh telemetry networks,' 2017.

Sugita, M., Matsue, H., Yamaguchi, K., Shimodaira, T., Shirotori, M., and Nanamatsu, S., 'Development strategy of disaster-resistant wifi mesh networks and the disaster monitoring and reporting system in a local area,' in '2015 International Conference on Information Networking (ICOIN),' 2015 pp. 139–144, doi:10.1109/ICOIN.2015.7057871.

The Weather Company - IBM, 'A new era of alerting,' https://weather.com/apps/ibm/meshnetworkalerts, 2017.

III. MEASUREMENT OF INTERNAL SELF-INTERFERENCE OF USRP FAMILY OF DEVICES IN FULL-DUPLEX OPERATIONS

I. Arul Mathi Maran Chandran, II. Maciej Zawodniok

Department of Electrical & Computer Engineering

Missouri University of Science and Technology

Rolla, Missouri 65409

Email: ac62f@mst.edu, mjzx9c@mst.edu

ABSTRACT

It is always been desirable to operate radios in full-duplex (FDX) mode to harness the maximum spectral efficiency despite the challenges it puts forth. Before validating any FDX schemes using a radio, we should know the characteristics of the radio in FDX operation. In this paper, the results from the measurement are presented for a set of widely used software-defined radio (SDR) platform, universal serial radio peripheral (USRP) such as N210, B210, and E310. The measurements includes the measurement of internal leakage suffered by these radios, operational range of transmitter gain to operate in FDX mode and their limitations. The internal leakage suffered by the USRPs is not uniform and varies across the family of devices.

Keywords: Full-Duplex (FDX), Self Interference (SI), Software defined radio (SDR), Universal Serial Radio Peripheral (USRP), N210, B210, E310, GNU Radio

1. INTRODUCTION

In the field of telecommunications, new methodologies and techniques are proposed to address the increasing demand in bandwidth and support the growing number of users. One of the parameters of interest that can be improved to address the demands is the

spectral efficiency of the radio. The spectral efficiency of the existing half-duplex (HDX) mode of operation is less than fifty percent since the radios take turns to transmit and receive. The spectral efficiency can be doubled by operating the radios in full-duplex (FDX) mode. In FDX, the transmission and the reception occur simultaneously. However, FDX presents a set of challenges. Self-interference (SI) is a key challenge that inhibits the radios to operate in FDX. During FDX communication, the transmitter signal overwhelms the highly sensitive receiver due to a significant difference in power levels. For example, the maximum signal strength that USRP N210 can transmit is +20 dBm (100 mW), which is large compared to its typical receiver sensitivity of -100 dBm (10^{-10} mW). SI occurs at two levels: external and internal to radio electronics. The direct feedback and reflections from the environment contribute to the external SI, whereas the internal SI is due to the leakage or RF coupling across internal components including printed circuit board (PCB), cables, circulators, switches, etc. as shown in Figure 1. The internal SI is prevalent in radios which multiplex its antennas or employing any switching interconnection between the transmitter (TX) chain and receiver (RX) chain. It occurs due to the lower isolation offered by multiplexing components such as couplers, switches. The internal SI is commonly observed in most SDR since they use multiplexing switches on their RF ports.

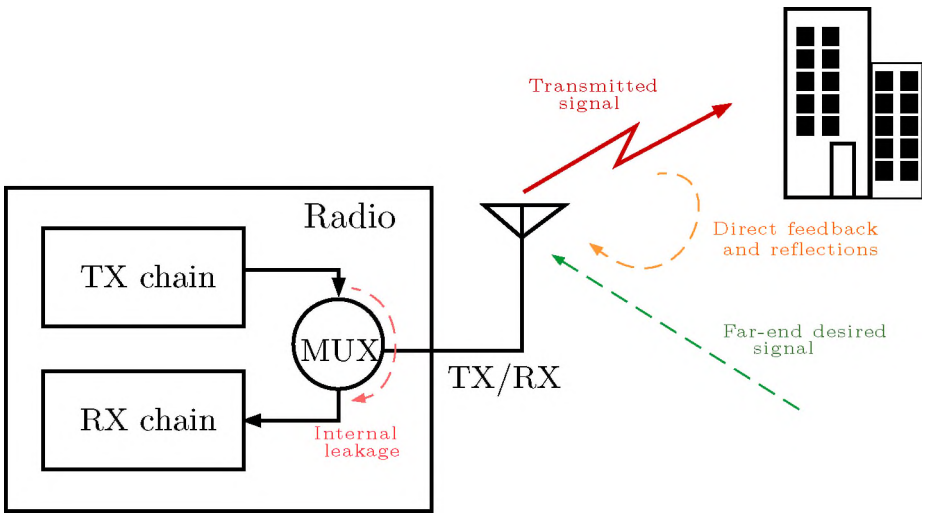

Figure 1. Radio suffering external SI during FDX operation.

SDR popularity is due to the ease in the development and reconfiguration of the radio modules Dominicis *et al.* (2012); Ghannouchi and Kwan (2015); Lahouli *et al.* (2014); Muradi *et al.* (2018); Shahin *et al.* (2013); Voet and Moer (2011). It is used in research for the rapid development and evaluation of new schemes and approaches. It is suitable for applications that demand flexibility and radio reconfiguration. There are different varieties of SDRs available in the market. USRP Ett (2018) is one such SDR platform. USRPs find their application in different fields such as research, monitoring, networking, cognitive radios, etc.

There are families of USRP products such as N210, E310, B210, etc. These devices have different capabilities, performance, and features. USRPs have at least two RF ports; one for transmission and other for the reception, allowing USRPs to operate in FDX mode. Table 1 tabulates the operating range of frequencies and available RF ports for different USRPs. These USRPs uses RF switches to multiplex their RF ports for transmission and reception. The metrics consider for the self-interference characterization are receiver leakage power, the cross-correlation between the transmitted and received signal. Understanding USRPs' capabilities and limitations for its FDX operation is a prerequisite for employing these radios to validate different schemes.

Table 1. Specification of different USRPs.

USRP	Frequency Range	RF ports	RF Switch
N210	50MHz to 2.2GHz	TX/RX & RX2	HMC174MS8
B210	70MHz to 6GHz	A: TX/RX & RX1 B: TX/RX & RX2	SKY13335-381LF
E310	70MHz to 6GHZ	A: TX/RX & RX1 B: TX/RX & RX2	SKY13373-460LF

USRPs are used as testbed to evaluate different schemes related to telecommunication Alexandris *et al.* (2014); Dobre *et al.* (2016); Guo *et al.* (2018); Hussain *et al.* (2016); Ridwan *et al.* (2016); Saafan and El-Badawy (2017); Tong *et al.* (2015); Yoon *et al.* (2016); Zitouni *et al.* (2015). They are used in the evaluation of spectrum access Saafan and El-Badawy (2017) and implementation of power estimation Dobre *et al.* (2016). They are also used in the development of fiber wireless testbed to simulate passive optical network Ridwan *et al.* (2016). USRPs were used in the performance analysis of cooperative protocols for MIMO systems Hussain *et al.* (2016) and also used in MIMO systems evaluation Yoon *et al.* (2016). These works used USRP in half duplex mode.

The specification of individual components of USRPs are available, but it is always a good practice to validate as a whole before it is used as a testbed to validate any schemes. On such validation of USRP N210 with SBX radio daughter card was performed in HDX mode Zitouni *et al.* (2015). The results revealed there was a deviation from the specification. The output power of the transmitter decreases with the increase in operating frequency, and an increase in transmitter gain increases the total harmonic distortion (THD) in addition to out-of-bound emissions. These results provided insight into the operation of the USRP N210, where it can be used reliably to validate different schemes. USRPs are been used to validate or demonstrate the full-duplex communication Guo *et al.* (2018); Tong *et al.* (2015). There is a lack of information on the performance of the USRPs in full-duplex operations, especially the internal self-interference over the operating frequencies. The knowledge of USRP in FDX operation enables us to test and evaluate different suppression techniques to overcome SI. USRPs are not built for FDX operation, but before it being used to validate different FDX schemes it has to be validated. These validations will be useful in the design of customized hardware platform for the final target.

The preliminary results have been presented Chandran and Zawodniok (2015) focusing only on USRP N210 and measurement of internal SI in a single radio scenario. In contrast, the paper contributions are: (a) measured and characterized internal SI for three

different radios as shown in Table 1, (b) characterized the capabilities and limitations in FDX mode. This allows the employment of USRPs for evaluation and to select the suitable frequency band for FDX operation.

2. OVERVIEW

The paper is organized as follows. First, we discuss the internal self-interference suffered by the USRPs due to the switches used to multiplex the transmitter and the receiver chains among the RF ports. Second, the experimental setup to determine the optimal transmitter gain such that the USRPs can be operated in FDX mode. Finally, we discuss the results which include the measured internal SI over the operating frequencies of the USRPs, and the correlation results to related the received signal at the RUT with its own signal and the far-end signal.

2.1. SELF-INTERFERENCE IN USRPS

In this section, we discuss the experimental setup and how internal SI of the USRPs N210, B210, and E310 are measured. The RF ports of USRP devices are in pairs, TX/RX and RX2. The TX/RX port can be used to transmit as well as receive, whereas RX2 can only be used to receive. The internal SI occurs due to the multiplexing transmitter and receiver chain between these two RF ports. USRP B210 and E310 have two pairs of a similar arrangement of RF ports.

Figure 2 shows the isolation plot across the RF ports of Single Pole Double Throw (SPDT) switch used in USRP N210. The maximum isolation offered by the SPDT switch over different operating frequencies of USRP N210 is -27 dB. The total isolation between the transmitter and receiver offered by two SPDT switches is -64 dB.

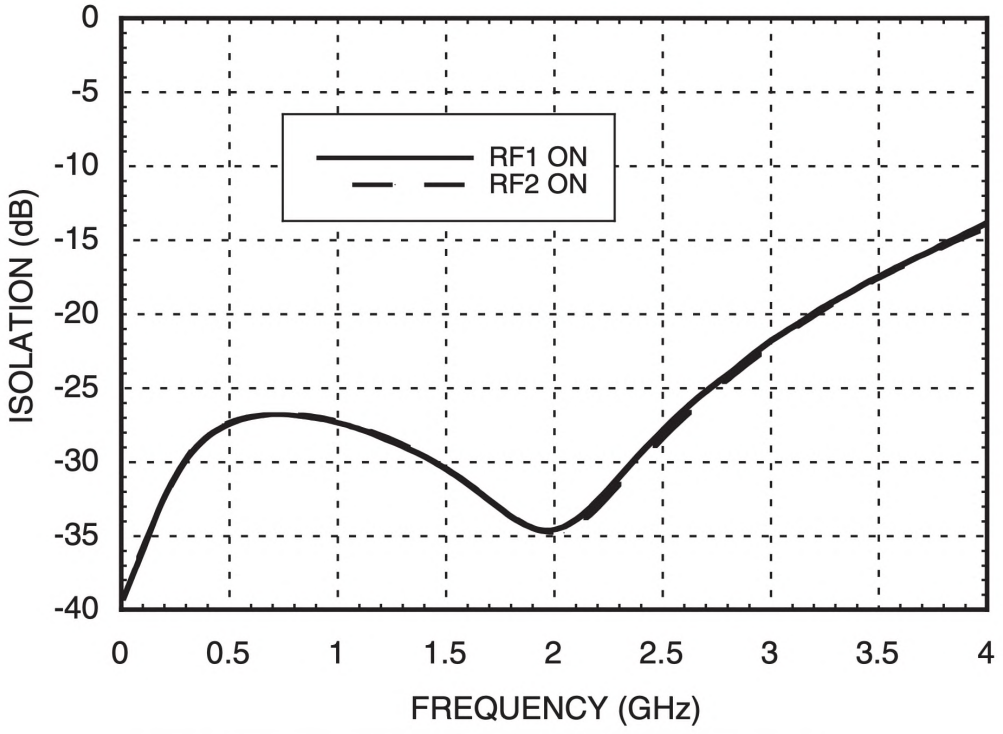

Figure 2. Isolation plot of HMC174MS8 switch used in USRP N210-RFswitch (2012).

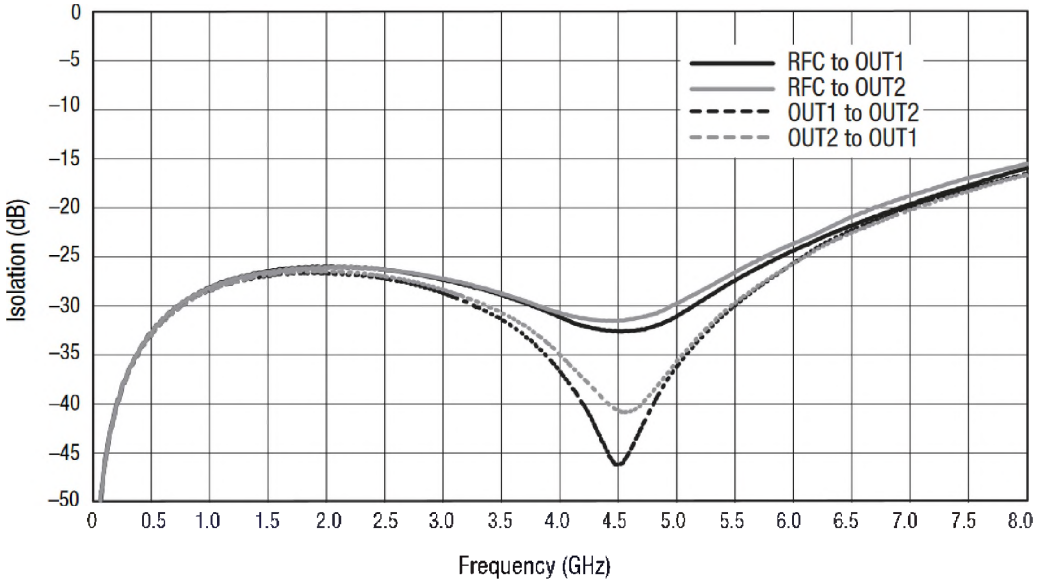

Figure 3. Isolation plot of SKY13335-381LF switch used in USRP B210-RFswitch (2014).

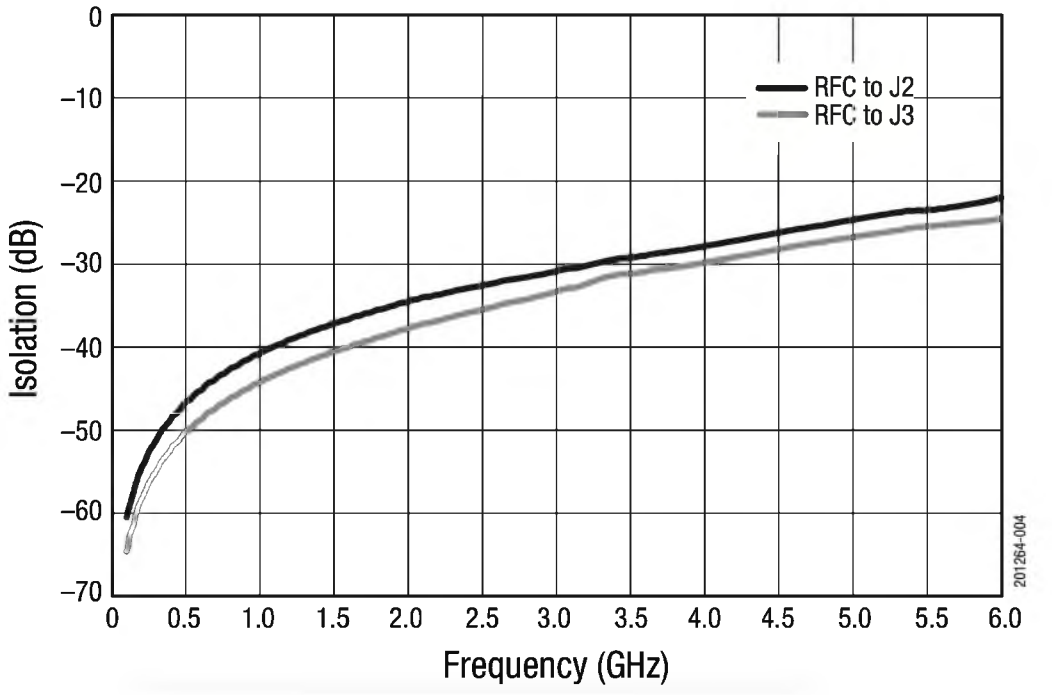

Figure 4. Isolation plot of SKY13373-460LF switch used in USRP E310-RFswitch (2016).

In the case of USRP B210 and E310 which have two pairs of RF ports as mentioned in Table 1. The measurements were done at both the receive-only ports (A: RX1 and B: RX1) while transmitting through one of the TX/RX port. All the RF ports other than the transmitting RF port was terminated using 50 Ω terminators. The SPDT switch (SKY13335-381LF) is used in USRP B210, and Figure 3 shows its isolation plot across its RF ports. The Single Pole Three Throw (SP3T) switch (SKY13373-460LF) is used in USRP E310, and Figure 4 shows its isolation plot across its RF ports.

The TX chain was configured to TX/RX port and RX chain to RX2 port. The RX2 port was terminated with 50 Ω, to stop feedback or reflections (external SI) reaching the receive chain. The power level at the receiver chain was monitored during transmission, and thus measuring internal SI. A similar experiment setup was used to measure the internal SI occurring in USRP B210 and E310.

The cross-correlation between the transmitted signal and received signal relates these two signals and confirms there is a leakage of the transmitter signal to the receiver chain. The transmitted signal leaked to the receiver chain suffers power loss due to the isolation offered by the SPDT switches. This loss has to be considered while comparing the autocorrelation of the transmitted signal with cross-correlation results. The measurements were done with different transmitter gain across respective radio's operating frequencies.

GNU Radio application was used to build the radio blocks and measurements were done on the IQ samples received by this application. The IQ samples received by the application are the baseband samples for the received signal.

2.2. FULL-DUPLEX OPERATION OF USRPS

This subsection discusses the experimental setup to determine the operational range of the USRPs in FDX mode. A pair of USRPs were used and each connected to GNU Radio application via Universal Hardware Driver (UHD). Typically the USRP devices are networked to computer with GNU Radio through interfaces such as ethernet and USB3. USRPs N210, B210, and E310 were used as the radio under test (RUT) and a USRP N210 was used as a far-end emulator. The experiment was performed in two parts, (a) determine the TX gain bound for FDX operation, and (b) determine the maximum coverage range using the determined TX gain bound. The TX gain range was determined since the internal SI is directly proportional to the transmitted signal strength. By varying the TX gain, the internal SI can be varied. This variation in TX gain also impact the coverage area of the radio, lower the TX gain lesser the coverage area. So, the experiment aims to determine the trade-off point such that the USRPs can be operated in FDX mode which can be deployed for short-range communication.

During the determination of TX gain bound, the RUT and the far-end emulator USRPs are physically connected with an attenuator. To avoid the external SI the USRPs are physically connected and the attenuator was introduced to emulate real-world attenuation

suffered by the far-end desired signal. Once, the TX gain bound was determined, the physical link with the attenuator was removed and the range experiment was performed under lab conditions with controlled external SI.

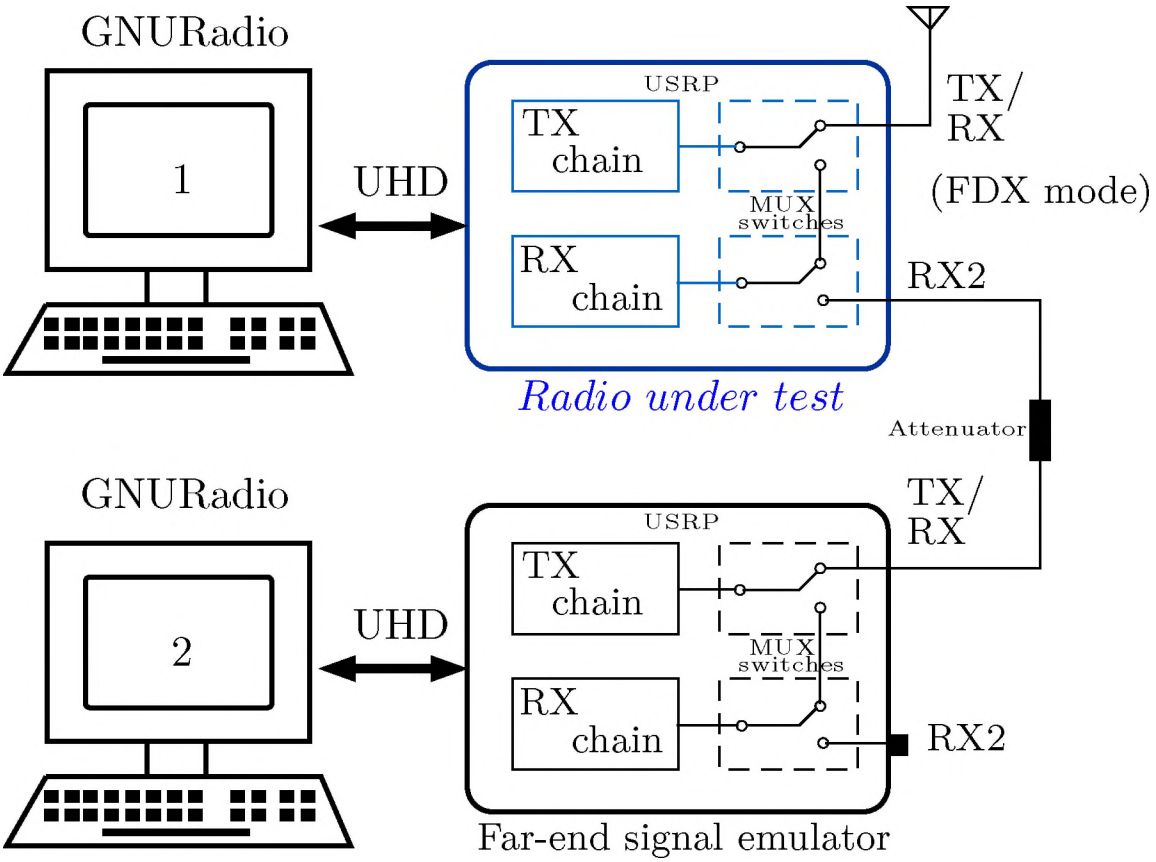

Figure 5. Experimental setup to operate USRPs in FDX mode.

The experimental setup to determine the transmitter gain threshold to operate the radios in FDX mode is shown in Figure 5. At RUT, the TX/RX port is configured to transmit and RX2 port to receive. The RX2 port of RUT was connected to the TX/RX port of the radio emulating the far-end signal via RF cable with 50 dB attenuation. The 50 dB attenuation emulates real-world attenuation suffered by the far-end signal. This ensures the RUT listens only to the far signal emulator and external SI can be avoided. The MIMO cable can be connected if the RUT is USRP N210, which allows sharing the clock between

RUT and the far-end signal emulator. This helps correlate signals between the USRPs. The connection between the radios is removed and measured the coverage distance with the identified optimum TX gain.

2.3. SUMMARY

In summary, the following steps can be followed before operating a radio in FDX mode.

1: Identify whether TX and RX chains of the given radio are independent of its specification or schematics
2: **if** TX and RX chains of the radio are multiplexed **then**
3: Internal SI exists and influences the radio performance
4: Perform experiments as discussed in Section 2.1
5: Characterize internal SI over the entire operating frequency range of the radio
6: **if** internal SI of operating frequency is above the desired threshold **then**
7: Tune TX gain such that internal SI is minimal. Reduces coverage area.
8: Employ suppression techniques for better coverage
9: **end if**
10: **else**
11: The radio can be operated in full-duplex mode for the chosen operating frequency
12: **end if**

3. MEASUREMENTS & RESULTS

In this section, internal SI measurements are presented for USRPs N210, B210, and E310. These radios operated in FDX mode and discussed their capability and limitations.

3.1. SELF-INTERFERENCE IN USRPS

Before the measurement of transmitter leakage, the signal strength of the transmitter was measured and repeated the same for different transmitter gains. The transmitter gain for USRP N210 ranges from 0 dB to 30 dB.

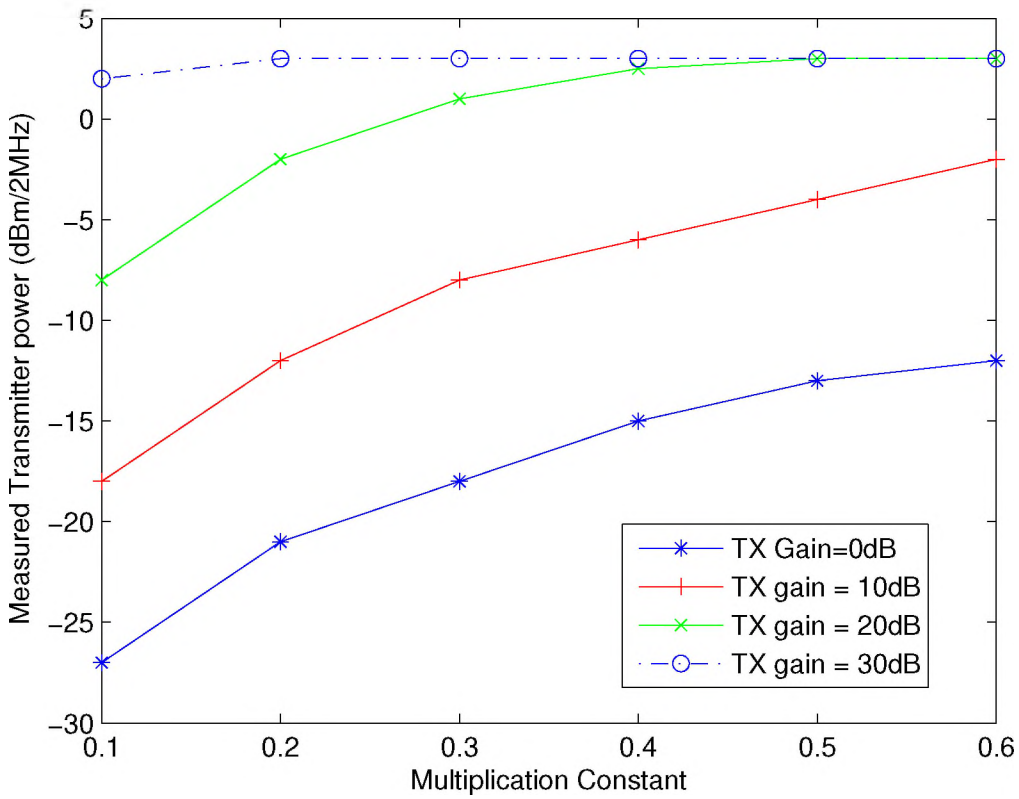

Figure 6. Measured transmitter power for different transmitter gain and multiplication constant using USRP N210.

The signal strength measured using a signal analyzer from USRP N210 for different transmitter gain with its center frequency configured to 650 MHz is shown in Figure 6. In addition to transmitter gain, a constant is multiplied before the baseband signal passed to passband which is also considered during the measurement. The operating range is from 0.1 to 0.6, above 0.6 the signal gets saturated at the passband. There is a non-linear relationship between the TX signal strength and TX gain.

The SI measurements for USRP N210 was discussed in Chandran and Zawodniok (2015). The SI measurements for USRP B210 and E310 are captured, observing the transmitter leakage (internal SI) at the receiver (RX1) of both pairs while transmitting at one (TX/RX). Figure 7 illustrates the observed power at the receivers of B210, and Figure 8 illustrates the observed power at the receivers of E310. It can be observed that internal SI is at its maximum between 1 GHz to 2.5 GHz for USRP B210 and a similar trend for USRP E310 with maximum leakage of -45 dBm.

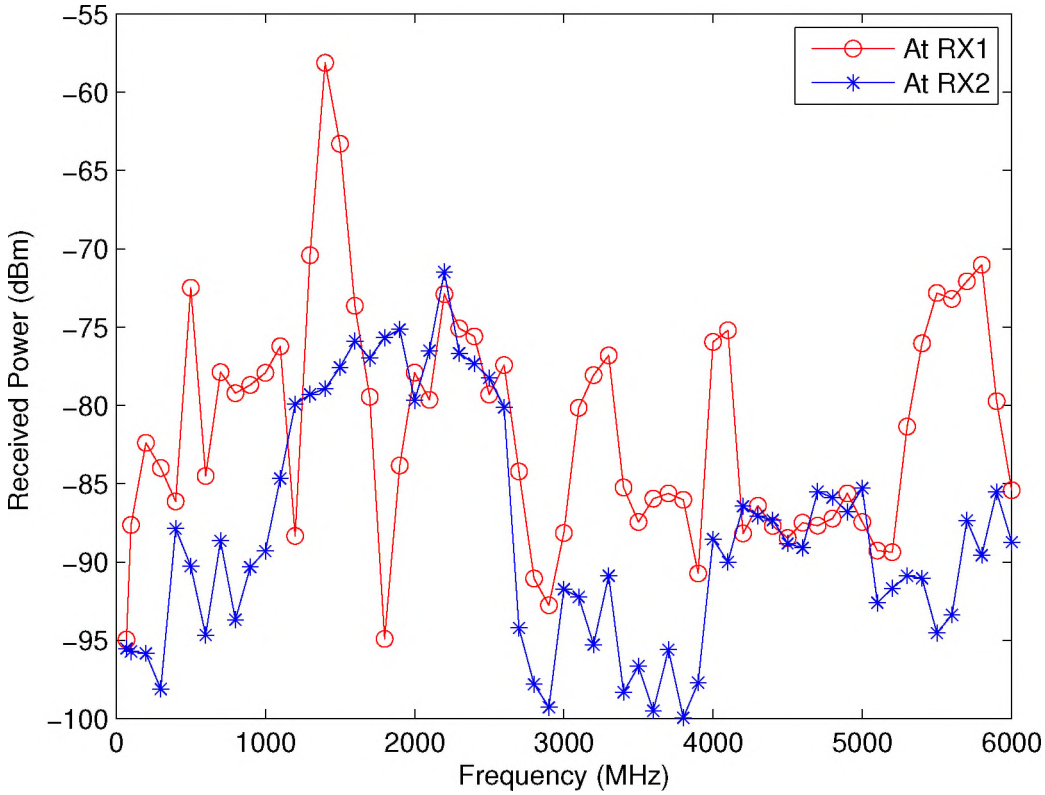

Figure 7. Internal SI observed in USRP B210 across its operating frequencies 70 MHz to 6 GHz with TX gain = 90.

The relationship between the transmitted signal and the received signal was determined by performing cross-correlation on samples captured by the GNU Radio application.

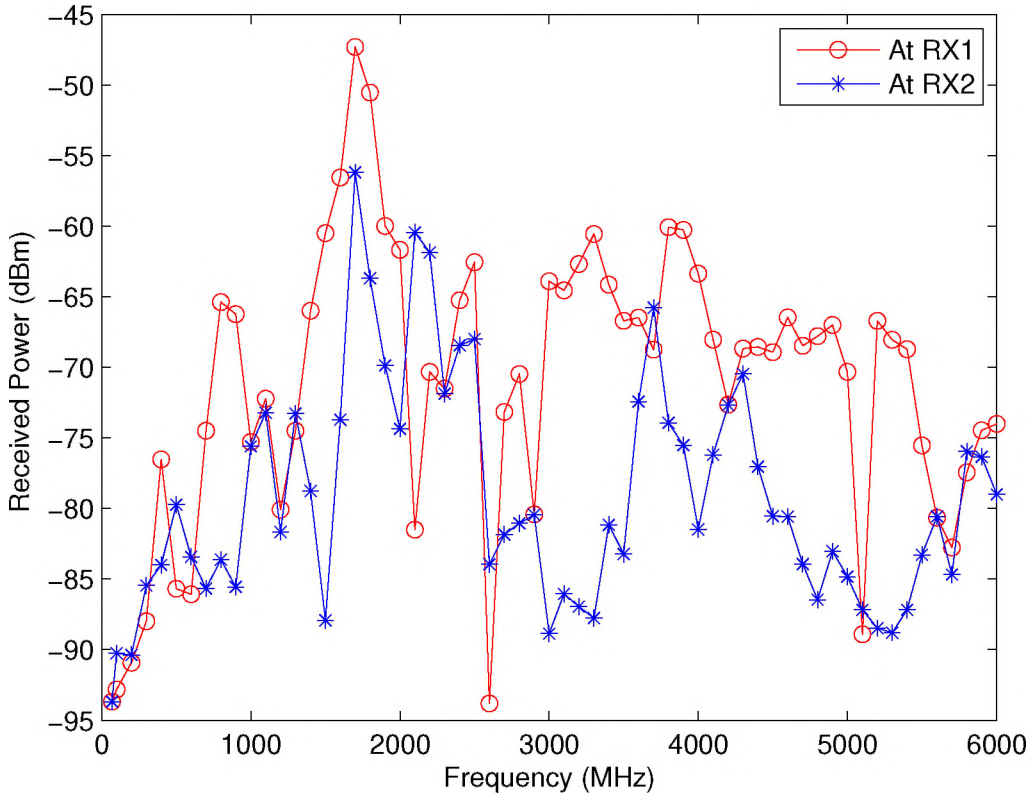

Figure 8. Internal SI observed in USRP E310 across its operating frequencies 70 MHz to 6 GHz with TX gain = 90.

The autocorrelation of the transmitted signal and the cross-correlation of the transmitted signal with the internal leakage (SI) signal is illustrated in Figure 9 . The difference in the maximum value of the cross-correlation to the autocorrelation of the transmitter's signal is due to the reduction of power through the SPDT switches. Thus using the correlation results the received signal can be related to the transmitted signal which leaked through the multiplexing switches. The internal leakage was observed without any external feedback since the RX2 port is terminated with 50 Ω terminator. The offset between the peaks varies due to offset introduced by the switches and also the application capturing the samples. In addition to cross-correlation, the received signal was demodulated and the decoded data. The decoded data is then compared with the transmitted data.

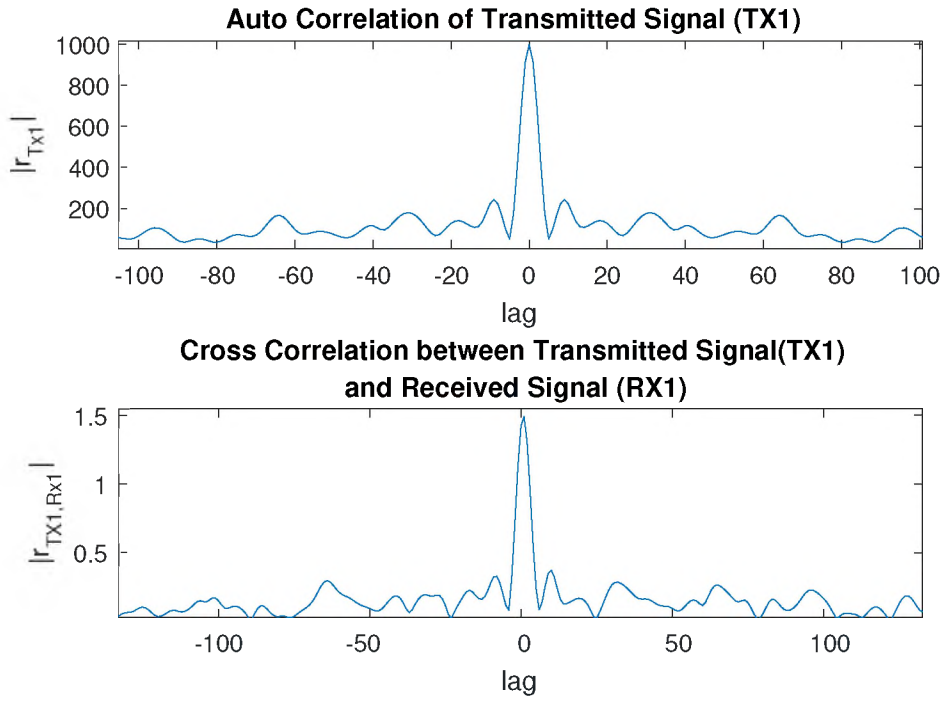

Figure 9. Relationship between the transmitter and received leakage signal.

3.2. FULL-DUPLEX OPERATION OF USRPs

In this subsection, we analyze the results and determine the configuration which enables USRPs to operate in full-duplex mode. The measurements were done using the experimental setup shown in Figure 5, and the operating frequency was 650 MHz. The noise floor was measured to be -95 dBm when the experiment was performed. The transmitter gain was varied from 0 dB to 30 dB, incremented in steps of 1 dB. Figures 9 to 11 shows the cross-correlation between the transmitter signal with the received signal at RUT for different TX gain at the RUT. The TX gain for the far-end signal emulator was fixed and the TX gain of RUT was varied to observe the impact of internal SI suffered by the USRPs.

The IQ samples of the transmitter and receiver at the baseband are captured by the GNURadio application and offline correlation analysis was performed. The correlations are performed on the raw IQ samples before demodulation. The lags in the correlation result are due to the random offset introduced by UHD and also during IQ sample capture. The

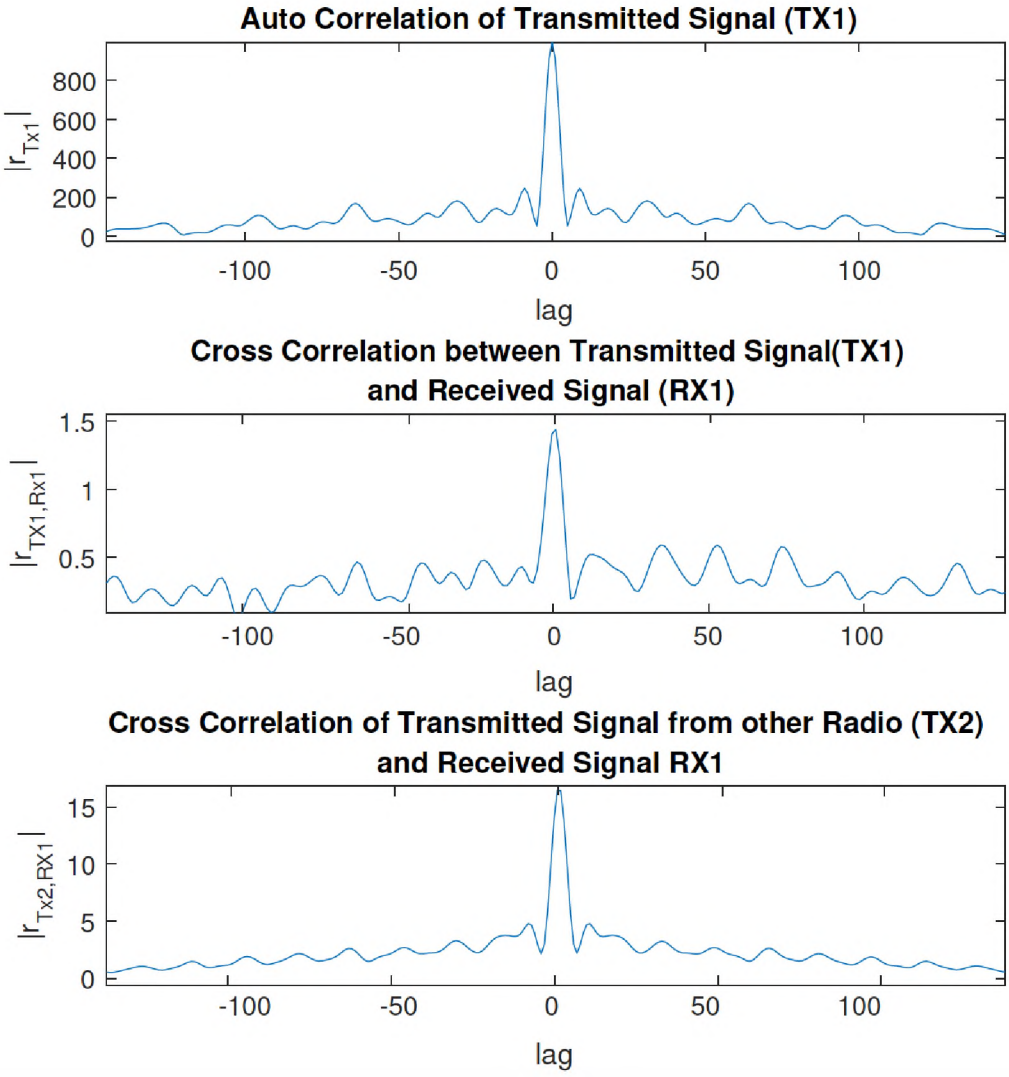

Figure 10. Relationship between the received signal with transmitter signals (TX1 and TX2) with TX1 gain = 1 dB.

lag of the cross-correlations are relative and the zero corresponds to the peak correlation with the tranmitted signal from the RUT. The networking interfaces such as ethernet, USB3 between the USRP devices and GNU Radio also contribute to the offset between the transmitter and receiver samples. The objective of illustrating correlation results is to show the close relationship of which signal dominating at the receiver. The lag/offset can be removed during frame synchronization after demodulation. Besides, the USRPs are not synchronized to a single clock for operation and they are independent.

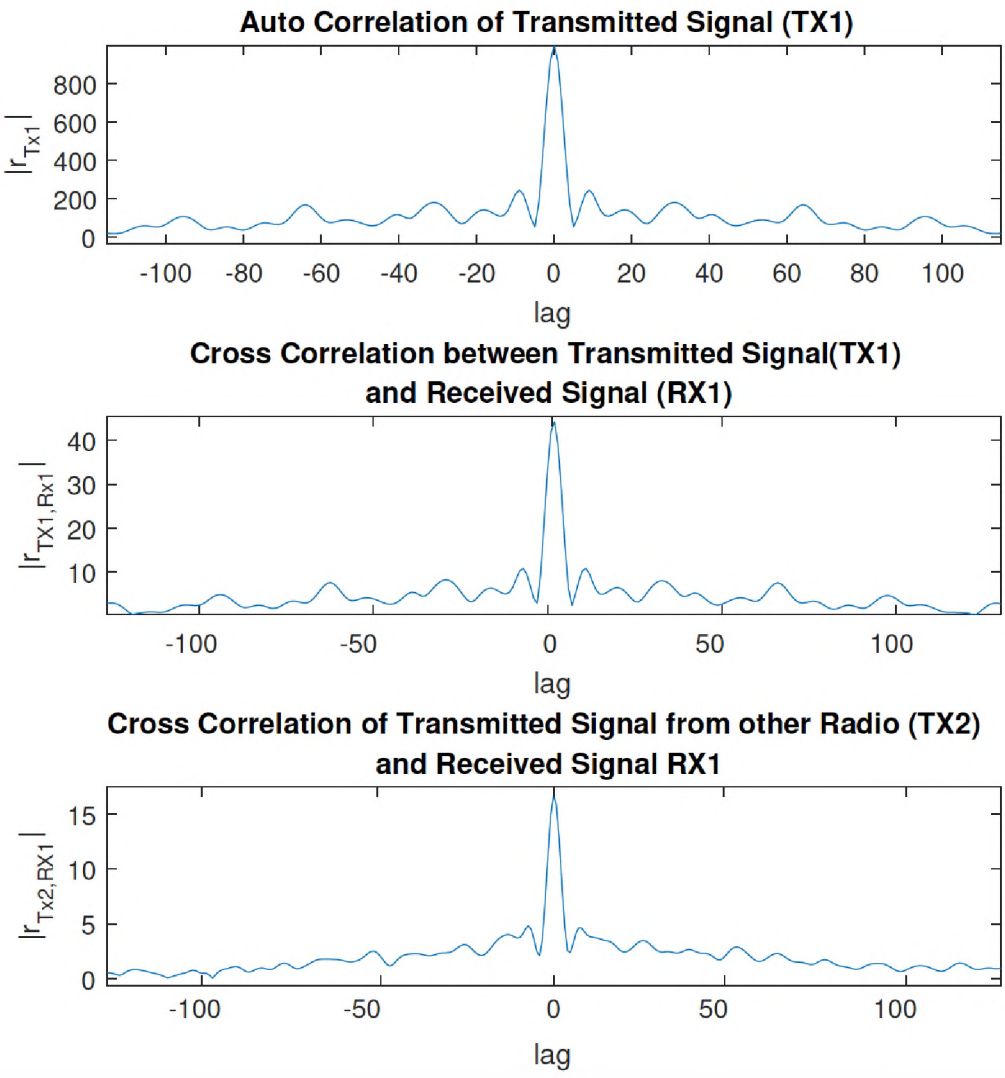

Figure 11. Relationship between the received signal with transmitter signals (TX1 and TX2) with TX1 gain = 30 dB.

When the RUT was operated at minimum TX gain (1 dB), the cross-correlation between the received signal at RUT and the far-end desired signal is greater than its signal as shown in Figure 10. When the TX gain of the RUT was increased (30 dB), the cross-correlation of the received signal at RUT and its signal increase, and greater than that of the far-end desired signal as shown in Figure 11. This correlation results reflected in the data when the received IQ samples were demodulated and decoded. In the first case, the data from the far-end emulator was decoded at the RUT, whereas in the latter case the data from

RUT was decoded overwhelming the far-end data. Though the cross-correlation between the RUT received signal and the far-end desired signal was the same, the decoded data showed the impact of the internal SI.

These observations help us to understand the impact of the internal SI suffered by the USRPs and can be used in FDX operation tailored to operate in the identified frequency range and TX gain.

4. CONCLUSION

The internal self-interference varied between USRPs N210, B210, and E310. USRP B210 has the least internal SI, whereas USRP N210 suffers the most. Table 2 tabulates the frequency bands where internal SI is maximum and minimum for USRPs N210, B210, and E310, and provides a choice where the respective USRPs can be operated in full-duplex mode.

Table 2. Minmum and maximum internal SI frequency bands for different USRPs.

USRP	Frequency Range	
	Minimum SI	Maximum SI
N210	600 MHz, 850 MHz 1.9 GHz to 2.2 GHz	600 MHz to 800 MHz
B210	50 MHz to 1 GHz 3 GHz to 6 GHz	1 GHz to 2.5 GHz
E310	50 MHz to 1 GHz 3 GHz to 3.5 GHz 5 GHZ to 5.75 GHz	1.2 GHz to 2.2GHz

The full-duplex operation was successfully performed between two USRP devices with limitations on the transmitter gain and the testing environment. USRP N210 achieved a coverage range of about 10 feet, in contrast, USRP B210 achieved 22 feet under lab conditions.

REFERENCES

'Ettus Research, a National Instruments Company,' https://kb.ettus.com/Knowledge_Base, 2018.

Alexandris, K., Balatsoukas-Stimming, A., and Burg, A., 'Measurement-based characterization of residual self-interference on a full-duplex MIMO testbed,' in '2014 IEEE 8th Sensor Array and Multichannel Signal Processing Workshop (SAM),' ISSN 1551-2282, 2014 pp. 329–332, doi:10.1109/SAM.2014.6882408.

B210-RFswitch, 'SKY13335-381LF: 0.1-6GHz GaAs SPDT Switch,' https://www.skyworksinc.com/-/media/SkyWorks/Documents/Products/301-400/SKY13335_381LF_201093D.pdf, 2014.

Chandran, A. M. M. and Zawodniok, M., 'Transmitter leakage analysis when operating USRP (N210) in duplex mode,' in '2015 IEEE International Instrumentation and Measurement Technology Conference (I2MTC) Proceedings,' ISSN 1091-5281, 2015 pp. 340–345, doi:10.1109/I2MTC.2015.7151291.

Dobre, E. I., Marţian, A., and Vlădeanu, C., 'USRP-based experimental platform for energy detection in cognitive radio systems,' in '2016 International Conference on Communications (COMM),' 2016 pp. 185–188, doi:10.1109/ICComm.2016.7528275.

Dominicis, C. M. D., Ferrari, P., Sisinni, E., Flammini, A., Pivato, P., and Macii, D., 'Timestamping performance analysis of ieee 802.15.4a systems based on sdr platforms,' in '2012 IEEE International Instrumentation and Measurement Technology Conference Proceedings,' ISSN 1091-5281, 2012 pp. 2034–2039, doi:10.1109/I2MTC.2012.6229356.

E310-RFswitch, 'SKY13373-460LF: 0.1-6GHz SP3T Switch,' https://www.skyworksinc.com/-/media/SkyWorks/Documents/Products/601-700/SKY13373_460LF_201264N.pdf, 2016.

Ghannouchi, F. M. and Kwan, A. K., 'Software defined radio subsampling receiver for wireless monitoring and sensing medical applications,' in '2015 IEEE International Conference on Ubiquitous Wireless Broadband (ICUWB),' ISSN 2162-6588, 2015 pp. 1–5, doi:10.1109/ICUWB.2015.7324513.

Guo, H., Xu, J., Zhu, S., and Wu, S., 'Realtime Software Defined Self-Interference Cancellation Based on Machine Learning for In-Band Full Duplex Wireless Communications,' in '2018 International Conference on Computing, Networking and Communications (ICNC),' 2018 pp. 779–783, doi:10.1109/ICCNC.2018.8390351.

Hussain, N., Ziri-Castro, K., Jayalath, D., and Arafah, M., 'Experimental Evaluation of DCOOP Protocol Using USRP-RIO Based Testbed at 5.8 GHz,' in '2016 IEEE 84th Vehicular Technology Conference (VTC-Fall),' 2016 pp. 1–6, doi:10.1109/VTCFall.2016.7881005.

Lahouli, R., Ben-Romdhane, M., Rebai, C., and Dallet, D., 'Towards flexible parallel sigma delta modulator for software defined radio receiver,' in '2014 IEEE International Instrumentation and Measurement Technology Conference (I2MTC) Proceedings,' ISSN 1091-5281, 2014 pp. 1041–1046, doi:10.1109/I2MTC.2014.6860901.

Muradi, V. S., Paithane, R. K., Ahmed, A., and Pawar, A., 'Spectrum sensing in cognitive radio using Labview and NI USRP,' in '2018 2nd International Conference on Inventive Systems and Control (ICISC),' ISSN null, 2018 pp. 1316–1319, doi:10.1109/ICISC.2018.8399019.

N210-RFswitch, 'HMC174MS8/174MS8E,' http://www.analog.com/media/en/technical-documentation/data-sheets/hmc174.pdf, 2012, rev. 04.0109.

Ridwan, M. A., Radzi, N. A. M., Abdullah, F., Din, N. M., and Al-Mansoori, M. H., 'Fiber wireless testbed using universal software radio peripheral (usrp),' in '2016 IEEE Region 10 Conference (TENCON),' 2016 pp. 3601–3604, doi:10.1109/TENCON.2016.7848729.

Saafan, A. M. and El-Badawy, H. M., 'Automated testbed for spectrum allocation in hostile environment based on usrp cognitive radio system,' in '2017 34th National Radio Science Conference (NRSC),' 2017 pp. 178–185, doi:10.1109/NRSC.2017.7893502.

Shahin, N., LaSorte, N. J., Rajab, S. A., and Refai, H. H., '802.11g channel characterization utilizing labview and NI-USRP,' in '2013 IEEE International Instrumentation and Measurement Technology Conference (I2MTC),' ISSN 1091-5281, 2013 pp. 753–756, doi:10.1109/I2MTC.2013.6555516.

Tong, Z., Russ, C., Vanka, S., and Haenggi, M., 'Prototype of Virtual Full Duplex via Rapid On-Off-Division Duplex,' IEEE Transactions on Communications, 2015, **63**(10), pp. 3829–3841, doi:10.1109/TCOMM.2015.2465958.

Voet, K. and Moer, W. V., 'Design of a software-defined radio for use in the IEEE L- and S-band,' in '2011 IEEE International Instrumentation and Measurement Technology Conference,' ISSN 1091-5281, 2011 pp. 1–4, doi:10.1109/IMTC.2011.5944002.

Yoon, H., Park, J.-S., and Jang, B.-J., 'Testbed for analyzing performance degradation of MIMO-OFDM WLAN due to WPAN interferer using USRP,' in '2016 Eighth International Conference on Ubiquitous and Future Networks (ICUFN),' 2016 pp. 487–489, doi:10.1109/ICUFN.2016.7537079.

Zitouni, R., Ataman, S., Mathian, M., and George, L., 'Radio frequency measurements on a SBX daughter board using GNU Radio and USRP N-210,' in '2015 IEEE International Workshop on Measurements Networking (M N),' 2015 pp. 1–5, doi: 10.1109/IWMN.2015.7322969.

IV. TRANSMITTER LEAKAGE ANALYSIS WHEN OPERATING USRP (N210) IN DUPLEX MODE

I. Arul Mathi Maran Chandran, II. Maciej Zawodniok

Department of Electrical & Computer Engineering

Missouri University of Science and Technology

Rolla, Missouri 65409

Email: ac62f@mst.edu, mjzx9c@mst.edu

ABSTRACT

The main challenge of operating a radio in full duplex mode, is the direct feedback from its transmission to its reception which is the self interference. However, the internal leakage within the radio has the potential to distort the received signal. This paper presents the measured leakage observed in N210 one of the Universal Serial Radio Peripheral (USRP) family of devices. Also, suppression mechanism has been evaluated in both in hardware and software.

Keywords: Transmitter leakage, self interference, Software Defined Radio (SDR), Universal Serial Radio Peripheral (USRP), Single Pole Double Throw (SPDT), GNU Radio.

1. INTRODUCTION

Radios in full duplex mode establish bidirectional communication link operating simultaneously, in other words the transmitter and the receiver are operated in the same time. Generally, separate antennas are used by the transmitter and the receiver. In addition, the RF carriers can be same frequency or different frequencies for the transmitter and receiver

Choi *et al.* (2010). There is a ongoing interest to operate a single antenna in full duplex mode with single RF carrier frequency especially in the field of Radar communication Beasley *et al.* (1990); Li and Murch (2011).

Most of the radios today are generally half duplex, which means there is no simultaneous operation of transmitter and receiver. One main challenging factor which prohibits us to achieve full duplex is transmitter feedback to the receiver Sta (2010). There are many cancellation technique put forth to cancel out the feedback from the transmitter. The solution to achieve full duplex can redefine the entire schematic for building the radio. Nowadays the radios are supporting MIMO where there multiple antennas for transmission and reception, which increased the complexity to achieve full-duplex because the self interference is not from a single antenna but from multiple antennas Duarte and Sabharwal (2010); Jain *et al.* (2011).

The advantage of full duplex wireless radio has a large scope to increase the efficiency by utilizing the transition period between transmission to reception. There are three main benefits which can be achieved by full duplex namely, timing efficiency, nodes no more wait for the other node to response (no handshake to avoid collision), both the entity transmitter and receiver enjoy full bandwidth.

In addition to the self interference, most radio suffer transmitter leakage due to the design and inability to isolate the transmitter and receiver path significantly. Due to the design constraint, transmitter and receiver paths are multiplexed, thus yielding to internal transmission bleed to the receiver path distorting the weak received signal. It also occur when a duplexer is used when a single antenna is deployed for transmission and reception. Though there are many cancellation technique to overcome the self interference, the transmitter leakage can be avoided by better design and choice of better isolators between transmitter and receiver path.

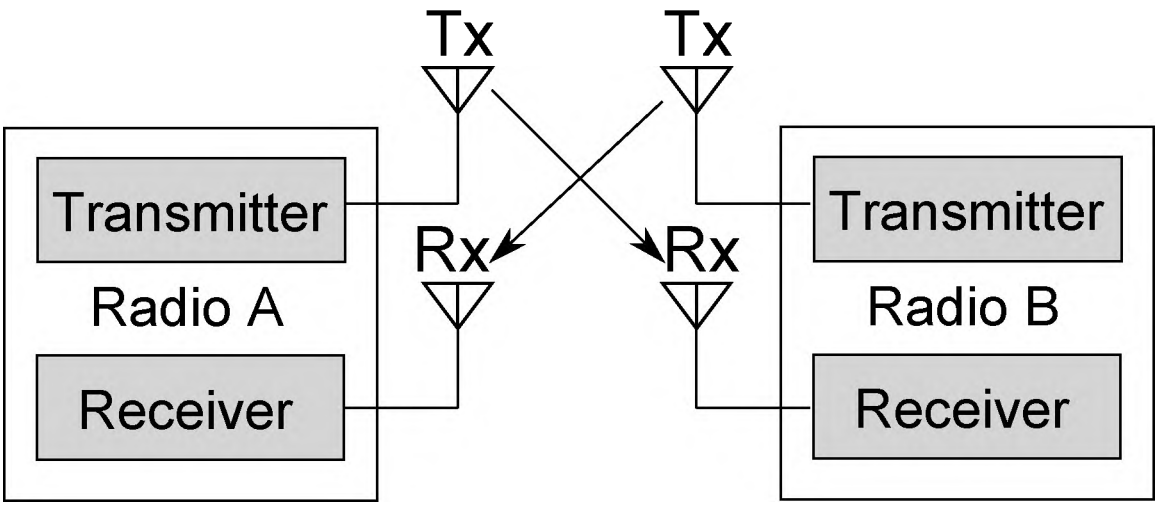

Figure 1. Radio A and B operating in full-duplex mode using separate antennas for transmitter and receiver.

In case of full duplex radio with single antenna, where the transmitter and receiver path shares the same antenna, the transmission leak from the transmitter to receiver path can be avoided by deploying isolator providing high isolation between them. Recently, the signal cancellation based on electrical balance using hybrid transformers has been proposed to improve isolation between transmitter and receiver path Abdelhalem *et al.* (2013).

2. USRP N210 RADIO

The USRPs are general purpose the Software Defined Radios (SDA), which are mostly used in academic and research field. The USRP N210 version provides high-bandwidth, high-dynamic range processing capability with modular design supporting it to operate from DC to 6GHz. The radio typically used in N210 is WBX, which operates in wide frequencies ranging from 50 MHz to 2.2 GHz and provides 40 MHz of bandwidth capability.

The radio offers two antenna ports TX/RX and RX2. TX/RX port one can be operated both as transmitter and receiver, whereas RX2 can be operated only as receiver. Both the antenna ports can be used simultaneously enabling radio to support full duplex

mode. The selection of the antenna ports for transmission and reception are controlled by application like GNURadio which is supported by USRP Hardware Driver (UHD), providing the host driver and APIs. The Gigabit Ethernet connectivity is available to stream data to and from the host system.

3. TRANSMITTER LEAKAGE CANCELLATION

Transmitter Leakage is a key challenge as discussed before, since the adverse effect caused at the receiver end brings down the performance of the radio. In general the common cancellation technique is to cancel or suppress by mixing the phase shifted version of the known transmitted signal to the received signal. This is the most adopted method to suppress the transmitter signal in the receiver path.

The phase shift can be fixed or computed dynamically on the fly and then applied to the transmitter signal. The dynamic estimation can be achieved by deploying a micro-controller Jung *et al.* (2008) which processes the received signal and estimate the phase to be applied to the transmitted signal for mixing. These cancellation techniques hold good for single tone transmission but for real-time data transmission, the micro-controller will face hard to estimate and counter the leakage in a timely manner.

There are implementations of transmitter leakage estimation and cancellation in the digital front end which is independent of the RF front-end used. Though these cancellation techniques are capable of cancelling the leakage, they fail when the transmitter leakage is significant such that the Low Noise Amplifier (LNA) gets saturated and there is no room to retrieve the information from its output Frotzscher and Fettweis (2008); Frotzscher and Fettweis (2012). Even if the transmitter leakage is not enough to saturate the LNA, they will be amplified and still increase the difficulty in retrieving the information. Even in case of Frequency Division Duplexing (FDD) systems where the transmitter and receiver use

different frequency, the transmitter leakage still prevail key issue which has to be mitigated since high power transmitter signal leaked to receiver path can saturate the receiver or interfere the weak received signal Kiayani *et al.* (2013).

Current CMOS technology is exploited to nullify the transmitter leakage. In some application like CDMA, a transmitter leakage canceller circuit Kim *et al.* (2013) was proposed and implemented in 0.18-μm CMOS technology. This circuitry is a feed-forward canceller sampling the reference transmitter signal and injects its amplitude-adjusted and phase-rotated signal in the receiver path.

4. TRANSMITTER LEAKAGE IN WBX

The WBX radio supports operating the transmitter and receiver port simultaneously. Besides the self interference is caused by the transmitter distorting the received signal, there is another factor in the WBX radio which significantly affects the received signal due to the internal bleed of transmitter signal to the receiver path. This is by the design, since the transmitter antenna which can perform the reception shares the receiver path of the other antenna which does only reception.

This leakage issue was earlier noticed and hardware workaround was proposed. However, these do not address the underlying issue Rub (2012).

Table 1. Specification of USRP N210.

USRP	Frequency Range	RF ports	RF Switch
N210	50MHz to 2.2GHz	TX/RX & RX2	HMC174MS8

The WBX daughter card uses two Single Pole Doupbe Throw (SPDT) switches (HMC174MS8 N210-RFswitch (2012)).

One of the switches switch transmitter adn receiver path feeding to/from TX/RX port as indicated in Table 1. The second switch switches between the receive path from TX/RX and RX2 port to the receiver. The transmitter leakage is observed because of the second SPDT switch where the transmitter chain TX/RX leaks to the receiver chain of RX2.

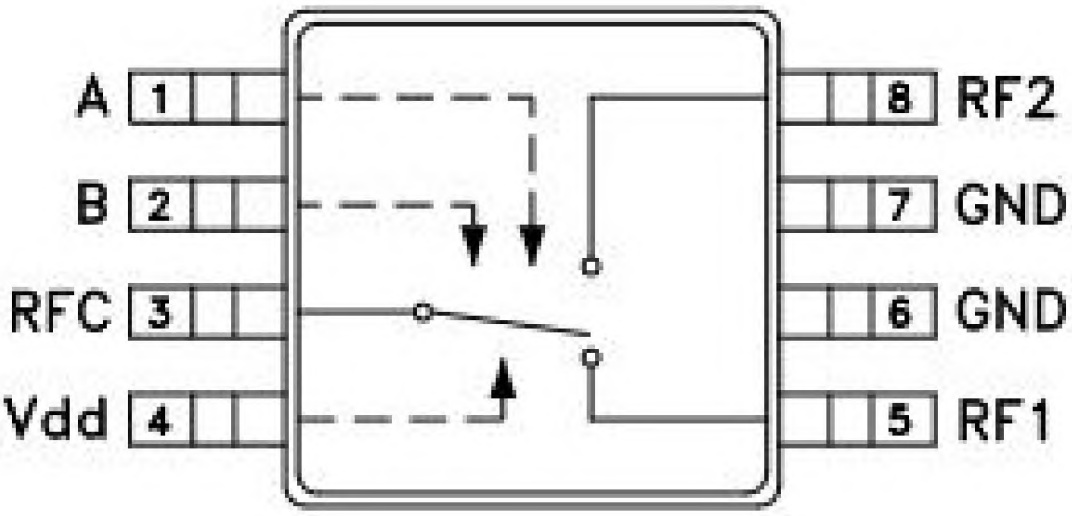

Figure 2. Functional diagram of HMC174MS8 SPDT switch N210-RFswitch (2012).

Figure 2 shows the functional diagram the deployed SPDT switch in WBX radio card. The port RFC selects signal between RF1 and RF2.

Figure 3 and Figure 4 illustrates the schematics TX/RX and RX2 ports of the WBX granddaughter card. The common connection between the SPDT switches *TX_RX* got encircled in the Figure 3 and Figure 4.

Figure 5 illustrates more clear representation of the two SPDT switches and their respective connections with the transmitter and receiver path.

When operating simultaneously the TX/RX port as transmitter and the RX2 port as receiver, the RF port of TX/RX SPDT switch receives a portion of energy from the transmitter chain and a portion from the transmitted signal port. This is then propagated

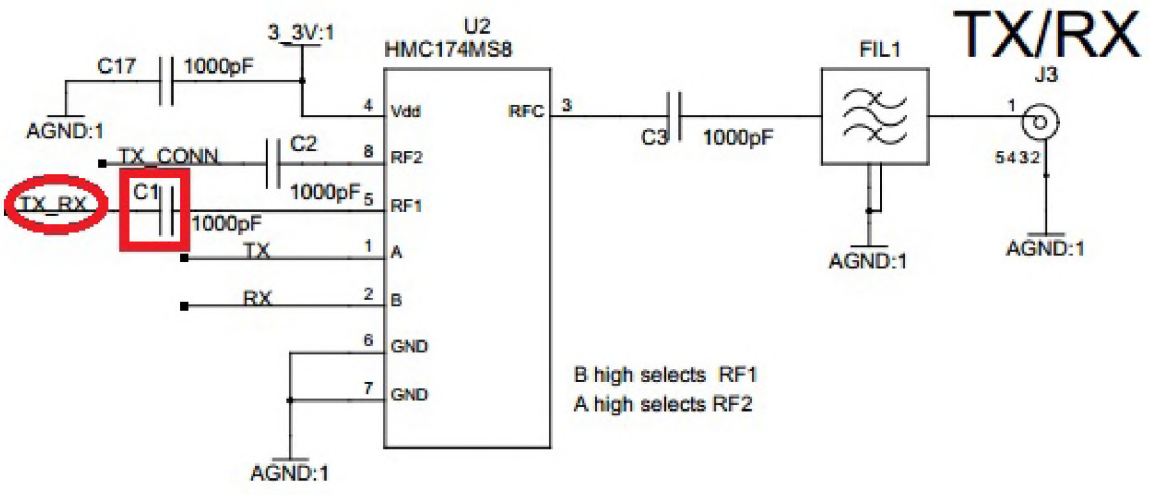

Figure 3. Schematic of WBX granddaughter card TX/RX antenna port, based on WBX (2012).

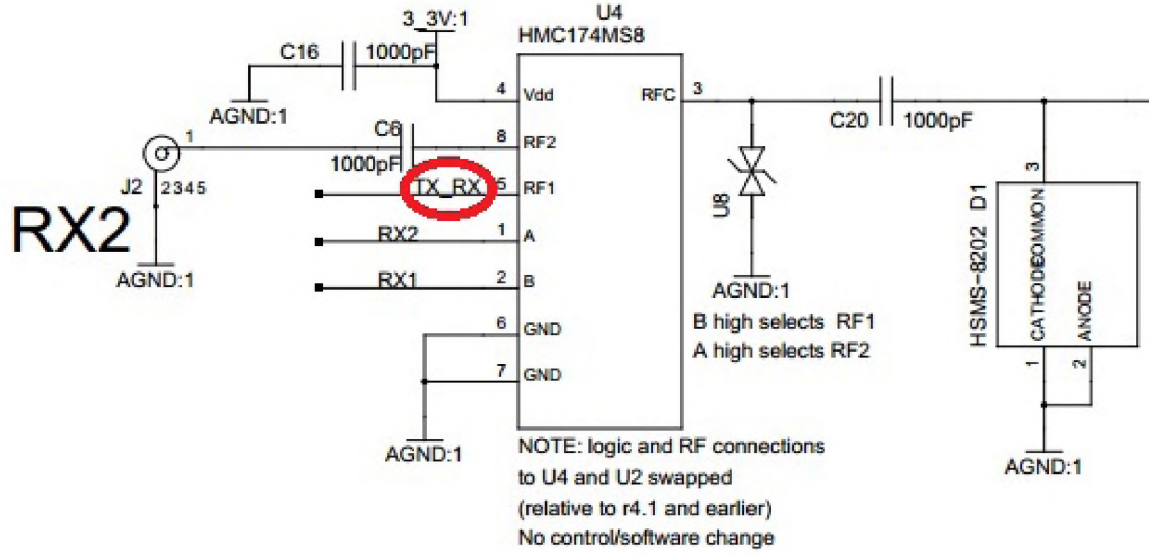

Figure 4. Schematic of WBX granddaughter card RX2 antenna port, based on WBX (2012).

to the receiver chain's SPDT switch and affects the received signal. This is due to SPDT switch providing lower the isolation between the two RF input ports, and between input and output ports of SPDT switch.

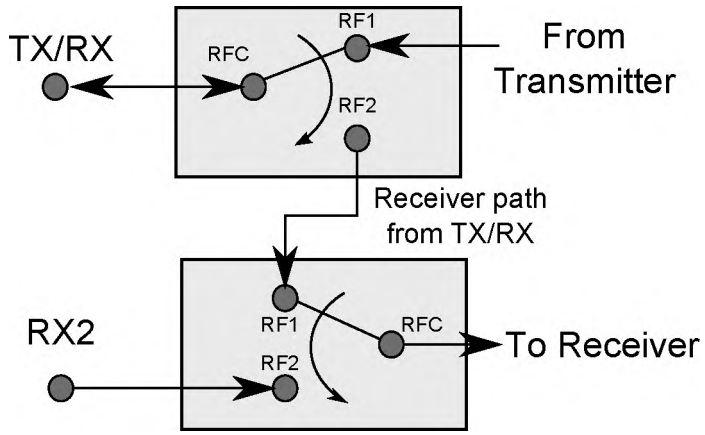

Figure 5. Block diagram of transmitter and receiver path connections between SPDT switches.

The isolation between the two RF ports RF1 and RF2 of HMC174MS8 is in the range of -25 dB to -30 dB for the frequency range of 500 MHz to 1 GHz. For the same frequency range, the isolation between RF ports RF1/RF2 to RFC is -26 dB. Typically, the desired isolation is more than -60 dB.

4.1. HARDWARE FIX

As mentioned the primary cause of transmitter leakage across the SPDT switches in the RF board is due to the common connection. Hence, the better option is to remove the common connections between the switches and physically isolating them. This was achieved by removing the coupling capacitor C1 which is encircled in Figure 3.

Figure 6a shows the WBX granddaughter card with the coupling capacitor and Figure 6b shows the WBX granddaughter card without the coupling capacitor between the SPDT switches.

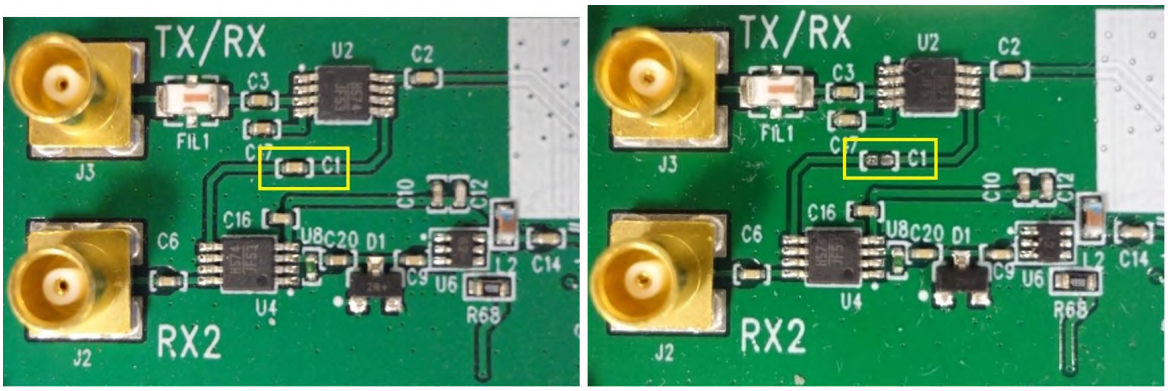

(a) With C1. (b) Without C1.

Figure 6. WBX granddaughter card with hardware fix.

4.2. DIGITAL FILTERING APPROACH

Beyond the hardware fix provided to the RF board, there can be transmitter leakage because of the existence of the open circuit between the switches. Irrespective of hardware fix, we can perform adaptive cancellation technique to suppress the transmitter leakage. The output of this block to suppress the transmitter leakage, if the LNA is not saturated by the leakage.

Recursive Least Squares (RLS) filter is a FIR of length M with coefficients $b_k, k = 0, 1, 2, \ldots M-1$. The input stream $f\,(n)$ is passed through the filter to produce the sequence $y\,(n)$. At each time-step the filter coefficients are updated using an error $e\,(n) = d\,(n) - y\,(n)$, where $d\,(n)$ is the desired response (usually based on $f\,(n)$) Rowell (2008).

$$y\,(n) = \Sigma_{k=0}^{M-1} b_k f\,(n-k) \tag{1}$$

Filter Coefficients, $b\,(n) = b\,(n-1) + k\,(n)\,e\,(n)$ where, λ is weighting factor.

$$KalmanGain, k\,(n) = \frac{R^{-1}\,(n-1)\,f\,(n)}{\lambda + f^{T}\,(n)\,R^{-1}\,(n-1)\,f\,(n)}$$

$$R\,(n) = \sum_{i=0}^{n} \lambda^{n-i} f\,(i)\,f^{T}\,(i)$$

$$e(n) = d(n) - y(n) \tag{2}$$

RLS Rowell (2008) adaptive filtering can be used to suppress the transmitter leakage. Since the transmitter signal is known, the RLS adaptive filter algorithm rapidly converges in estimating the filter coefficients.

5. RESULTS AND ANALYSIS

The measurements were collected using two USRPs (N210), one with original WBX and other with coupling capacitor C1 removed as shown in the Figure 7. A 10 dB attenuator was connected to the RX2 port to prohibit any reception of transmitter power. Addition of attenuators to the RX2 port did not affected the received power and hence 10 dB attenuator was connected for the experiment. The TX/RX port was connected to an antenna such that the reflection power is nominal. GNU Radio GNU (2018) application was used to perform

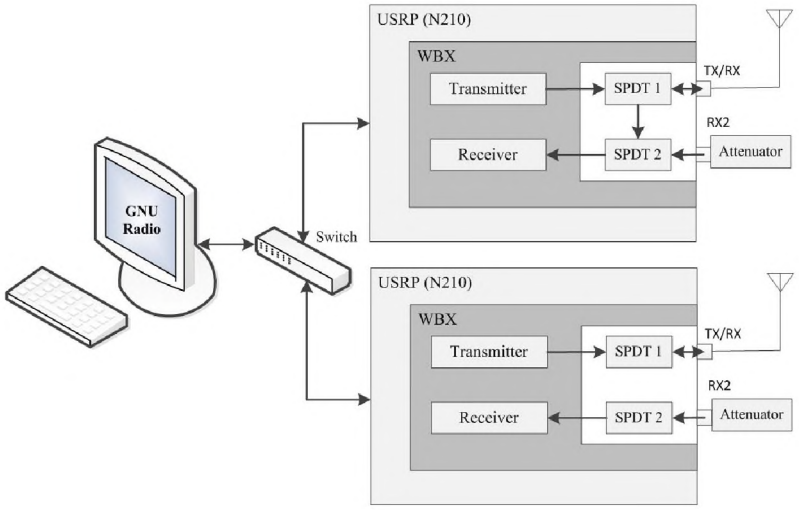

Figure 7. Block diagram of the experiment setup.

the analysis which connects to the radio via UHD drivers. The project was set up to monitor the power level of received signal without connecting an antenna to the RX2 port such that

there is no received signal. Both the radios are fed with the same signal for transmission. The received signal from the radios have been captured and analysed for frequencies ranging from 50 MHz to 2.2 GHz.

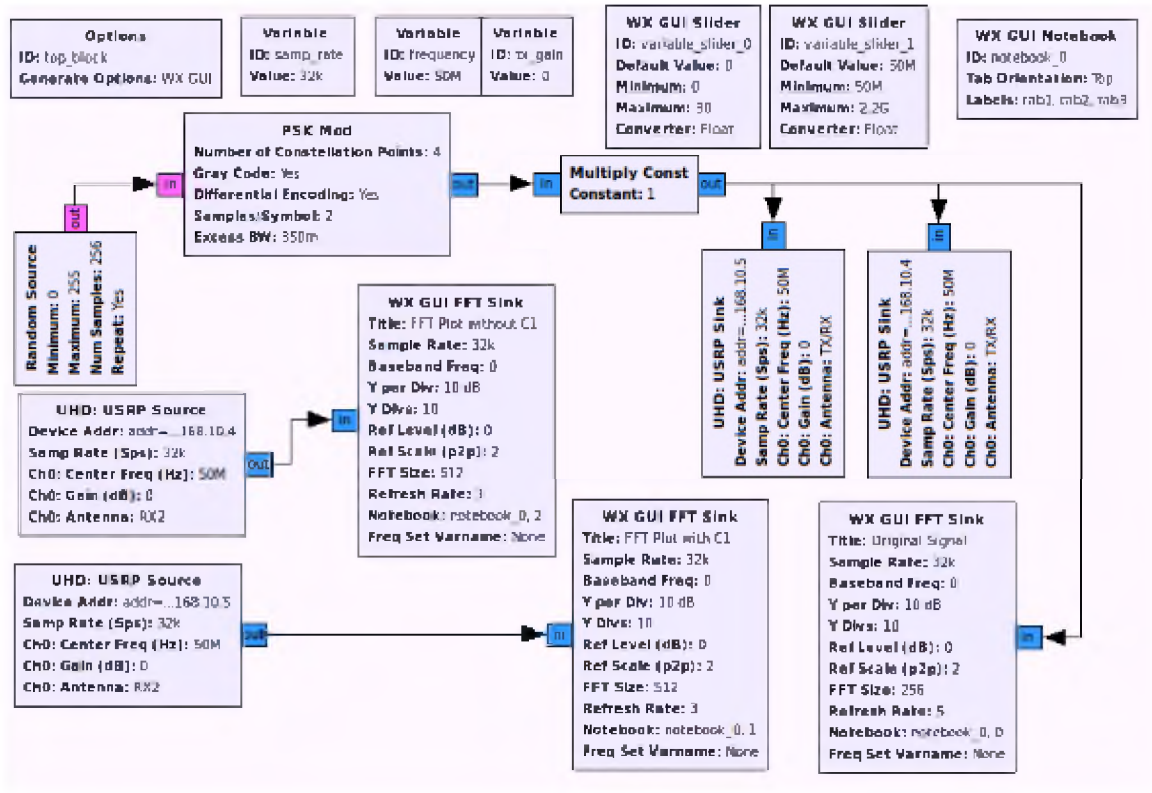

Figure 8. GNURadio project for the analysis of transmitter leakage.

Figure 8 shows the GNURadio project which was developed to record the transmitter power leakage to the receiver path for different transmitter gain with the receiver gain being zero.

Figure 9 shows the power of the generated signal fed to the USRPs for transmission. The parameter which control the transmitter gain provides 1 dB for every increment by one.

The maximum power output by the transmitter can be achieved by the lower frequencies and drops when proceeding with higher frequencies.

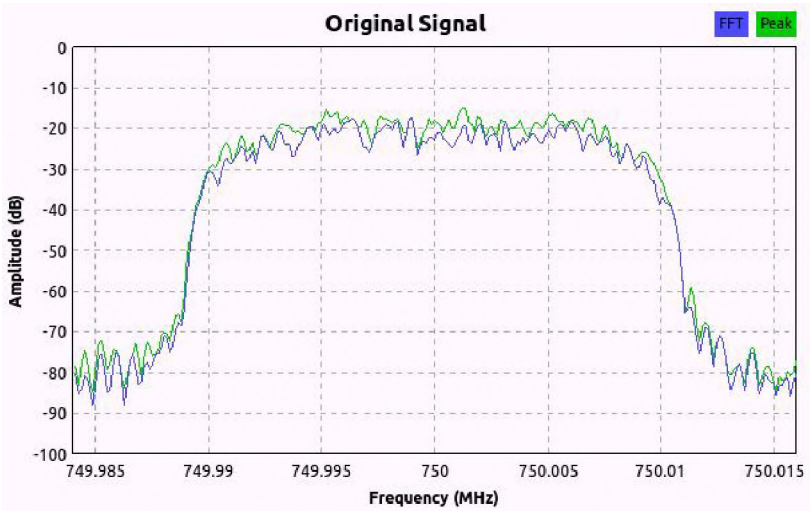

Figure 9. FFT plot of signal fed to the transmitter (f = 750 MHz).

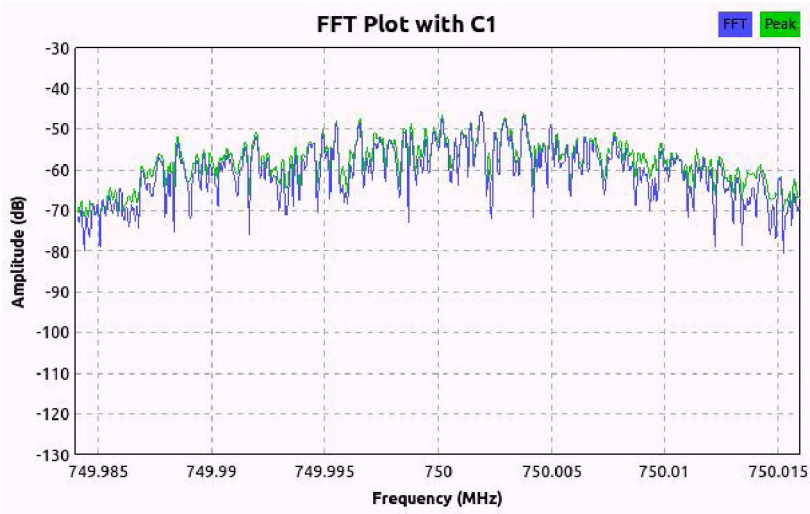

Figure 10. FFT plot of received power with connection between TX/RX and RX2 (f = 750 MHz, TX gain = 30).

As shown in Figure 9, the generated signal strength is equal to -20 dBm. Hence, the transmitter gains 0, 10, 20 and 30 corresponds to transmit output power equal to -20 dBm, -10 dBm, 0 dBm and +10 dBm respectively.

Figures 10 and 11 are the received power of the receivers when operated with maximum transmitter gain, 30 dB. Receiver gain set to 0 dB in GNU Radio project and the

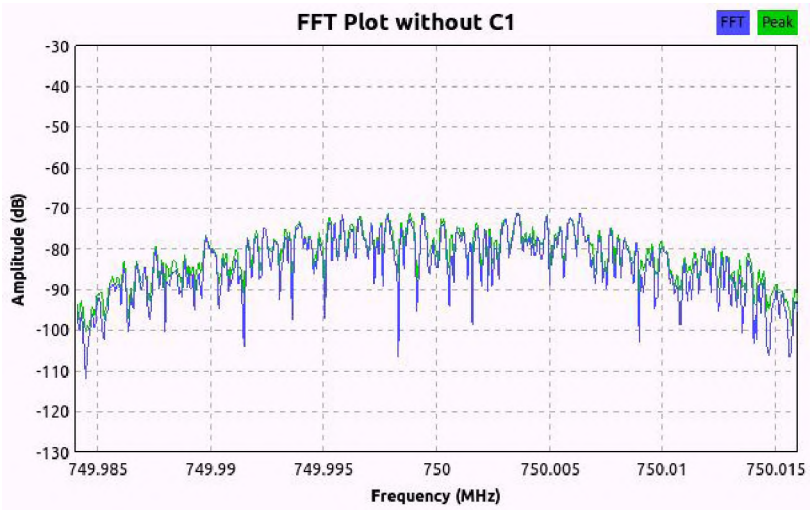

Figure 11. FFT plot of received power without connection between TX/RX and RX2 (f = 750 MHz, TX gain = 30).

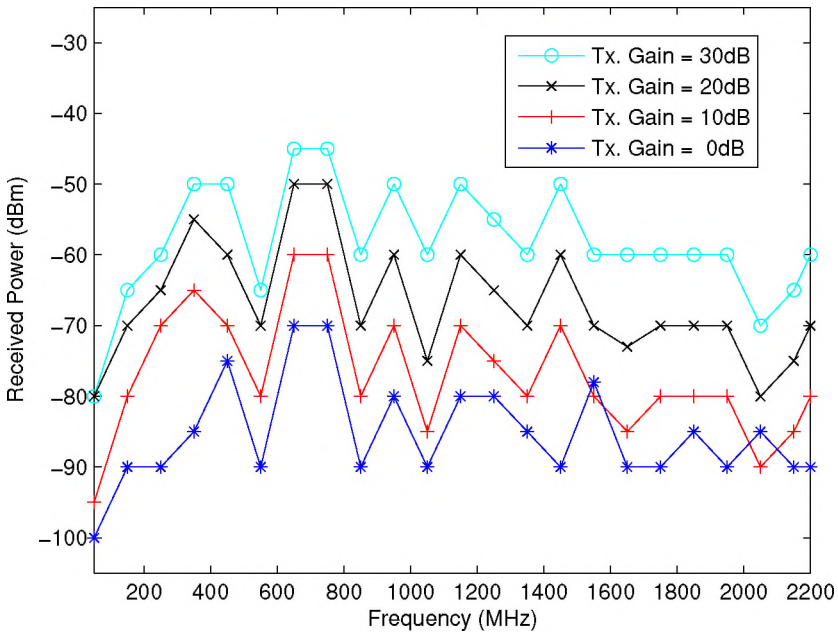

Figure 12. Received power for different TX gain with the connection between TX/RX and RX2 path.

Figure 10 and 11 show the reduction in leakage power when the transmitter and receiver path between the SPDT switches was open.

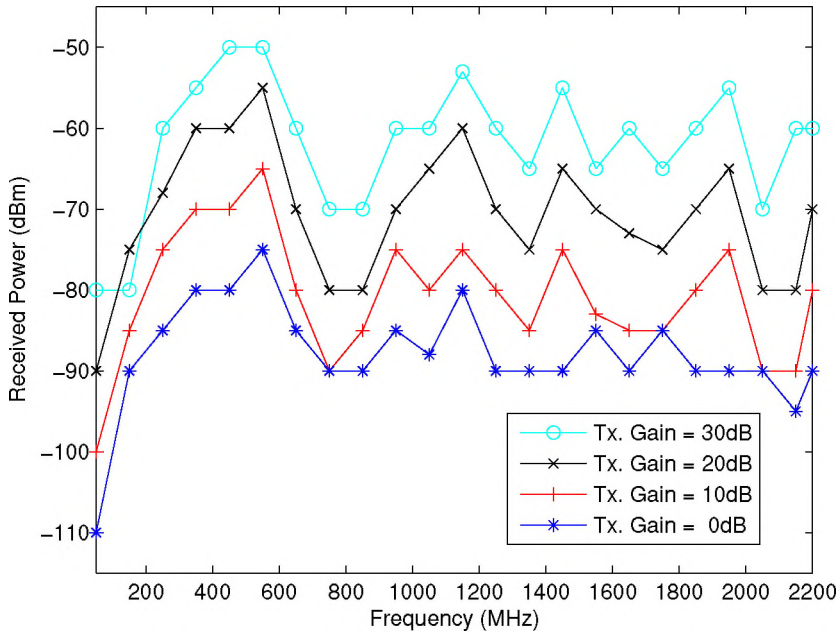

Figure 13. Received power for different TX gain without the connection between TX/RX and RX2 path.

Figures 12 and 13 show the received signal power for different transmitter gain across the frequencies ranging from 50 MHz to 2.2 GHz.

Comparing the received power from Figures 12 and 13, the difference was calculated and plotted for different transmitter gains as shown in Figure 14. It was observed that the best range of frequencies with maximum isolation between the transmitter and receiver was achieved in the range from 650 MHz to 950 MHz (UHF band). For frequencies between 550 MHz and 1.05 GHz the performance got degraded where the isolation was reduced. There was no improvement for other frequencies. The transmitted and received signals from the radio are saved into files and performed adaptive filtering using MATLAB RLS (2013). The RLS algorithm was employed to perform adaptive filtering to remove the transmitted signal leaked to the receiver block.

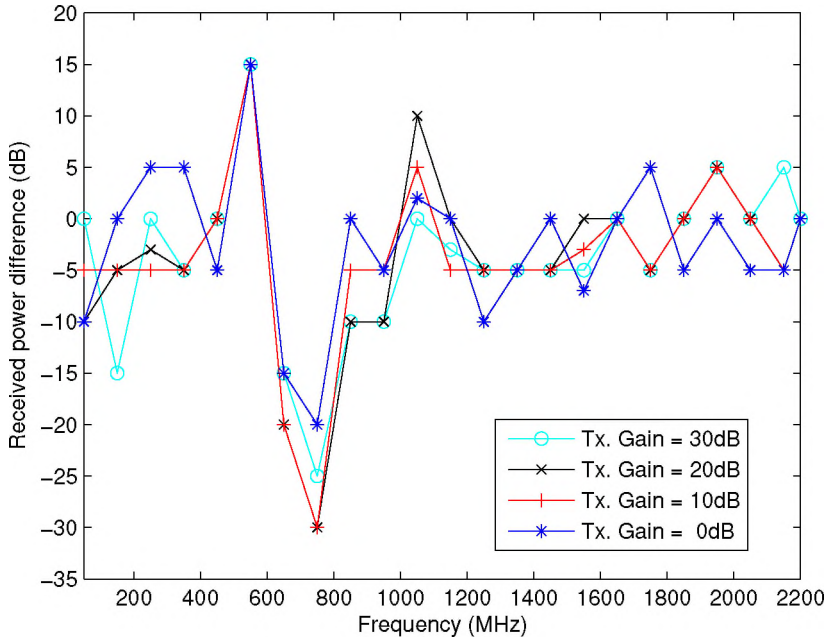

Figure 14. Power difference observed for different TX gains with and without the coupling capacitor.

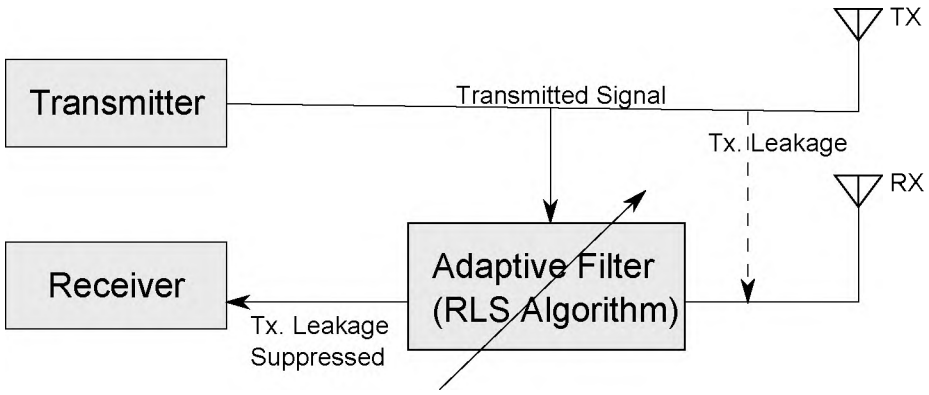

Figure 15. Block diagram of adaptive filter using RLS algorithm.

The transmitted signal was fed to the RLS algorithm to estimate the filter coefficients which was later applied to the received signal. Figure 15 shows the block diagram on the deployment of adaptive filter between the transmitter and receiver.

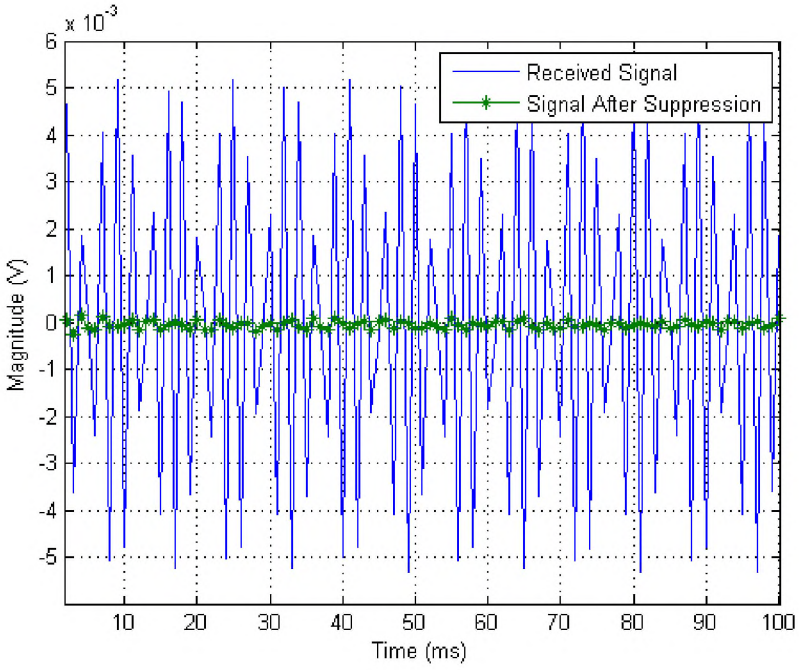

Figure 16. Received signal and the signal after suppression at the receiver.

Figure16 shows the transmitter leakage observed at the receiver and the output of the adaptive filter using RLS algorithm. Figure 17 shows the difference in the recieved power using adaptive filtering using the radios with and without coupling capacitor. As observed from Figure 14 the maximum isolation was achieved in range between 650 MHz to 950 MHz.

Figure 18 shows the received power difference for different transmitter gains between the received powers from radio with and without adaptive filtering using RLS algorithm, in addition to the removal of the coupling capacitor.

Figure 19 shows the received power difference for different transmitter gains between the received powers from radio with and without adaptive filtering using RLS algorithm, with the coupling capacitor intact on WBX. It is observed that from Figures 19 and 18 the adaptive filtering was effective in the suppression of the transmitter leakage irrespective of the hardware fix.

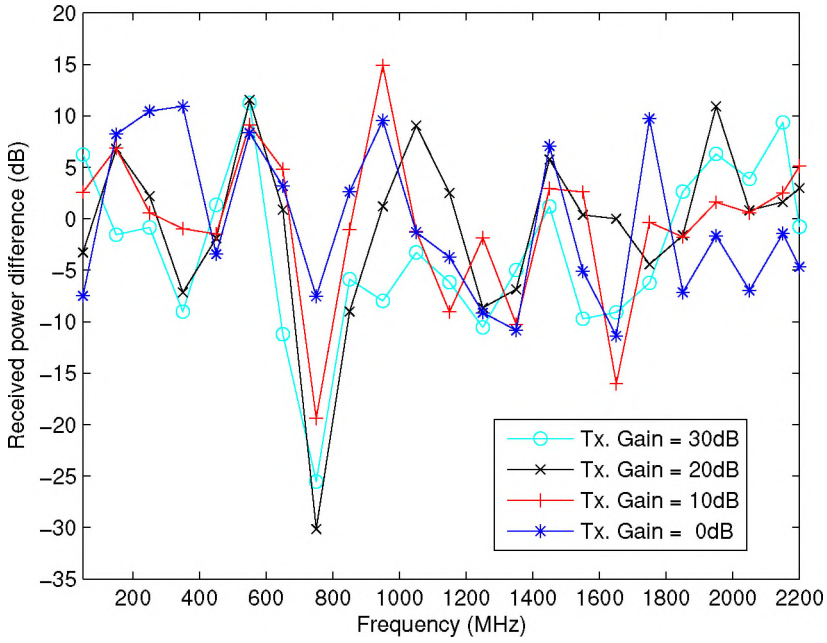

Figure 17. Power difference observed for different TX gains with and without coupling capacitor, and with adaptive filtering.

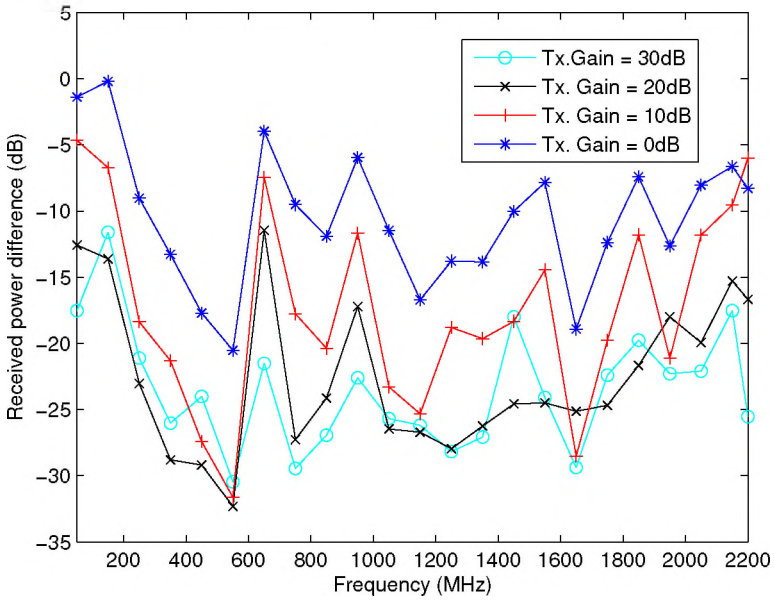

Figure 18. Power difference observed for different TX gains with and without adaptive filtering, and coupling capacitor removed.

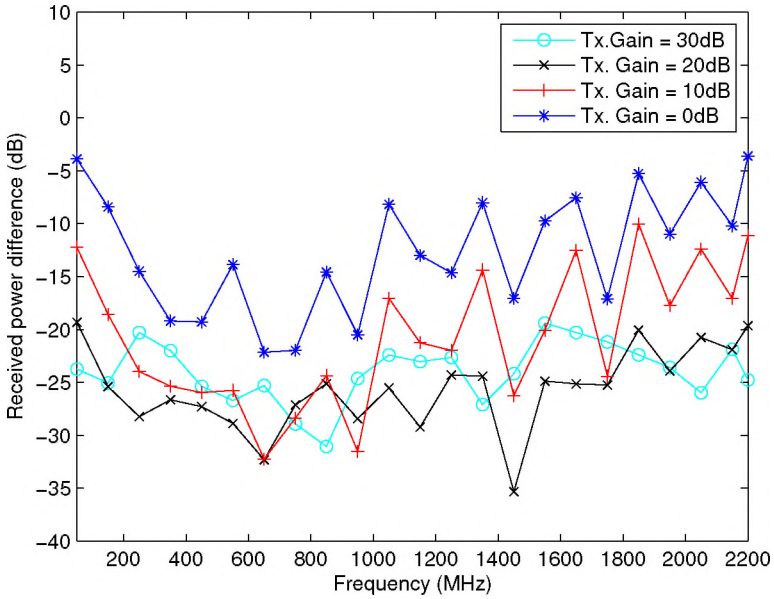

Figure 19. Power difference observed for different TX gains with and without adaptive filtering, and coupling capacitor intact.

6. CONCLUSION

Hardware solution of physically removing the coupling capacitor, C1 isolating transmitter and receiver has mixed outcome. The removal of the coupling capacitor selectively improved the isolation between the transmitter and the receiver for the frequency ranging from 650 MHz to 950 MHz. Maximum isolation of -30dB was achieved in the mentioned frequency range. The performance was degraded for lower frequencies between 50 and 500 MHz, where there was 15 dB decrease in isolation. There was no improvement across frequencies from 950 MHz to 2.2 GHz.

The inclusion of adaptive filter at the reception improved the performance by suppressing the transmitter leakage signal irrespective of the hardware fix. But, this suppression technique holds good until the leakage from the transmitter does not saturated the LNA in the initial stage of the receiver. Saturation of initial blocks of the receiver can be avoided by deploying SPDT switch which offers higher isolation more than -50 dB between its throw

ports. Thus enhancing the performance of the digital cancellation using adaptive filtering. The adaptive filtering using RLS algorithm achieved maximum isolation of -35 dB between the transmitter and receiver blocks of WBX radio used in USRP N210.

REFERENCES

'Stanford Information Networks Group Full-Duplex Wireless Design,' http://sing.stanford.edu/fullduplex, 2010.

'USRP inserts a peak in the carrier frequency,' https://www.ruby-forum.com/topic/4019305, 2012.

'WBX daughter card schematics,' https://files.ettus.com/schematics/wbx/WBX.pdf, 2012.

'Adaptive Noise Cancellation Using RLS Adaptive Filtering,' http://www.mathworks.com/help/dsp/examples/adaptive-noise-cancellation-using-rls-adaptive-filtering.html, 2013.

'GNURadio,' https://wiki.gnuradio.org/index.php/Main_Page, 2018.

Abdelhalem, S., Gudem, P., and Larson, L., 'Hybrid Transformer-Based Tunable Differential Duplexer in a 90-nm CMOS Process,' Microwave Theory and Techniques, IEEE Transactions on, 2013, **61**, pp. 1316–1326, doi:10.1109/TMTT.2013.2243748.

Beasley, P. D. L., Stove, A. G., Reits, B. J., and As, B., 'Solving the problems of a single antenna frequency modulated CW radar,' in 'IEEE International Conference on Radar,' 1990 pp. 391–395.

Choi, J. I., Jain, M., Srinivasan, K., Levis, P., and Katti, S., 'Achieving Single Channel, Full Duplex Wireless Communication,' in 'Proceedings of the Sixteenth Annual International Conference on Mobile Computing and Networking,' MobiCom '10, ACM, New York, NY, USA, ISBN 978-1-4503-0181-7, 2010 pp. 1–12, doi:10.1145/1859995.1859997.

Duarte, M. and Sabharwal, A., 'Full-duplex wireless communications using off-the-shelf radios: Feasibility and first results,' in '2010 Conference Record of the Forty Fourth Asilomar Conference on Signals, Systems and Computers,' 2010 pp. 1558–1562.

Frotzscher, A. and Fettweis, G., 'Baseband analysis of TX leakage in WCDMA Zero-IF-receivers,' in '2008 3rd International Symposium on Communications, Control and Signal Processing,' 2008 pp. 129–134.

Frotzscher, A. and Fettweis, G., 'Digital compensation of transmitter leakage in FDD zero-IF receivers,' European Transactions on Telecommunications, 2012, **23**, pp. 105–120, doi:10.1002/ett.1514.

Jain, M., Choi, J. I., Kim, T., Bharadia, D., Seth, S., Srinivasan, K., Levis, P., Katti, S., and Sinha, P., 'Practical, real-time, full duplex wireless,' in 'Proceedings of the 17th annual international conference on Mobile computing and networking - MobiCom '11,' ACM Press, New York, New York, USA, ISBN 9781450304924, 2011 p. 301, doi:10.1145/2030613.2030647.

Jung, J., Roh, H., Kim, J., Kwak, H., Jeong, M. S., and Park, J., 'TX Leakage Cancellation via a Micro Controller and High TX-to-RX Isolations Covering an UHF RFID Frequency Band of 908–914 MHz,' IEEE Microwave and Wireless Components Letters, 2008, **18**(10), pp. 710–712.

Kiayani, A., Anttila, L., and Valkama, M., 'Modeling and dynamic cancellation of TX-RX leakage in FDD transceivers,' in '2013 IEEE 56th International Midwest Symposium on Circuits and Systems (MWSCAS),' 2013 pp. 1089–1094.

Kim, H., Woo, S., Jung, S., and Lee, K., 'A CMOS Transmitter Leakage Canceller for WCDMA Applications,' IEEE Transactions on Microwave Theory and Techniques, 2013, **61**(9), pp. 3373–3380.

Li, S. and Murch, R. D., 'Full-Duplex Wireless Communication Using Transmitter Output Based Echo Cancellation,' in '2011 IEEE Global Telecommunications Conference - GLOBECOM 2011,' 2011 pp. 1–5.

N210-RFswitch, 'HMC174MS8/174MS8E,' http://www.analog.com/media/en/technical-documentation/data-sheets/hmc174.pdf, 2012, rev. 04.0109.

Rowell, D., 'Introduction to Recursive-Least-Squares(RLS) Adaptive Filters,' 2008.

V. CHANNEL ESTIMATORS FOR FULL-DUPLEX COMMUNICATION USING ORTHOGONAL PILOT SEQUENCES

I. Arul Mathi Maran Chandran, II. Maciej Zawodniok

Department of Electrical & Computer Engineering

Missouri University of Science and Technology

Rolla, Missouri 65409

Email: ac62f@mst.edu, mjzx9c@mst.edu

III. Lei Wang

Computer Science Department

University of Wisconsin - La Crosse

La Crosse, Wisconsin, USA

Email: lwang@uwlax.edu

ABSTRACT

Full-duplex communication is desirable to maximize the spectral efficiency, despite the challenges it puts forth. The key challenge inhibiting the operation of radios in full-duplex mode is self-interference. In this paper, we propose a pilot-based channel estimation to estimate both self-interference and communication channels simultaneously at both ends of a full-duplex link using orthogonal sequences. The Cramer-Rao Lower Bound for estimators of both the channels were determined and compared with the half-duplex channel estimator. We performed simulations varying sequence length and channel taps and studied the performance of the estimators. We also studied the effect of synchronization between the sequences on the performance of the estimators. Thus, providing a solution to balance the trade-off between the accuracy of the channel estimation and the overhead added to the transmissions for full-duplex communication.

Keywords: Channel estimation, orthogonal m-sequences, full-duplex (FDX), half-duplex (HDX), self-interference (SI), Cramer-Rao Lower Bound (CRLB)

1. INTRODUCTION

Rapid evolution in telecommunication and increasing population penetration demands more bandwidth to support new users in addition to the existing users with reliable high-speed data services. Most existing technologies operate in half-duplex (HDX) mode by performing only transmission or reception at any instance of time, achieving only fifty percent of the spectral efficiency. The full-duplex (FDX) mode of operation where the transmission and reception are performed simultaneously which can potentially achieve double the spectral efficiency of the existing mode of operation. Thus, FDX mode proves to be a promising solution for future wireless systems. FDX also provide solutions faced by the existing HDX operations such as a hidden terminal, throughput bottlenecks due to congestion, large end-to-end delays Choi *et al.* (2010). There are existing applications that deploy FDX operations, especially in relay systems. The use of FDX in relay systems increases the coverage and throughput. FDX is been considered a potential solution in the next-generation telecommunication technologies such as 5G Xiang *et al.* (2016), Non-orthogonal multiple access (NOMA) Chu and Zepernick (2018); Ding *et al.* (2018); Makled *et al.* (2019); Mohammadi *et al.* (2019); Zheng *et al.* (2018).

The major challenge of FDX operation is rooted in its operation. Since transmission and reception occur simultaneously, the transmitted signal interferes with its own receiver's operation. This is called self-interference (SI) which affects the throughput and potentially degrading the communication. In addition to the reflection of the transmitted signal, SI also occurs across the transmitter and receiver chain within the radio. To harness the benefits of FDX, suppression/cancellation of SI is necessary. Since the SI signal strength is high compared to the weak desired signal, multiple stages of SI cancellation both in analog and digital has been proposed in the literature. Though full-duplex is considered a potential

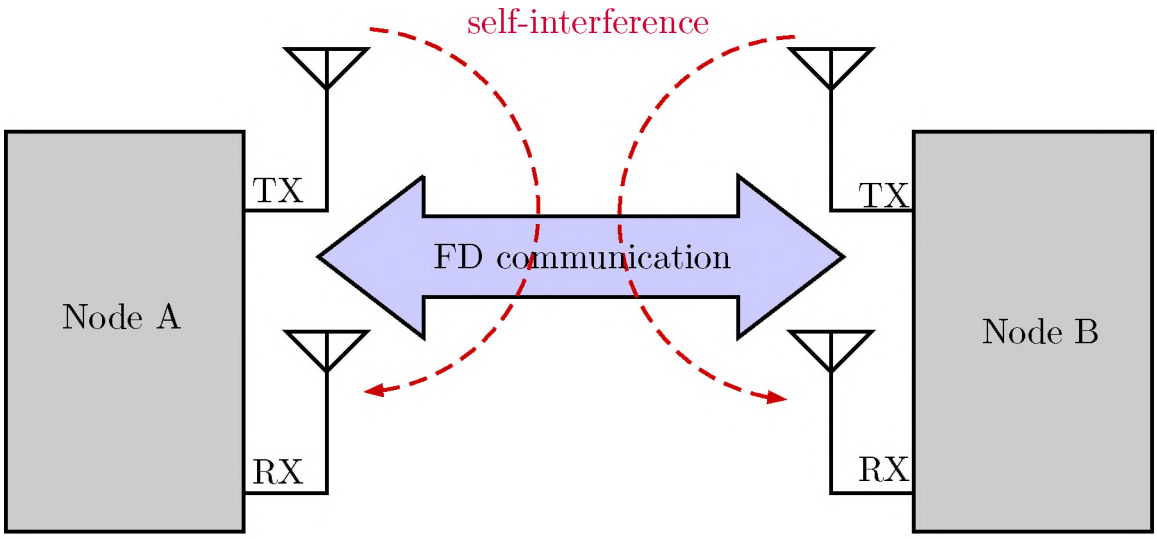

Figure 1. Block diagram of full-duplex operation.

methodology in the next-generation systems, the lack of a feasible solution to estimate and mitigate self-interference lost its appeal to adopt in commercial mobile applications. Instead, the industry sought to move towards higher frequencies of operation to meet the demand. There is an increased interest to operate in a non-licensed band such as LTE-U, LTE-LAA. Unfortunately, operating in high-frequency bands such as millimeter operations also pose challenges such as shorter range, limited mobility, channel modeling Hemadeh *et al.* (2018).

The estimation of SI channel coefficients plays a vital role in the mitigation of self-interference. To achieve the best estimation possible, we should able to separate the SI and communication channel components at the reception. This separation can be achieved by orthogonality which already used in code-division multiple access (CDMA) and orthogonal frequency division multiplexing (OFDM) which operates in HDX mode. The signals orthogonal to each other do not interfere with each other and can be evaluated separately without the influence of the other. Generally, the channels are estimated using known pilot sequences, and the orthogonal sequences are proposed to be used as a pilot sequence to estimate SI and communication channel.

The contribution of this paper is as follows. We proposed the system model and defined the correlation properties of both autocorrelation and cross-correlation requirements for the sequences to be used as pilot sequences in the proposed method. We proposed to use a set of selected orthogonal m-sequences which are closely compliant with the expected correlation properties as orthogonal pilot sequences to achieve separation and estimation of SI and communication channels. We also determined the Cramer-Rao Bound of the estimators for full-duplex operations and compared them with the half-duplex operations.

The paper is organized as follows. Section 2 discuss the various existing works to achieve full-duplex operation. Section 3 describes briefly the system model proposed and the proposed method to use the orthogonal m-sequence as pilots to estimate both the SI and communication channels. We also briefly discussed the effect of synchronization offset in the performance of the estimators. The CRLB of the proposed method is formulated in Section 2.2. Finally, Section 4 discuss the simulation and results of the proposed methodology.

Notations. The matrices are denoted by upper-case letters and the vectors by lower-case letter with a macron. $(\cdot)^T$, $(\cdot)^H$, and $E(\cdot)$ denotes transpose, hermitian, expectation operations respectively. $\mathcal{CN}\left(\mu, \sigma^2\right)$ denotes complex Gaussian distribution with mean μ and variance σ^2.

2. RELATED WORKS

In this section, we discuss the related works from the literature on the solutions to suppress and mitigate self-interference during FDX operation. The proposed work improves on the existing works by optimizing the accuracy of the channel estimation while minimizing the overhead.

The majority of the works in the literature consider relay systems L. Weizheng (2017); Senol *et al.* (2018) for FDX operations. In the relay systems, only the relaying nodes operate in FDX mode forwarding the received signal to the next communication link

and all other nodes operate in HDX mode. FDX operation finds its application in relay nodes since they are stationary and physically able to isolate transmitter and receiver. Therefore, the effects of self-interference are considered negligible. In more general scenarios, the effects of SI are significant in FDX operation and must be addressed. The target solution for an effective FDX operation is to estimate and mitigate the self-interference caused by the transmitter. A theoretical analysis was performed and showed that for a bidirectional communication system with multiple antennas, FDX can be more efficient than HDX even with channel estimation error Kim *et al.* (2013).

The critical step to mitigate the effects of SI channel from the received signal is to estimate the SI channel coefficients. Different estimators are proposed for FDX systems to estimate the SI channel and perform cancellation at different stages of data recovery. The suppression of self-interference is addressed at different stages of processing both in analog Beamforming *et al.* (2018); Bojja Venkatakrishnan *et al.* (2018); Keating *et al.* (2016); Khaledian *et al.* (2018); Korpi *et al.* (2014); Lee and Byung-Wook (2017); Liu *et al.* (2017), and digital domains Bharadia *et al.* (2013); Chandran and Zawodniok (2015); Duarte *et al.* (2012); Figwer *et al.* (2017); Korpi *et al.* (2017); Li *et al.* (2015); Luan *et al.* (2016); Masmoudi and Le-Ngoc (2016); Tian *et al.* (2016). An additional receiver chain was proposed Korpi *et al.* (2014) to obtain a reference signal for digital SI cancellation. The analog cancellation techniques do not remove 100% of the SI signal. However, analog cancellation techniques are necessary to reduce the SI signal strength down to an acceptable range of the transceiver to continue further cancellation in the digital domain. The proposed method in this paper is performed in the digital domain after the received signal strength is reduced to the operational level of the digital domain by analog cancellation using one of the solutions listed above.

The residual SI signal reaching the digital domain is significant enough to affect the performance of decoding the signal of interest. Hence, the residual SI cancellation must be performed in the digital domain to improve the performance of the FDX operation.

The characterization of the distribution of the SI before and after cancellation mechanisms and the effect of performing digital cancellation after analog cancellation is discussed in Duarte *et al.* (2012). A design prototype and implementation of full-duplex operation using WiFi radios were presented in a constrained indoor environment, presenting the throughput values closer to the expected theoretical doubling of spectral efficiency in Bharadia *et al.* (2013); Choi *et al.* (2010).

There are different methods proposed in the literature to estimate the self-interference. The use of an auxiliary receiver is one of the common approaches towards the estimation of the SI channel. A Kalman filter is used to estimate the SI channel from a copy of the transmitted signal via an auxiliary receiver in Shammaa *et al.* (2019). The joint estimation of the SI channel and communication channel using the ML criterion was presented in Masmoudi and Le-Ngoc (2016). The estimation exploits the known transmitted signal from the auxiliary receiver and second-order statistics of the unknown signal for the identification of respective channels. These techniques focus on the SI cancellation but lack the effect of SI cancellation on the signal-of-interest and the dynamicity of the channels. Recently, there is a proposed work in the literature to separate pilots from different nodes by placing the pilots in non-overlapping time slots Hua and Chang (2019).

The solution we propose improves the channel estimation for both SI and communication channels by employing known orthogonal sequences as pilots which can be transmitted simultaneously. These sequences remove the uncertainty to distinguish pilots from the received signal using the orthogonality property. The orthogonality property of these sequences is already being used in various applications such as MIMO Wang *et al.* (2017); Wu *et al.* (2018); Xing *et al.* (2010) for channel estimation, to reduce pilot contamination in cellular cells Wang *et al.* (2017); Wu *et al.* (2018), in detection algorithms to provide robustness against eavesdroppers Hou *et al.* (2016), scramble and accommodate multiple users transmission simultaneously.

3. FULL-DUPLEX OPERATION

In this section, we discuss the proposed method to operate an OFDM system in full-duplex mode and discussed the desired correlation properties of the sequences for the proposed method. In the following discussions, we considered two nodes A and B communicating in full-duplex mode. The discussion of the proposed method considers the reception at node A, which is also applicable to node B.

3.1. PROPOSED METHOD

The block diagram of the OFDM operating in FDX mode considered for the proposed method is shown in Figure 2. Both the nodes A and B operate in FDX mode and at the reception of node A signals from both node A and node B are received. The channel effect on these signals is independent. The proposed method is performed in the digital domain after analog cancellation which reduces the received signal to operational range of the digital domain.

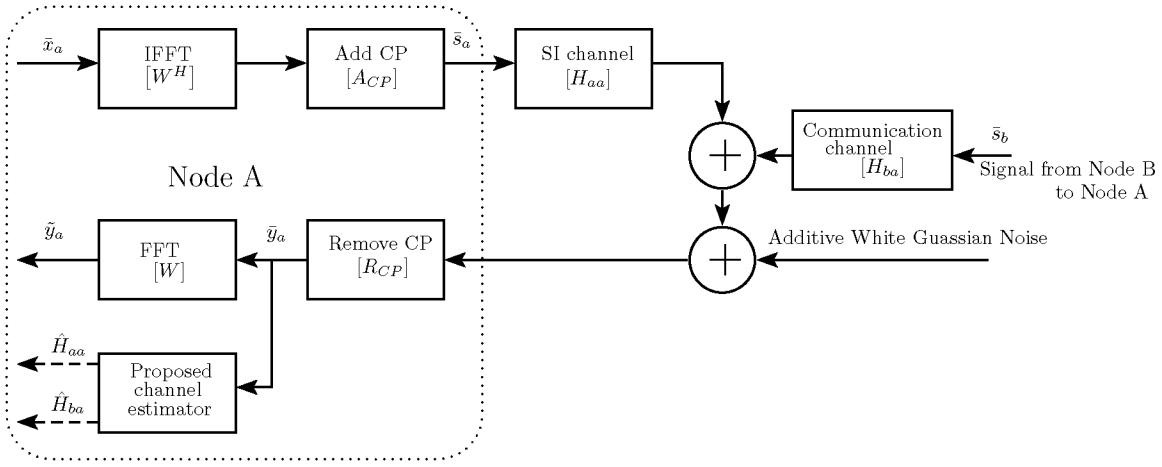

Figure 2. Block diagram of OFDM system with the proposed method for full-duplex operation.

The analog cancellations techniques in the literature as listed in earlier section shows potential suppression to perform digital cancellation to remove the residual self-interference and shown it is efficitive by performing digital cancellation after analog cancellation Duarte *et al.* (2012).

Considering an OFDM system with L equispaced subcarrier and cyclic prefix of length L_{CP} forming an OFDM block of length, N. The symbol sequence contains both the data and pilot symbols. In general, the receivers may use the pilot symbols for synchronization in time and frequency, offset correction, estimate the channel, etc. The OFDM block transmitted in the k^{th} block is given by

$$s\left[k\right] = A_{CP}W^{H}x\left[k\right], \tag{1}$$

where, $x\left[k\right]$ is the symbols of length L to be transmitted containing the data and pilot symbols. A_{CP} is the $N \times L$ matrix which insert the cyclic prefix of length L_{CP} and W is the $L \times L$ unitary discrete Fourier transform (DFT) matrix whose elements are given by $W_{mn} = (1/L)\, exp\left(-j2\pi mn/L\right)$, $0 \geq (m,n) \leq L-1$.

Then, the received symbols at the reception of node A is given by

$$\bar{r}_{a}\left[k\right] = H_{aa}\left[k\right]\bar{s}_{a}\left[k\right] + H_{ba}\left[k\right]\bar{s}_{b}\left[k\right] + \bar{\eta}\left[k\right], \tag{2}$$

where, s_a and s_b are the symbol vectors transmitted by the nodes A and B respectively. H_{aa} and H_{ba} are the SI and communication channels at the receiver of node A. After removing the cyclic prefix for pilot slot,

$$\begin{aligned}
\bar{y}_{a} &= R_{CP}\left(\bar{r}_{a}\right) \\
&= R_{CP}H_{aa}A_{CP}W^{H}\left(W\bar{x}_{pa}\right) + R_{CP}H_{ba}A_{CP}W^{H}\left(W\bar{x}_{pb}\right) + \bar{\eta} \\
&= R_{CP}H_{aa}A_{CP}\left(W^{H}W\right)\bar{x}_{pa} + R_{CP}H_{ba}A_{CP}\left(W^{H}W\right)\bar{x}_{pb} + \bar{\eta}
\end{aligned}$$

$$\begin{aligned}\bar{y}_a &= H_{at}\bar{x}_{pa} + H_{bt}\bar{x}_{pb} + \bar{\eta} \\ &= X_{pa}\bar{h}_{at} + X_{pb}\bar{h}_{bt} + \bar{\eta}. \end{aligned} \tag{3}$$

To remove the SI channel component from (3), multiply X_{pb}^T on both sides of the equation as shown in (4), where 0_L is zero matrix and I_L is identity matrix of size L.

$$X_{pb}^T\bar{y}_a = X_{pb}^T X_{pa}\bar{h}_{at} + X_{pb}^T X_{pb}\bar{h}_{bt} + X_{pb}^T\bar{\eta} \tag{4}$$

$$= 0_L + I_L\bar{h}_{bt} + X_{pb}^T\bar{\eta} \qquad \left[\because X_{pb}^T X_{pa} = 0_L; X_{pb}^T X_{pb} = I_L\right] \tag{5}$$

$$= \bar{h}_{bt} + X_{pb}^T\bar{\eta}, \tag{6}$$

Similarly, the SI channel component can be extracted from (3), multiply X_{pa}^T on both sides of the equation as shown in (7)

$$X_{pa}^T\bar{y}_a = X_{pa}^T X_{pa}\bar{h}_{at} + X_{pa}^T X_{pb}\bar{h}_{bt} + X_{pa}^T\bar{\eta} \tag{7}$$

$$= I_L\bar{h}_{at} + 0_L + X_{pa}^T\bar{\eta} \qquad \left[\because X_{pa}^T X_{pb} = 0_L; X_{pa}^T X_{pa} = I_L\right] \tag{8}$$

$$= \bar{h}_{at} + X_{pa}^T\bar{\eta}. \tag{9}$$

From Equations (6) and (9), the maximum likelihood estimate of the communication and SI channel estimates can be written as

$$\tilde{h}_{bt} = X_{pb}^T\,\bar{y}_a, \tag{10}$$

$$\tilde{h}_{at} = X_{pa}^T\,\bar{y}_a. \tag{11}$$

3.2. SYNCHRONIZATION

In addition to self-interference, synchronization between the two channels is another key issue to be considered in full-duplex communication. The SI signal and the signal of

interest is not necessarily aligned at the reception. The offset between the SI signal and the signal of interest at the reception, depends on the propagation delay between the nodes and the reflections from the environment. The effect of propagation delay is propositional to the distance between the nodes. For short range communication, this effect is minimum to negligible well below the tolerance of the system. For example, OFDM suffers from inter-Carrier-interference when timing variance of the channel during one OFDM symbol interval affects the orthogonality and results in power leakage among the subcarriers.

In the proposed method, this offset can be measured from the correlation peaks of the orthogonal sequences. The correlation yields two peaks aligned to respective orthogonal sequences of the nodes. This offset can be tracked and used to compensate at the mitigation of the channel effects at the equalization for both SI and communication channel. The tolerance depends on the correlation property once it overlaps with data signal in the other channel. The scope of this paper does not include the synchronization and all results discussed are with synchronized SI signal and signal of interest at the reception.

3.3. SELECTION OF PSEUDORANDOM SEQUENCES

The desired correlation properties of the orthogonal sequence are (a) the autocorrelation of the sequence should have its peak only with its zero shifted version and zero for all other linear shifts, (b) the cross-correlation of the sequence with any other sequence should be zero as shown in Equation (12) and Equation (13).

$$r_{xx}(\tau) = \begin{cases} 2^N, & \text{if } \tau = 0, \\ 0, & \text{if } \tau \neq 0 \end{cases}, \tag{12}$$

$$r_{xy}(\tau) = 0, \forall \tau. \tag{13}$$

The orthogonal sequence with the correlation properties as mention in Equation (12) and Equation (13) is not available in the literature. The cross-correlation of the orthogonal sequences are by definition is zero, but their autocorrelation varies with one or more peaks with non-zero values for different shifts. These variations in the autocorrelation of the sequences introduce error to the estimation. The sequences with the correlation properties closed to the requirements are orthogonal m-sequence. The Gold and Kasami sequences are not suitable candidates because their autocorrelation is not two-valued and not as good as that of m-sequences. The orthogonal Walsh sequence does not match the requirement since the autocorrelation swings between positive peak (+1) and negative peak (-1) across even and odd shifts respectively.

The autocorrelation of the m-sequence of length N is given by

$$r_{xx}(j) = \begin{cases} N, & \text{if } j = 0, \\ -1, & \text{if } 1 \leq j \geq N-1 \end{cases} \tag{14}$$

and the cross-correlation in general may have large peaks which can be exhibited as three-valued cross-correlation with values $\{-1, -t\,(n)\,, t\,(n) - 2\}$, where

$$t\,(n) = \begin{cases} 2^{\frac{(n+1)}{2}} + 1, & \text{if n is odd} \\ 2^{\frac{(n+2)}{2}} + 1, & \text{if n is even} \end{cases} \tag{15}$$

The preferred orthogonal m-sequences are the ones with the closest correlation properties for the proposed method to separate and estimation individual channel coefficients.

The m-sequence defined in Buračas and Boynton (2002) whose properties are closer to the desired properties is chosen for the proposed method. The orthogonal m-sequence is derived from the m-sequence whose length is $2^M - 1$, where M is a positive integer. The length of the orthogonal m-sequence is 2^M and the sequences are binary sequences $\in [-1, +1]$.

4. CRLB FOR THE PROPOSED METHOD

In this section, we derive the Cramer-Rao Lower Bound (CRLB) of the channel estimators both SI and communication channels for the proposed method. For the defined system model,

$$\bar{y_a} = X_{pa}\bar{h}_{at} + X_{pb}\bar{h}_{bt} + \bar{\eta}, \tag{16}$$

where, $\bar{h}_{at}$ and $\bar{h}_{bt}$ are channel coefficient of the SI and the communication channel. These two parameters are the parameters of interest to be estimated which is indicated by $\bar{\theta} = \left[\bar{h}_{at}\ \bar{h}_{bt}\right]^T$.

The probability density function of the received slot with N symbols is given by

$$P\left(\bar{y_a}, \bar{\theta}\right) = \frac{1}{\left(2\pi\sigma^2\right)^{\frac{N}{2}}}.exp\left[\frac{-1}{2\sigma^2}\left\|\bar{y}_a - X_{pa}\bar{h}_{at} + X_{pb}\bar{h}_{bt}\right\|^2\right]. \tag{17}$$

To determine the CRLB of the estimator, the Fisher information matrix $\mathbf{I}\bar{\theta}$ has to be evaluated which is given by

$$\mathbf{I}\bar{\theta} = \begin{bmatrix} -E\left[\dfrac{\partial^2 \ln P\left(\bar{y_a}, \bar{\theta}\right)}{\partial h_{at}^2}\right] & -E\left[\dfrac{\partial^2 \ln P\left(\bar{y_a}, \bar{\theta}\right)}{\partial h_{at}\partial h_{bt}}\right] \\ -E\left[\dfrac{\partial^2 \ln P\left(\bar{y_a}, \bar{\theta}\right)}{\partial h_{bt}\partial h_{at}}\right] & -E\left[\dfrac{\partial^2 \ln P\left(\bar{y_a}, \bar{\theta}\right)}{\partial h_{bt}^2}\right] \end{bmatrix}. \tag{18}$$

Recall that for the estimation of vector parameter, $\bar{\theta} = [\theta_1\ \theta_2\ \ldots\ \theta_n]^T$. If $\hat{\theta}_i$ is an unbiased estimator, then the CRLB of $\hat{\theta}_i$ is ii^{th} element of the inverse of the Fisher information matrix Kay (1993), $\mathbf{I}\left(\bar{\theta}\right)$

$$var\left(\hat{\theta}_i\right) \geq \left[\mathbf{I}^{-1}\bar{\theta}\right]_{ii}. \tag{19}$$

Now, we evaluate the individual element of the Fisher information matrix. The logarithm

of the probability density function of the reception is

$$\ln P\left(\bar{y_a},\bar{\theta}\right) = \frac{-N}{2}\ln\left(2\pi\sigma^2 I\right) + \frac{-1}{2\sigma^2 I}\left\|\bar{y}_a - X_{pa}\bar{h}_{at} + X_{pb}\bar{h}_{bt}\right\|^2, \tag{20}$$

and expanding the contents within the norm square yields

$$\bar{y_a}^H\bar{y_a} - 2\bar{h}_{at}^H X_a^H\bar{y_a} - 2\bar{h}_{bt}^H X_b^H\bar{y_a} + 2\bar{h}_{at}^H X_a^H X_b\bar{h}_{bt} + \bar{h}_{at}^H X_a^H X_a\bar{h}_{at} + \bar{h}_{bt}^H X_b^H X_b\bar{h}_{bt}. \tag{21}$$

Then, the partial derivatives of Equation (20) using Equation (21) to build the Fisher information matrix are given by

$$\begin{aligned}
\frac{\partial \ln P\left(\bar{y_a},\bar{\theta}\right)}{\partial\bar{h}_{at}} &= \frac{-1}{\sigma^2 I}\left[-2X_a^H\bar{y_a} + 2X_a^H X_b\bar{h}_{bt} + X_a^H X_a\bar{h}_{at}\right],\\
\frac{\partial \ln P\left(\bar{y_a},\bar{\theta}\right)}{\partial\bar{h}_{bt}} &= \frac{-1}{\sigma^2 I}\left[-2X_b^H\bar{y_a} + 2X_b^H X_b\bar{h}_{bt} + X_b^H X_b\bar{h}_{bt}\right],\\
\frac{\partial^2 \ln P\left(\bar{y_a},\bar{\theta}\right)}{\partial\bar{h}_{at}^2} &= \frac{-1}{\sigma^2 I}\left[X_a^H X_a\right], &(22)\\
\frac{\partial^2 \ln P\left(\bar{y_a},\bar{\theta}\right)}{\partial\bar{h}_{bt}^2} &= \frac{-1}{\sigma^2 I}\left[X_b^H X_b\right], &(23)\\
\frac{\partial^2 \ln P\left(\bar{y_a},\bar{\theta}\right)}{\partial\bar{h}_{bt}\partial\bar{h}_{at}} &= \frac{-1}{\sigma^2 I}\left[2X_a^H X_b\right], &(24)\\
\frac{\partial^2 \ln P\left(\bar{y_a},\bar{\theta}\right)}{\partial\bar{h}_{bt}\partial\bar{h}_{at}} &= \frac{-1}{\sigma^2 I}\left[2X_a^H X_b\right]. &(25)
\end{aligned}$$

Now using Equations (22), (24), (25), and (23) in Equation (2.6), then the Fisher information matrix can written as

$$\mathbf{I}\left(\bar{\theta}\right) = \frac{1}{\sigma^2 I}\begin{bmatrix} E\left[X_a^H X_a\right] & E\left[2X_b^H X_a\right] \\ E\left[2X_a^H X_b\right] & E\left[X_b^H X_b\right] \end{bmatrix}. \tag{26}$$

Inverting the Fisher information matrix from Equation (26) yields

$$\mathbf{I}\left(\bar{\theta}\right)^{-1} = \frac{\sigma^2 I}{D}\begin{bmatrix} E\left[X_b^H X_b\right] & -E\left[2X_b^H X_a\right] \\ -E\left[2X_a^H X_b\right] & E\left[X_a^H X_a\right] \end{bmatrix}. \tag{27}$$

where, D is the determinant of the Fisher information matrix given by

$$D = E\left[X_a^H X_a\right].E\left[X_b^H X_b\right] - E\left[2X_a^H X_b\right].E\left[2X_b^H X_a\right]. \tag{28}$$

The variance of the parameter also the CRLB of the $\bar{h}_{at}$ and $\bar{h}_{bt}$ are the diagonal elements of the inverse Fisher information matrix Equation (2.7) using Equation (27) are:

$$var\left(\bar{h}_{at}\right) \geq \frac{\sigma^2 I}{D} E\left[X_b^H X_b\right], \tag{29}$$

$$var\left(\bar{h}_{bt}\right) \geq \frac{\sigma^2 I}{D} E\left[X_a^H X_a\right]. \tag{30}$$

Furthermore (29) and (30) can be simplified for the orthogonal sequence whose cross-correlation is zero $\left[X_a^H X_b = X_b^H X_a = 0\right]$ and assuming perfect autocorrelation where $E\left[X_a^H X_a\right] = E\left[X_b^H X_b\right] = NI$, the variance of the estimators can be written as

$$var\left(\bar{h}_{at}\right) \geq \frac{\sigma^2 I}{E\left[X_a^H X_b\right]} \geq \frac{\sigma^2}{N}, \tag{31}$$

$$var\left(\bar{h}_{bt}\right) \geq \frac{\sigma^2 I}{E\left[X_b^H X_b\right]} \geq \frac{\sigma^2}{N}. \tag{32}$$

From (31) and (32), the bound depend on the autocorrelation of the orthogonal sequence. Lower the autocorrelation, the variance of the estimators' increases which yields lower performance in the estimation of the channel parameters. The results also matches the variance of the channel estimator in a half-duplex communication.

5. RESULTS

In this section, we discuss and analyze different simulation resuts for the proposed method.

The autocorrelation and cross-correlation of the orthogonal sequence are shown in Figure 3. The cross-correlation of the selected orthogonal m-sequence is zero with any other sequence. The autocorrelation is non-zero with most of its linear shifts. The maximum peak occurs only when correlated with itself without any linear shift. The non-zero autocorrelation of the orthogonal sequence will introduce error since it does not yield an identity matrix in (5) and (8). For a given number of channel taps and sequence length only certain linear shifts yield a better result than the other. As the number of channel taps increases there is fewer sequence are suitable for the FDX operation.

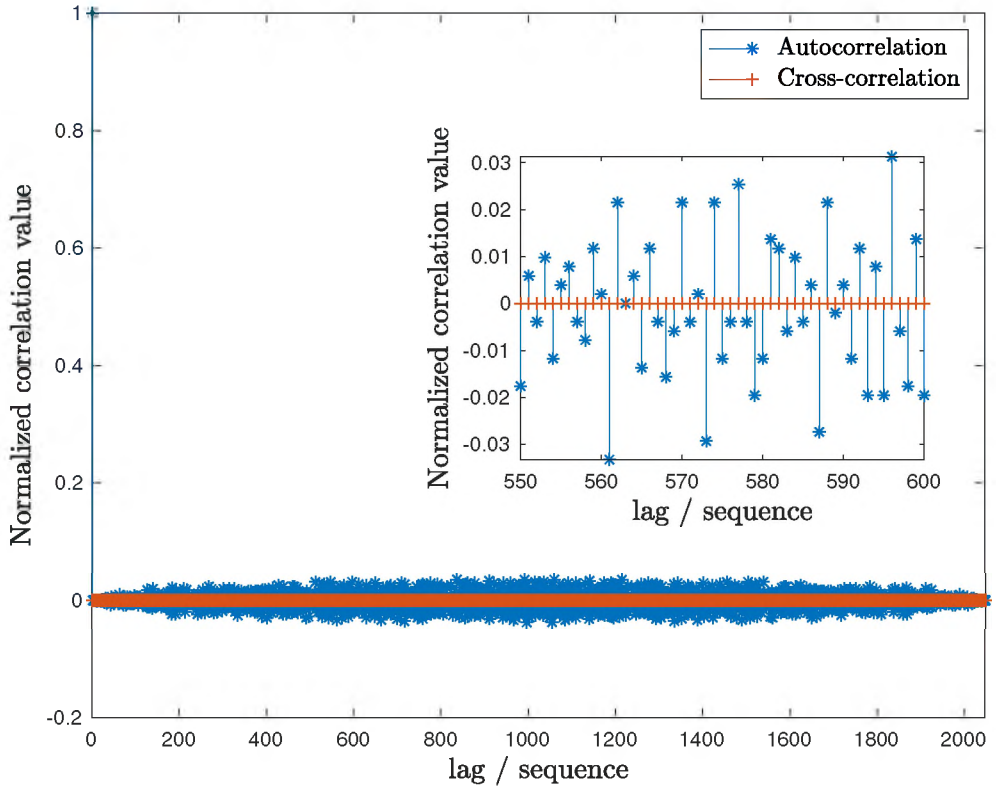

Figure 3. Autocorrelation and cross-correlation of the selected orthogonal m-sequence.

The simulation is built in MATLAB using the system model as shown in Figure 2. The channel coefficients are generated using improved Jake's model Xiao *et al.* (2006). Due to a lack of actual model representing the self-interference available in the literature, we used the channel model used for the communication channel with different parameters. Both the channels introduce frequency selective fading. The average error of the estimators of both the channels is evaluated from 50 000 frames in the simulation over different noise levels in the communication link. The performance of the channel estimators was evaluated for different scenarios listed in Table 1.

Table 1. Different scenarios evaluating the proposed method.

Scenarios
Different channel sequences
Different channel taps
Impact of synchronization

The channel estimation for the SI and communication channels are performed for different sequence length. Figure 4 shows the mean square error (MSE) of the channel estimate with five channel taps each for different sequence length. It can be observed the estimation error decreases with the increase in the sequence lengths since more information are available from usage of longer sequences. As the length of the pilot sequences increases, the performance of the estimation increases but saturates to the minimum error introduced by the sequence while performing the extraction and estimation.

The channel estimation for both SI and communication channels is performed for a different number of channel taps. Figure 5 shows the MSE of the channel estimate for a different number of channel taps. Figure 6 shows a close up look on the MSE plots for different channel taps for a given noise level (15 dB). There is a noticable increase in estimation error with the increase in channel taps resulting in more inter-symbol interference.

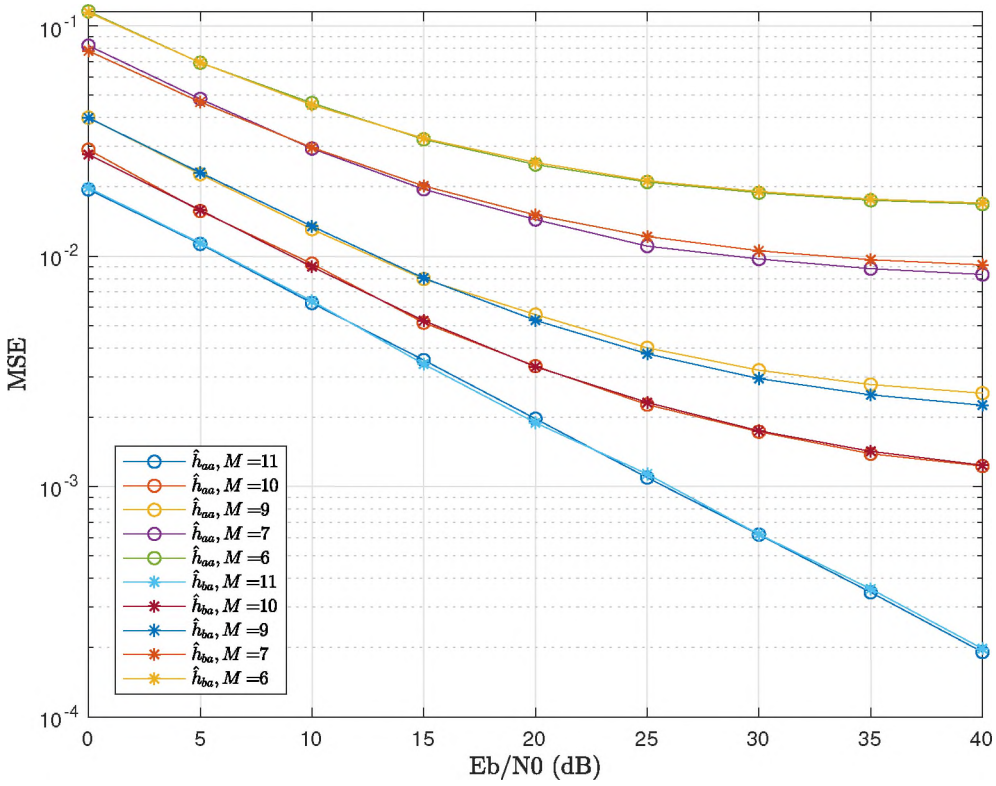

Figure 4. MSE of the channel estimates using different sequence length.

The use of OFDM in the proposed method allowed mitigation of frequency selective fading to a set of parallel flat fading across the sub-carriers. This mitigation is limited to slow fading and the revision to handle fast fading is planned in the future works.

In addition to the channel estimation error for different channel taps with sequence length is 2048 (M = 11), the CRLB of the estimators is also plotted. The MSE of the estimate can get closer to the CRLB plot shown in Figure 5, when the orthogonal sequence used can achieve the desired correlation property as discussed in Section 3.3. The autocorrelation of the selected orthogonal m-sequence used is not zero for all its shifts. This deviation in the autocorrelation for certain shifts introduces error in addition to the noise which moves the MSE plots away from the CRLB. In addition, to both the channel estimator's CRLB being the same, it is also the CRLB for the channel estimator operated in half-duplex. Though

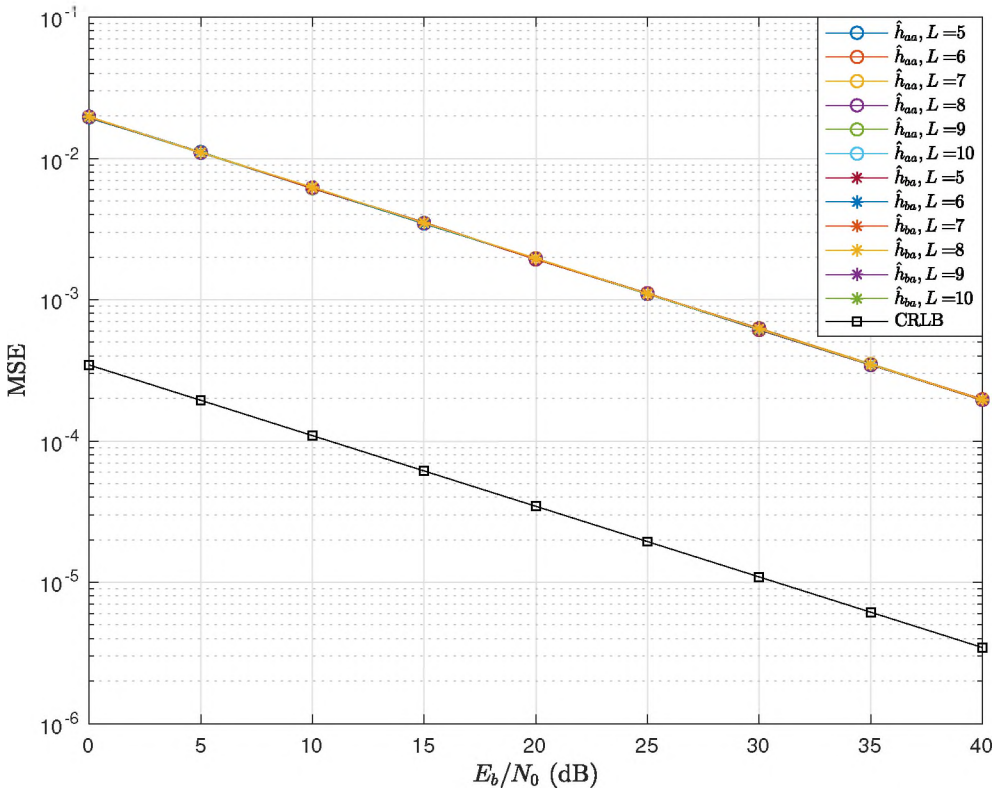

Figure 5. MSE of the channel estimation with CRLB for different channel taps and M = 11.

both the FDX and HDX communication have the same bound and HDX achieving better performance, FDX excels in the bandwidth efficiency. The channel estimators of the HDX performs better than the FDX due to the absence of the SI but the bandwidth utilization of FDX is doubled compared to HDX.

The comparison of channel performance between HDX operation with FDX for different sequence alignments is shown in Figure 7. The pilot-based channel estimator was used in HDX same as that used in FDX operation. The FDX plots comprise of sequences with offsets reducing the cross-correlation between the pilot sequences. The offsets are introduced only to the far-end signal which is the signal of interest to be decoded. The plot comprises of three sets of channel estimation with no offset and two different offsets and compared with the HDX operation. The channel estimation performance of HDX and FDX

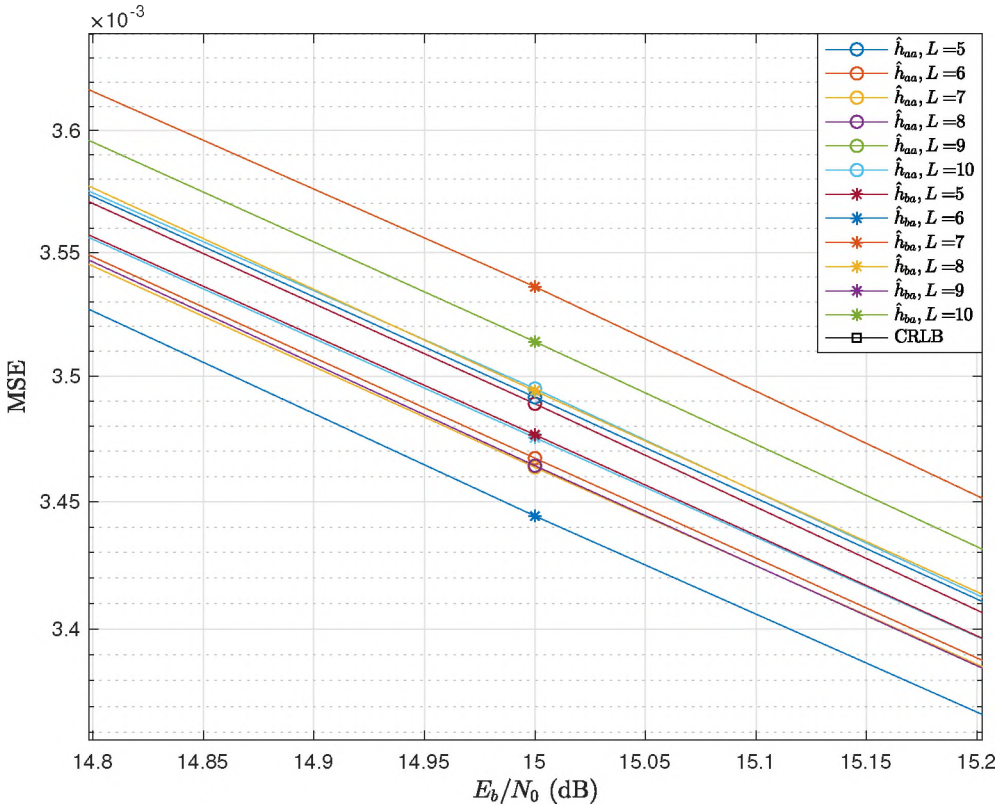

Figure 6. MSE of the channel estimation with CRLB for different channel taps and M = 11 (zoomed).

with no offset aligns with each other since channels in FDX are orthogonal resulting HDX performance. In contrast, when the offsets get introduced the channel estimation of FDX degrades due to the loss of orthogonality and the performance saturates quickly with to the errors introduced. The estimation of SI channel suffers more due to error introduced by the poor cross-correlation with sequence from the far-end node. This implies the maximum channel estimation performance can be obtained only by maintaining the alignment of the sequence and preserving orthogonality.

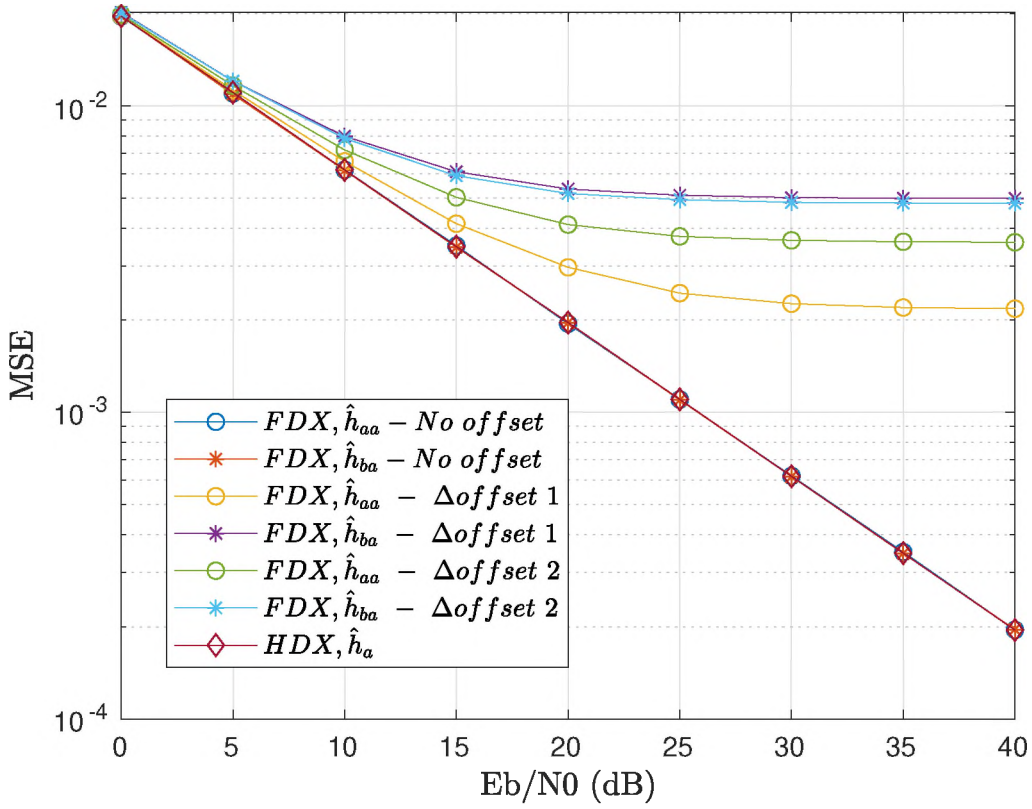

Figure 7. Comparison of channel estimation error between half-duplex and full-duplex with different sequence alignments.

6. CONCLUSION

We demonstrated the separation and estimation of both self-interference and communication channels in full-duplex communication using the proposed method. The performance of the channel estimators depends on the correlation properties preserving the orthogonality and synchronization between the seqeunces. The deviation in cross-correlation affects performance of both the channel estimators. The effect on the performance depends on the which sequences not synchronized at the reception. The results of the theoretical limits of both the full-duplex estimators equal to half-duplex estimators shows the potential doubling of the spectral efficiency. Since the sequences are assigned to individual users,

it can be reused in adjacent non-interfering cells. The proposed method can benefit the upcoming next-generation 5G and future generations of wireless communication where full-duplex operation considered to play a key role.

ACKNOWLEDGEMENTS

This work was supported in part by the Intelligent Systems Center (ISC), Missouri University of Science and Technology, Rolla, MO, USA.

REFERENCES

Beamforming, S.-i. C., Dastjerdi, M. B., Reiskarimian, N., Chen, T., Zussman, G., and Krishnaswamy, H., 'Full Duplex Circulator-Receiver Phased Array Employing,' 2018 IEEE Radio Frequency Integrated Circuits Symposium (RFIC), 2018, (i), pp. 108–111.

Bharadia, D., McMilin, E., and Katti, S., 'Full duplex radios,' ACM SIGCOMM Computer Communication Review, 2013, **43**(4), pp. 375–375–386–386, ISSN 0146-4833, doi:10.1145/2534169.2486033.

Bojja Venkatakrishnan, S., Alwan, E. A., and Volakis, J. L., 'Wideband rf self-interference cancellation circuit for phased array simultaneous transmit and receive systems,' IEEE Access, 2018, **6**, pp. 3425–3432, ISSN 2169-3536, doi:10.1109/ACCESS.2017.2788179.

Buračas, G. T. and Boynton, G. M., 'Efficient design of event-related fMRI experiments using m-sequences,' NeuroImage, 2002, **16**(3 I), pp. 801–813, ISSN 10538119, doi:10.1006/nimg.2002.1116.

Chandran, A. M. M. and Zawodniok, M., 'Transmitter leakage analysis when operating USRP (N210) in duplex mode,' in '2015 IEEE International Instrumentation and Measurement Technology Conference (I2MTC) Proceedings,' IEEE, ISBN 978-1-4799-6114-6, 2015 pp. 340–345, doi:10.1109/I2MTC.2015.7151291.

Choi, J. I., Jain, M., Srinivasan, K., Levis, P., and Katti, S., 'Achieving Single Channel, Full Duplex Wireless Communication,' in 'Proceedings of the Sixteenth Annual International Conference on Mobile Computing and Networking,' MobiCom '10, ACM, New York, NY, USA, ISBN 978-1-4503-0181-7, 2010 pp. 1–12, doi:10.1145/1859995.1859997.

Chu, T. M. C. and Zepernick, H. J., 'Performance of a Non-Orthogonal Multiple Access System with Full-Duplex Relaying,' IEEE Communications Letters, 2018, **22**(10), pp. 2084–2087, ISSN 15582558, doi:10.1109/LCOMM.2018.2852308.

Ding, Z., Fan, P., and Poor, H. V., 'On the coexistence between full-duplex and NOMA,' IEEE Wireless Communications Letters, 2018, **7**(5), pp. 692–695, ISSN 21622345, doi:10.1109/LWC.2018.2811492.

Duarte, M., Dick, C., and Sabharwal, A., 'Experiment-driven characterization of full-duplex wireless systems,' IEEE Transactions on Wireless Communications, 2012, **11**(12), pp. 4296–4307, ISSN 15361276, doi:10.1109/TWC.2012.102612.111278.

Figwer, J., Michalczyk, M., and Główka, T., 'Accelerating the rate of convergence for LMS-like on-line identification and adaptation algorithms. Part 1: Basic ideas,' 2017 22nd International Conference on Methods and Models in Automation and Robotics, MMAR 2017, 2017, **0**(1), pp. 347–350, doi:10.1109/MMAR.2017.8046851.

Hemadeh, I. A., Satyanarayana, K., El-Hajjar, M., and Hanzo, L., 'Millimeter-Wave Communications: Physical Channel Models, Design Considerations, Antenna Constructions, and Link-Budget,' IEEE Communications Surveys and Tutorials, 2018, **20**(2), pp. 870–913, ISSN 1553877X, doi:10.1109/COMST.2017.2783541.

Hou, X., Gao, C., Zhu, Y., and Yang, S., 'Detection of active attacks based on random orthogonal pilots,' 2016 8th International Conference on Wireless Communications and Signal Processing, WCSP 2016, 2016, doi:10.1109/WCSP.2016.7752543.

Hua, Y. K. and Chang, W., 'Time Shifted Pilots Scheme for Full-Duplex Massive MIMO Systems,' IEEE Transactions on Vehicular Technology, 2019, **68**(3), pp. 3022–3026, ISSN 00189545, doi:10.1109/TVT.2019.2893547.

Kay, S. M., 'Fundamentals of statistical signal processing,' Prentice Hall Signal Processing Series, 1993, ISSN 00401706, doi:10.2307/1269750.

Keating, R., Ratasuk, R., and Ghosh, A., 'Performance analysis of full duplex in cellular systems,' IEEE Vehicular Technology Conference, 2016, **2016-July**(5GArch), ISSN 15502252, doi:10.1109/VTCSpring.2016.7504406.

Khaledian, S., Farzami, F., Smida, B., and Erricolo, D., 'Inherent self-interference cancellation at 900 MHz for in-band full-duplex applications,' 2018 IEEE 19th Wireless and Microwave Technology Conference, WAMICON 2018, 2018, pp. 1–4, ISSN 00189480, doi:10.1109/WAMICON.2018.8363897.

Kim, D., Ju, H., Park, S., and Hong, D., 'Effects of channel estimation error on full-duplex two-way networks,' IEEE Transactions on Vehicular Technology, 2013, **62**(9), pp. 4666–4672, ISSN 00189545, doi:10.1109/TVT.2013.2265407.

Korpi, D., Aghababaeetafreshi, M., Piilila, M., Anttila, L., and Valkama, M., 'Advanced architectures for self-interference cancellation in full-duplex radios: Algorithms and measurements,' Conference Record - Asilomar Conference on Signals, Systems and Computers, 2017, (i), pp. 1553–1557, ISSN 10586393, doi:10.1109/ACSSC.2016.7869639.

Korpi, D., Anttila, L., and Valkama, M., 'Reference receiver based digital self-interference cancellation in MIMO full-duplex transceivers,' 2014 IEEE Globecom Workshops, GC Wkshps 2014, 2014, pp. 1001–1007, ISSN 16871499, doi:10.1109/GLOCOMW.2014.7063564.

L. Weizheng, T. X., 'Throughput Analysis of Full-Duplex Network Coding in Two-Way Relay Channel,' IEEE International Conference on Communication Technology, 2017, pp. 85–90.

Lee, D. and Byung-Wook, '2x2 MIMO in-band full-duplex radio front-end with 50 dB self-interference cancellation in 90 MHz bandwidt,' IEEE MTT-S International Microwave Symposium Digest, 2017, pp. 670–672, ISSN 0149645X, doi:10.1109/MWSYM.2017.8058658.

Li, Y., Sun, L., Zhao, C., and Huang, L., 'A Digital Self-interference Cancellation algorithm based on Spectral Estimation in Co-time Co- frequency Full Duplex System,' 2015 10th International Conference on Computer Science & Education (ICCSE), 2015, **1**(Iccse), pp. 412–415, doi:10.1109/ICCSE.2015.7250280.

Liu, D., Shen, Y., Shao, S., Tang, Y., and Gong, Y., 'On the Analog Self-Interference Cancellation for Full-Duplex Communications with Imperfect Channel State Information,' IEEE Access, 2017, **5**, pp. 9277–9290, ISSN 21693536, doi:10.1109/ACCESS.2017.2702713.

Luan, Z., Qu, H., Zhao, J., and Chen, B., 'Robust digital non-linear self-interference cancellation in full duplex radios with maximum correntropy criterion,' China Communications, 2016, **13**(9), pp. 53–59, ISSN 16735447, doi:10.1109/CC.2016.7582296.

Makled, E. A., Yadav, A., Dobre, O. A., and Haynes, R. D., 'Hierarchical Full-Duplex Underwater Acoustic Network: A NOMA Approach,' OCEANS 2018 MTS/IEEE Charleston, OCEAN 2018, 2019, pp. 1–6, doi:10.1109/OCEANS.2018.8604904.

Masmoudi, A. and Le-Ngoc, T., 'A Maximum-Likelihood Channel Estimator for Self-Interference Cancelation in Full-Duplex Systems,' IEEE Transactions on Vehicular Technology, 2016, **65**(7), pp. 5122–5132, ISSN 00189545, doi:10.1109/TVT.2015.2461006.

Mohammadi, M., Shi, X., Chalise, B. K., Ding, Z., Suraweera, H. A., Zhong, C., and Thompson, J. S., 'Full-Duplex Non-Orthogonal Multiple Access for Next Generation Wireless Systems,' IEEE Communications Magazine, 2019, **57**(5), pp. 110–116, ISSN 15581896, doi:10.1109/MCOM.2019.1800578.

Senol, H., Li, X., and Tepedelenlioglu, C., 'Rapidly time-varying channel estimation for full-duplex amplify-and-forward one-way relay networks,' IEEE Transactions on Signal Processing, 2018, **66**(11), pp. 3056–3069, ISSN 1053587X, doi:10.1109/TSP.2018.2824254.

Shammaa, M., Vogt, H., El-Mahdy, A., and Sezgin, A., 'Adaptive Self-Interference Cancellation for Full Duplex Systems with Auxiliary Receiver,' 2019 International Conference on Advanced Communication Technologies and Networking (CommNet), 2019, pp. 1–8, doi:10.1109/commnet.2019.8742358.

Tian, L., Wang, S., Cheng, Z., and Bu, X., 'All-digital self-interference cancellation in zero-IF full-duplex transceivers,' China Communications, 2016, **13**(11), pp. 27–34, ISSN 16735447, doi:10.1109/CC.2016.7781715.

Wang, H., Huang, Y., Jin, S., Du, Y., and Yang, L., 'Pilot contamination reduction in multi-cell tdd systems with very large mimo arrays,' Wireless Personal Communications, 2017, **96**(4), pp. 5785–5808, ISSN 1572-834X, doi:10.1007/s11277-017-4447-1.

Wu, Y., Liu, T., Cao, M., Li, L., and Xu, W., 'Pilot contamination reduction in massive mimo systems based on pilot scheduling,' EURASIP Journal on Wireless Communications and Networking, 2018, **2018**(1), p. 21, ISSN 1687-1499, doi:10.1186/s13638-018-1029-1.

Xiang, W., Zheng, K., and Shen, X. S., *5G mobile communications*, Springer, 2016, ISBN 9783319342085, doi:10.1007/978-3-319-34208-5.

Xiao, C., Member, S., Zheng, Y. R., and Beaulieu, N. C., 'Novel Sum-of-Sinusoids Simulation Models for Rayleigh and Rician Fading Channels,' IEEE Transactions on Wireless Communications, 2006, **5**(12).

Xing, H., Wei, D., and Yin, F., 'Channel estimation using orthogonal superimposed pilot for MIMO systems,' ICSPS 2010 - Proceedings of the 2010 2nd International Conference on Signal Processing Systems, 2010, **2**, pp. 625–628, doi:10.1109/ICSPS.2010.5555739.

Zheng, B., Chen, F., Wen, M., Li, Q., Liu, Y., and Ji, F., 'Secure NOMA Based Cooperative Networks with Rate-Splitting Source and Full-Duplex Relay,' Proceedings of the International Symposium on Wireless Communication Systems, 2018, **2018-August**, pp. 1–5, ISSN 21540225, doi:10.1109/ISWCS.2018.8491208.

VI. TARGETED LEARNING FOR THE DYNAMIC SELECTION OF CHANNEL ESTIMATION METHODOLOGY

I. Arul Mathi Maran Chandran, II. Maciej Zawodniok

Department of Electrical & Computer Engineering

Missouri University of Science and Technology

Rolla, Missouri 65409

Email: ac62f@mst.edu, mjzx9c@mst.edu

III. Akim Adekpedjou

Department of Mathematics and Statistics

Missouri University of Science and Technology

Rolla, Missouri 65409

Email: akima@mst.edu

ABSTRACT

The explosive expansion of collected data - in terms of dimensionality, diversity, volume - increases more rapidly than we can analyze to draw useful conclusions, make informed decisions, and provide specific recommendations. Various fields such as medical, healthcare, aviation, telecommunication require new tools to process the data which they collect to process effectively and economically and benefit from the estimated quantities that were learned from the data itself. In particular, there are different methodologies proposed and used in telecommunications to estimate the channel coefficients of different types of channels. All these methodologies are grounded based on the assumption of the statistical property of the channel. However, a flexible solution that can dynamically deploy different methods based on the received signal yields higher performance and maintained over time.

In this paper, we propose to apply targeted learning and explore the suitable parameters for a communication system. The initial results demonstrate it is possible to distinguish and identify the best methodology to fit the current channel conditions.

Keywords: Channel estimation, targeted learning, target parameters, targeted maximum likelihood estimator (TMLE)

1. INTRODUCTION

The notion of data has dramatically changed in recent decades in its nature, scope, and magnitude. In many fields, one is interested in collecting data and extracting information and knowledge from it. For examples electronic health records in medical studies, passengers biometric information when entering a country, sociology, the DNA sequence of a population, consumer information over a period of many years. Another potential application of autonomous data analysis is in signal processing such as identification of a human voice for authentication, channel estimation for radio frequency (RF) communication. Storage and processing of a large amount of collected data become cheaper thus allowing the collection of even more data. However, effective processing and reasoning based on such data at ever-increasing velocities remain a challenge due to a bottleneck of manual interpretation of these data. A more desired approach is to formulate a question of interest about the data and let the data speak. Such a question would quantify a casual or non-casual relationship within the data. In telecommunications, there is no single method that can estimate any channel model. These methods vary significantly with assumptions to the statistical property of the channel. Each new methods addressing a particular channel model or improving the estimation accuracy. There is a need in telecommunication where the channel estimation be performed by dynamically selecting a methodology with respect to the current channel condition.

Traditional statistical approaches towards the data required aprior knowledge of specific, parametric statistical model Cao *et al.* (2004). These may work in small-dimensionality problems with existing expert knowledge, i.e. these need often flawed human input. Moreover, many techniques are not well suited to process large datasets in a reasonable time due to slow convergence and computational complexity. Hence, to process large datasets and quickly discover the unknown knowledge from the data and automatically formulate appropriate predictive models with minimal humans input, machine/deep learning is preferred and deployed.

Machine Learning, a subset of artificial intelligence in the field of computer science, arose in the sixties as a way of dealing with such complex data. It focuses on prediction, based on known properties learned from the training data to give computers the ability to learn from the data without being explicitly programmed. It is closely related to computational statistics and is in sharp contrast to using misspecified parametric statistical models van der Laan and Rose (2010). However, the goal is often a whole prediction function, and the machines are tailored to fit this whole prediction function.

The statistical inference in terms of assessment of variability (for instance confidence intervals) is typically lacking in this field. Moreover, the algorithms developed via machine learning are not targeted, which is adapted to the availability of new information especially in longitudinal studies. Also, choosing the right algorithm for prediction turns out to be difficult. Besides, both approaches use irrelevant information from the data to estimate target quantities thereby injecting bias and variability in the estimation. Existing machine learning approaches often employ techniques that do not statistically sound and are based on strong assumptions about the underlying statistical model. If the assumptions are not correct, the estimator will have a large bias, low accuracy, or may diverge from the true value. In contrast, the super learning technique estimates the targeted parameter (TP) over a set of potential statistical models via the super learner algorithm. Recent works have begun

employing such super learners to learn from the data but these (a) are not applicable to complex models such as surface, nonsmooth and unbounded TP, and (b) assumes complete dataset without dealing with the possibility of missing observations.

Recently deep learning-based approaches are employed for the channel estimation Jiang *et al.* (2019); Joo *et al.* (2019); Liu *et al.* (2019); Ye *et al.* (2018). It is been shown that a deep learning-based approach is robust compared to the traditional methods when fewer pilots are used, omitting the cyclic prefix, and nonlinear clipping noise exists Ye *et al.* (2018). The future channel state information (CSI) was predicted using deep learning from the measurement campaign to obtain and analyze the real-world channel estimates Joo *et al.* (2019). These approaches require high computational complex deep neural networks and a channel model based offline training from the real-world measurement campaign. With the advent of millimeter-wave (mmWave) and 5G communication, the knowledge of its channels are being explored and constantly updated through different measurement campaigns Deng *et al.* (2015); Samimi *et al.* (2016); Samimi and Rappaport (2016). The complex deep learning algorithms have to evolve with the updates and also its training sets. In contrast, these updates or models can be added to the model set of the targeted learning and update the criteria of selection.

Targeted Statistical Learning (TSL) has been established as a reliable framework for constructing effect estimators and prediction functions and focuses on efficient machine learning-based substitution estimators of targeted parameters that are defined as features of the distribution of the relevant part of the data while providing inference mainly via the influence curve. It is a broad framework that includes Targeted Maximum Likelihood Estimator (TMLE) for effect estimation questions and Super Learning technique for prediction, and the efficient Influence Curve for inference van der Laan and Rose (2010, 2018). TMLE is the usual maximum likelihood, however, targeted toward the relevant parts of the data generating distribution instead of the overall distribution. It is tailored to handle difficult questions that standard statistical inferences and machine learning approaches can not solve.

The contributions of this paper are as follows. We provided the initial results show variation in error performance of channel estimation with respect to the selection of the model. We identify and propose the targeted learning to determine the best methodology which fits the current channel conditions from the observations at the receiver.

The paper is organized as follows. Section 2 introduces the general formulation of the targeted learning algorithm and the targeted maximum likelihood estimator. Section 3 discusses the proposed use of targeted learning for channel estimation in telecommunications. Finally, Section 4 discusses the results to show how the targeted learning algorithm can be used to address the estimation of coefficient(s) of a dynamic channel.

2. TARGETED LEARNING

In this section, we discuss the general formulation of a targeted learner and yhe targeted maximum likelihood estimator. The discussion includes the telecommunication model and how targeted learning can benefit the channel estimation.

2.1. GENERAL FORMULATION

Consider n units on which data is collected. Let $\mathbf{t} = (t_1, t_2, \ldots, t_k)$ be a $k-$dimensional vector of variables collection times. $\mathbf{x}(t) = (x_1(t), x_2(t), \ldots, x_p(t))$, a $p-$dimensional vector of covariates, some of which are time dependent. $\mathbf{I}_t = (I_{t1}, I_{t2}, \ldots, I_{tj})$ is the sequence of interventions performed or recommendations that the unit was exposed to (or given to) at each time t_j. $\mathbf{Y}_t$ is a vector of expected outcome at each time t_j given recommendation at time t_{j-1}. One may also have censoring which often occurs in biomedical studies in the form of $h(\mathbf{x}t, \mathbf{Y}_t)$, where $h(.,.)$ is some smooth function. Another very important generalization for example is the possible spatial aspect measured but a spatial correlation $\rho(\mathbf{l}_i, \mathbf{l}_j)$ between units locations, where $\mathbf{l}_i : i = 1, \ldots, n$ and each being a 2-dimensional vector describing longitude and latitude of the location. Environmental factors

usually induce a spatial correlation, and often occurs in epidemiology, communication, war zone, and climate. Therefore, depending on the situation, a data structure may be of the form $\mathbf{O} = (O_1, \ldots, O_n)$ with O_i being

$$O_i = \left(\mathbf{x}\left(t_i\right), \mathbf{I}_{t_i}, \mathbf{Y}_{t_i}, h\left(\mathbf{x}_i\left(t_i\right), \mathbf{Y}_{t_i}\right), \rho\left(\mathbf{l}_i, \mathbf{l}_j\right) \mathbf{I}\{i \neq j\}\right).$$

In traditional approach to data analysis, one usually assumes that $\mathbf{O} \sim P_0$, where P_0 has a known form. Clearly no model exists that can fit such a complex data structure.

2.2. TARGETED MAXIMUM LIKELIHOOD ESTIMATOR

The behavior of O say P_0 is completely unknown, but belongs to a family of semi-parametric or fully non-parametric models $\mathcal{M}$. Let ψ be a function that maps $\mathcal{M}$ to $\Re^d$, $d \geq 1$ such that for any $P_0 \in \mathcal{M}$, one is interested in learning from a $d-$dimensional feature ψP_0, so called target parameter. In communication systems, modeling wireless channel as sequence of received symbols Cao *et al.* (2004),

$$y\left(n\right) = \Sigma_{k=0}^{L} h\left(k\right) x\left(n-k\right) + \eta\left(n\right),$$

where h is a finite discrete channel coefficients, x is the transmitted sequence and η is the noise term. The existing works assume the noise vector to follow a specific distribution and formulate the probability density function of $y\left(n\right)$ conditioned on the knowledge of $h\left(k\right)$ and $x\left(n\right)$ as $P\left(\bar{y}|\bar{x}, \bar{h}\right)$. The channel estimation and equalization can be then formulated as a maximization problem, for example, $arg\ \min_{\bar{x},\bar{h}} \Sigma_{n=0}^{N-1} P\left(\bar{y}|\bar{x}, \bar{h}\right)$.

In contrast to existing works Cao *et al.* (2004); Ghavami and Naraghi-Pour (2018); Necker and Stuber (2004); Saci *et al.* (2017); Yu *et al.* (2014); Zhang *et al.* (2015) which assume specific distribution model, the proposed framework will learn from data what is the best model.

TMLE builds on the literature of loss-based estimation for an infinite-dimensional parameter in order to target lower-dimensional parameters. The goal is to target the outcome parameter by making an optional bias-variance tradeoff for the parameter instead of the overall probability P_0. Specifically, what are the relevant part of P_0 say Q_0 that is useful to optimize knowledge of ψP_0. The name is coined because the estimator is targeted towards the parameter via the super learner algorithm that estimates the relevant portion of the distribution P_0 Rubin (1976); van der Laan (2010a,b); van der Laan and Rubin (2006). The ideas are rooted in the theory of semiparametric-efficient estimating equations Bickel (1998). It targets outcome parameters by making an optimal bias-variance trade off for the parameter of interest instead of the overall probability P_0. It is double robust and asymptotically efficient. The standard error of the TMLE is obtained upon estimating the influence curve. However, the influence curve, which is one of the most important components of successful learning from TSL and TMLE of a given parameter can only be estimated when ψP_0 is smooth. If not, convergence issues may arise. Existing work approximates the target parameter using a kernel with a constant bandwidth for all training data. Accurate information cannot be extracted from the nonsmooth parameter in case the bandwidth varies from one training to another. That remains an open problem for researchers.

3. DYNAMIC CHANNEL ESTIMATION

This section discusses different available methods to address the channel estimation and how the targeted learning algorithm can be deployed to achieve a dynamic selection of methodology to estimate any given channel.

In traditional communication approaches to channel estimation and equalization assume a particular statistical model such as Gaussian, Weibull Gaeddert and Annamalai (2005); Tzeremes and Christodoulou (2002). In such a scenario two issues arise. First, the channel model has to be known a priori, which is a strong assumption as wireless

channel varies significantly with the environment. Second, often these approaches focus on improving the accuracy of channel parameters estimation without consideration for the true target parameter, i.e., improved accuracy of data decoding.

A better approach would be to target estimation with two key benefits. First, the targeted statistical learning will identify the most suitable statistical model for the current channel conditions. Second, the decoding accuracy can be maximized by selecting a corresponding targeted parameter for TMLE. The block diagram of how the targeted learner deployed in the selection of the estimator for the received samples is shown in Figure 1.

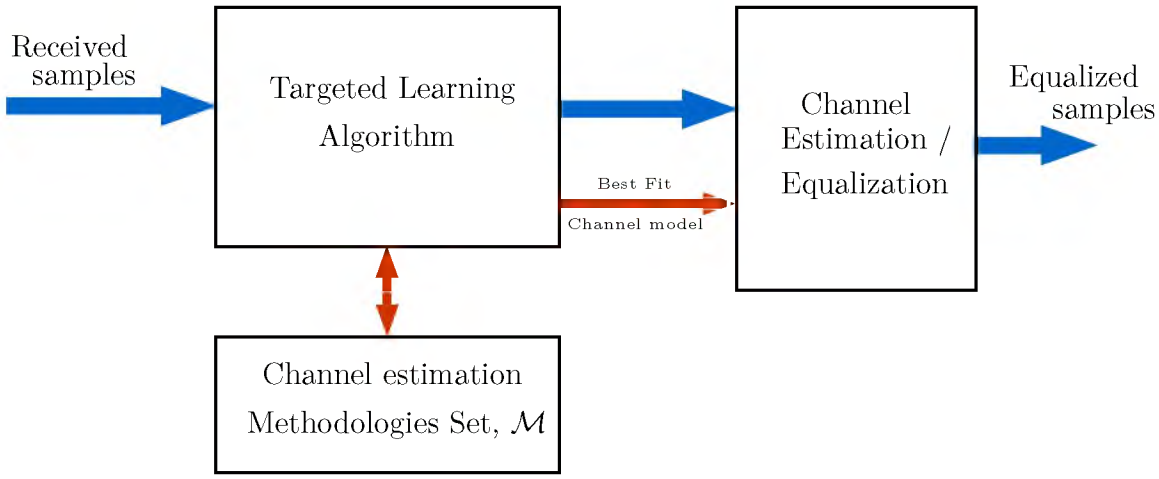

Figure 1. Block diagram of the targeted learner used in dynamic selection of channel estimator.

We evaluate how different methods to estimate the channel coefficients perform for different channel models as shown in Table 1. Three-channel estimators are analyzed for two different channel conditions where one of them is the channel for which they are designed and the other is different from the desired channel. The estimators are evaluated using the loss function which is given by

$$E_{m_0 \in \mathcal{M}}\left[L\left(\hat{h}, \bar{h}\right)\right] = Var\left(\hat{h}\right) + \left[Bias\left(\hat{h}\right)\right]^2 \tag{1}$$

where $\hat{h}$ is the estimated channel coefficient vector and $\bar{h}$ is the true channel coefficient vector. $\mathcal{M}$ is the set of the statistical models.

Table 1. Different channel fading model and distributions.

Channel fading	Flat-fading
	Frequency selective
Distributions	Rayleigh
	Racian
	Nakagami

Let us consider two-channel models. The first model considers the channel with a single tap coefficient, whereas in the second model the channel with two taps. There are two different channel estimators to estimate the channel coefficient(s) for the respective channel model. To show how targeted learning can be applied, the performance of these estimators are compared for both the channel models. Typically single-tap channel model can be associated with flat fading where are all reflection arriving the receiver during the symbol period can be summed up as one tap channel and channel model with more than one-tap which incur inter-symbol interference (ISI) is associated with frequency selective fading.

The system equation of the received symbols $\bar{y}$ of a given slot of length N at the receiver is given by

$$\bar{y} = X\bar{h} + \bar{\eta}, \tag{2}$$

where $\bar{h}$ is channel coefficient vector of length $LL \ll N$. $L = 1$ for single-tap channel and $L = 2$ for double-tap channel. X is L concatenated columns of transmitted symbol vector of length N. $\bar{\eta}$ is the noise vector of length N.

The system equation (2) for the two channel models can be written as

$$\begin{bmatrix} y0 \\ y1 \\ \vdots \\ yN-1 \end{bmatrix} = \begin{bmatrix} h & 0 & \cdots & 0 \\ 0 & h & \ddots & \vdots \\ \vdots & \ddots & \ddots & \vdots \\ 0 & 0 & \cdots & h \end{bmatrix} \begin{bmatrix} x0 \\ x1 \\ \vdots \\ xN-1 \end{bmatrix} + \begin{bmatrix} \eta 0 \\ \eta 1 \\ \vdots \\ \eta N-1 \end{bmatrix}, \tag{3}$$

In the single-tap channel model, only one channel coefficient h is estimated whereas, in the double-tap channel model, two-channel coefficients h_0 and h_1 are estimated. The two methodologies are designed specifically to estimate the coefficients of their respective channel models.

$$\begin{bmatrix} y0 \\ y1 \\ \vdots \\ \vdots \\ yN-1 \end{bmatrix} = \begin{bmatrix} h_0 & 0 & 0 & \cdots & 0 \\ h_1 & h_0 & 0 & \ddots & \vdots \\ 0 & h_1 & h_0 & \ddots & \vdots \\ \vdots & \ddots & \ddots & \ddots & \vdots \\ 0 & 0 & \cdots & h_1 & h_0 \end{bmatrix} \begin{bmatrix} x0 \\ x1 \\ \vdots \\ \vdots \\ xN-1 \end{bmatrix} + \begin{bmatrix} \eta 0 \\ \eta 1 \\ \vdots \\ \vdots \\ \eta N-1 \end{bmatrix}. \tag{4}$$

As discussed earlier in real-life scenarios, the channel is dynamic constantly varying with respect to the environment. For the evaluation of these methods in different channel models, we assume the true channel coefficients are known. The bias of the estimator demonstrates the deviation of the estimated channel coefficients from the true value and shows how the targeted learning can be a potential solution to dynamically select the methods based on the observation from received symbols. This evaluation is not limited to a simpler system model in Equation (2) and can be scaled to advanced system models such as OFDM, and MIMO systems.

Bias is introduced when the estimators are used for different channel models which they are not designed for. The target parameter for the learner is the bias of the estimators. From Equation (1), the loss function is equal to the variance of the estimator if the right estimator was selected to estimate the channel coefficients.

Bias of the estimator is given by

$$Bias\left(\hat{h}\right) = E_{y|h}\left[\hat{h} - \bar{h}\right]$$

where $\hat{h}$ and $\bar{h}$ are the estimated and true channel coefficients respectively.

The steps to estimate the channel coefficients differ for different methods and maximum likelihood is generally used. The simplest of all is the estimation of a single tap channel where only one coefficient is estimated by dividing the received symbol with the know transmitted symbol. This is possible in pilot slots where a known sequence is transmitted between the nodes. In the case of the multi-tap channel, the estimation of channel coefficients is difficult in the time domain and mostly performed in the frequency domain and transform the results back to the time domain. These are widely used in modern wireless communication technologies such as OFDM, MIMO systems. The channel coefficient(s) estimated by the respective estimators are:

$$\hat{h} = \left[\tilde{h}\right], \tag{5}$$

$$\hat{h} = \begin{bmatrix} \tilde{h}_0 \\ \tilde{h}_1 \end{bmatrix}. \tag{6}$$

Typically for an unbiased estimator, the expectation of the estimated value is equal to the true value. From Equation (3), for an unbiased estimator, the bias is equal to zero. The estimators which are considered for evaluation are unbiased while using the respective channel model. This difference can be used to determine which estimator(methodology) and an appropriate candidate for the target parameter of the targeted learning algorithm.

4. RESULTS

In section, we discuss the simulation results to show the performance of different methodologies to estimate the channel coefficients and demonstrate the feasibility of the targeted learner.

The simulation comprises three-channel estimators, one modeled to address the single-tap channel whereas the other to address the two-tap channel. The simulation was performed using MATLAB over 100 000 pilot slots. The noise vector $\bar{\eta}$ used in the simulation is additive white Gaussian noise (AWGN) with mean 0 and variance σ^2. For the Bayesian model, both the true mean, μ_h and true variance σ_h are assumed to be known. The pilots are the known sequences between the transmitter and the receiver. The simulation was performed for two different channel conditions. First, the channel was set to a single-tap channel and second, the channel was set to a two-tap channel. Both the scenarios were run over different SNR conditions and the estimators are deployed to estimate the channel coefficients. Figure 2 compares the variance of the estimated channel coefficients by the two methods with the true variance of the channel coefficients (single-tap channel) used in the simulation. From Figure 2, the true variance of the channel coefficients over the duration of the simulation is compared with the variance of the channel coefficients estimated by the two estimators. It can be observed the variance of the single-tap estimator is closer to the true variance than the double-tap estimator. This indicates the variance can be used as a parameter of interest to determine the best method which fits the current channel condition.

The estimated channel coefficients by the estimators are used to evaluate the error performance and plotted as shown in Figures 3 and 4.

The error performance plots of the single-tap and double-tap estimators used to estimate a single-tap channel (flat fading) are shown in Figure 3. It can be observed that the bayesian and single-tap estimators perform better than the double-tap estimator. The error

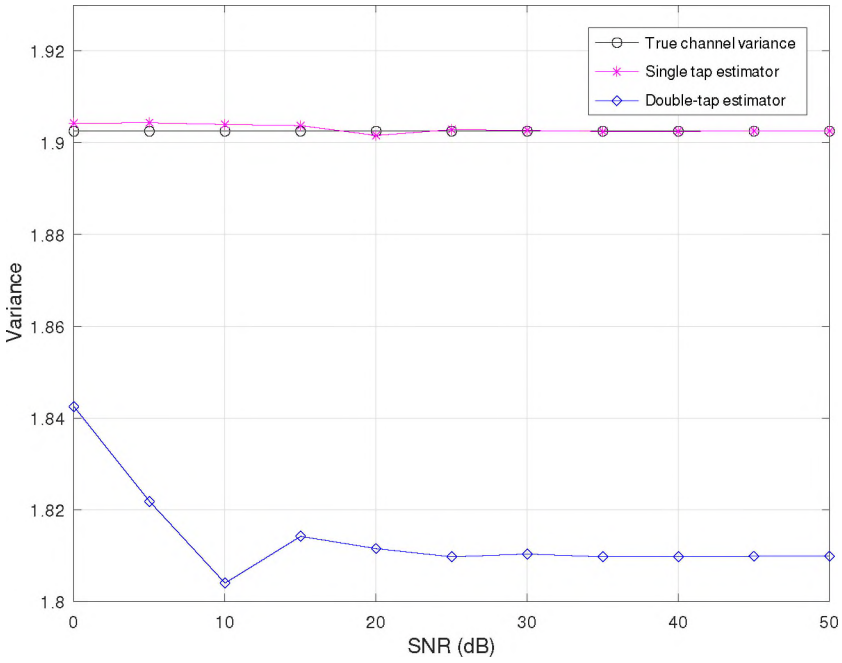

Figure 2. Comparison of variance of the estimated channel coefficients by the two methods with the true variance.

plot of the double-tap estimator follows the similar trend of the single-tap estimator and incurred error in its estimation of the h_0 and h_1. Here, h_1 should be zero but the estimated value is not equal to zero and has a similar error difference of h_0.

Similarly, in Figure 4 illustrates the error performance plots of the single-tap and double-tap estimators used to estimate a channel with two taps. In this case, the transmitted symbols suffer ISI and their impact can be observed on the poor performance of the single-tap estimator. By design, multi-tap estimators, in general, are built to overcome ISI to estimate the channel coefficients which is reflected in the error performance plot of the double-tap estimator. The Bayesian model performed better than the other two models with prior knowledge of the channel. If the prior knowledge of the channel is not available or not accurate then the error performance will be close to the other ML estimators.

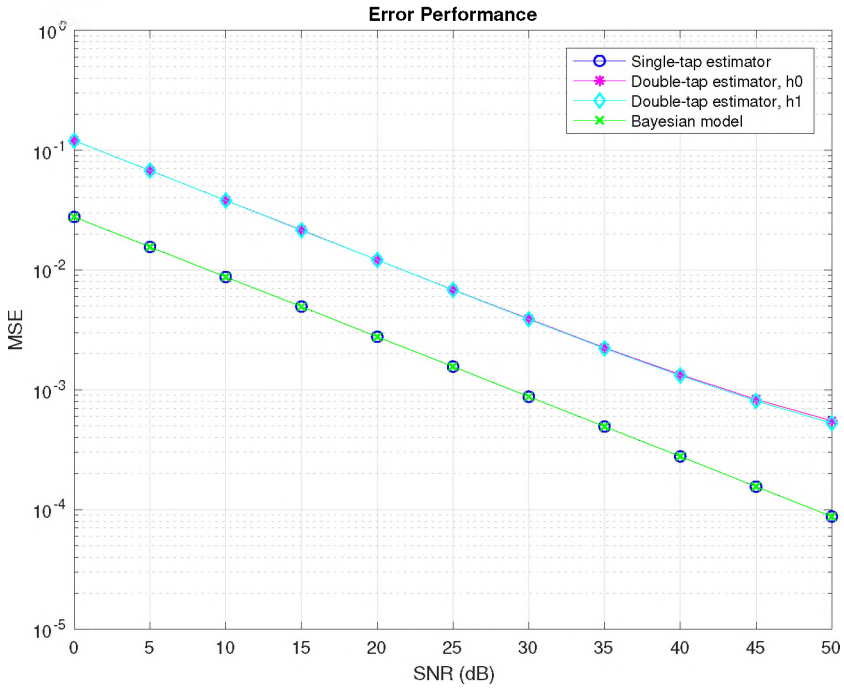

Figure 3. Mean square error of the channel estimators when applied to the single-tap channel.

From the above results, the estimators tailored to respective channel model performance best. There is no single solution that addresses any channel and estimates its coefficients. Deep learning is promising to address but with a huge cost on the complexity and offline training for learning. A deep learning algorithm can estimate a dynamic channel but they are complex with high computations which is not a suitable solution for compact mobile applications. However, a targeted learning algorithm can dynamically select the best methodology from its collection of models to estimate the channel coefficients using the received samples. There are many estimators available in the literature proposed to address channels of different environments. These methodologies can be considered as a set of estimators that can be selected dynamically with respect to the channel conditions observed from the samples.

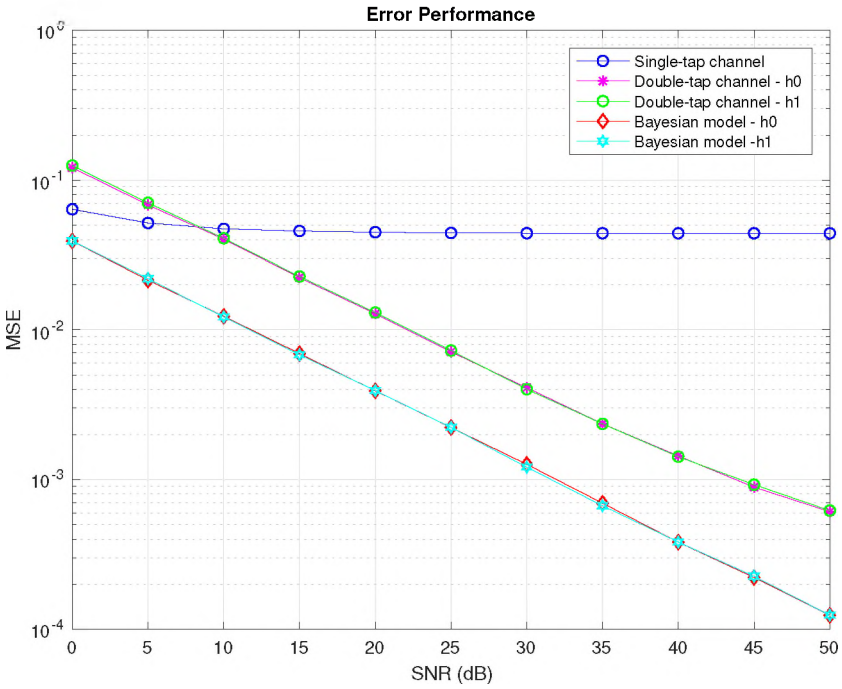

Figure 4. Mean square error of the channel estimators when applied to the multi-tap (2-taps) channel.

5. CONCLUSION

Different methodologies were used to estimate different channel conditions and evaluated their respective error performance. The results show that a single methodology to estimate the channel coefficients cannot maintain its performance for a dynamic channel. The targeted learning algorithm can perform the selection of methodology to estimate the channel coefficients based on the target parameter such as bias, bit error rate, speed of convergence, computation overhead. The formulation and regression model with the explored target parameters for different channel distributions such as Rayleigh, Racian, Nakagami are planned for OFDM, MIMO systems and evaluate the performance of the targeted learning.

REFERENCES

Bickel, K. C. R. Y. W. J., P.J., *Efficient and Adaptive Estimation for Semiparametric Models*, Springer-Verlag New York, 1998, ISBN 978-0-387-98473-5.

Cao, L., Chen, C. W., Orlik, P., Zhang, J., and Gu, D., 'A trellis-based technique for blind channel estimation and equalization,' Journal of Communications and Networks, 2004, **6**(1), pp. 19–25, ISSN 1229-2370, doi:10.1109/JCN.2004.6596983.

Deng, S., Samimi, M. K., and Rappaport, T. S., '28 ghz and 73 ghz millimeter-wave indoor propagation measurements and path loss models,' in '2015 IEEE International Conference on Communication Workshop (ICCW),' 2015 pp. 1244–1250, doi: 10.1109/ICCW.2015.7247348.

Gaeddert, J. and Annamalai, A., 'New estimators for the weibull fading parameters,' in 'VTC-2005-Fall. 2005 IEEE 62nd Vehicular Technology Conference, 2005.', volume 2, ISSN 1090-3038, 2005 pp. 1367–1371, doi:10.1109/VETECF.2005. 1558150.

Ghavami, K. and Naraghi-Pour, M., 'Blind Channel Estimation and Symbol Detection for Multi-Cell Massive MIMO Systems by Expectation Propagation,' IEEE Transactions on Wireless Communications, 2018, **17**(2), pp. 943–954, ISSN 1536-1276, doi:10.1109/TWC.2017.2772837.

Jiang, Z., He, Z., Chen, S., Molisch, A. F., Zhou, S., and Niu, Z., 'Inferring Remote Channel State Information: Crame r-Rae Lower Bound and Deep Learning Implementation,' 2018 IEEE Global Communications Conference, GLOBECOM 2018 - Proceedings, 2019, pp. 1–7, doi:10.1109/GLOCOM.2018.8648140.

Joo, J., Park, M. C., Han, D. S., and Pejovic, V., 'Deep Learning-Based Channel Prediction in Realistic Vehicular Communications,' IEEE Access, 2019, **7**, pp. 27846–27858, ISSN 21693536, doi:10.1109/ACCESS.2019.2901710.

Liu, J., Mei, K., Zhang, X., Ma, D., and Wei, J., 'Online Extreme Learning Machine-based Channel Estimation and Equalization for OFDM Systems,' IEEE Communications Letters, 2019, **PP**(X), pp. 1–1, ISSN 1089-7798, doi:10.1109/lcomm.2019. 2916797.

Necker, M. C. and Stuber, G. L., 'Totally blind channel estimation for OFDM on fast varying mobile radio channels,' IEEE Transactions on Wireless Communications, 2004, **3**(5), pp. 1514–1525, ISSN 1536-1276, doi:10.1109/TWC.2004.833508.

Rubin, D. B., 'Inference and missing data,' Biometrika, 1976, **63**(3), pp. 581–592, ISSN 0006-3444, doi:10.1093/biomet/63.3.581, with comments by R. J. A. Little and a reply by the author.

Saci, A., Al-Dweik, A., Shami, A., and Iraqi, Y., 'One-Shot Blind Channel Estimation for OFDM Systems Over Frequency-Selective Fading Channels,' IEEE Transactions on Communications, 2017, **65**(12), pp. 5445–5458, ISSN 0090-6778, doi:10.1109/TCOMM.2017.2740925.

Samimi, M. K., MacCartney, G. R., Sun, S., and Rappaport, T. S., '28 ghz millimeter-wave ultrawideband small-scale fading models in wireless channels,' in '2016 IEEE 83rd Vehicular Technology Conference (VTC Spring),' 2016 pp. 1–6, doi:10.1109/VTCSpring.2016.7503970.

Samimi, M. K. and Rappaport, T. S., 'Local multipath model parameters for generating 5g millimeter-wave 3gpp-like channel impulse response,' in '2016 10th European Conference on Antennas and Propagation (EuCAP),' 2016 pp. 1–5, doi:10.1109/EuCAP.2016.7481410.

Tzeremes, G. and Christodoulou, C. G., 'Use of weibull distribution for describing outdoor multipath fading,' in 'IEEE Antennas and Propagation Society International Symposium (IEEE Cat. No.02CH37313),' volume 1, 2002 pp. 232–235 vol.1, doi:10.1109/APS.2002.1016291.

van der Laan, M. J., 'Targeted maximum likelihood based causal inference. I,' Int. J. Biostat., 2010a, **6**(2), pp. Art. 2, 44, ISSN 1557-4679.

van der Laan, M. J., 'Targeted maximum likelihood based causal inference. II,' Int. J. Biostat., 2010b, **6**(2), pp. Art. 3, 33, ISSN 1557-4679.

van der Laan, M. J. and Rose, S., *Targeted Learning - Causal Inference for Observational and Experimental Data*, Springer, 2010, ISBN 9780387775005, doi:10.1007/978-0-387-98135-2.

van der Laan, M. J. and Rose, S., *Targeted Learning in Data Science - Causal Inference for Complex Longitudinal Studies*, Springer, 2018, ISBN 978-3-319-65303-7, doi:10.1007/978-3-319-65304-4.

van der Laan, M. J. and Rubin, D., 'Targeted maximum likelihood learning,' Int. J. Biostat., 2006, **2**, pp. Art. 11, 40, ISSN 1557-4679, doi:10.2202/1557-4679.1043.

Ye, H., Li, G. Y., and Juang, B. H., 'Power of Deep Learning for Channel Estimation and Signal Detection in OFDM Systems,' IEEE Wireless Communications Letters, 2018, **7**(1), pp. 114–117, ISSN 21622345, doi:10.1109/LWC.2017.2757490.

Yu, J.-L., Zhang, B., and Chen, P.-T., 'Blind and semi-blind channel estimation with fast convergence for MIMO-OFDM systems,' Signal Processing, 2014, **95**, pp. 1–9, ISSN 0165-1684, doi:10.1016/j.sigpro.2013.08.006.

Zhang, W., Gao, F., and Yin, Q., 'Blind Channel Estimation for MIMO-OFDM Systems With Low Order Signal Constellation,' IEEE Communications Letters, 2015, **19**(3), pp. 499–502, ISSN 1089-7798, doi:10.1109/LCOMM.2015.2393889.

SECTION

2. FULL-DUPLEX CHANNEL ESTIMATORS FOR FLAT FADING CHANNEL

The following contents are the initial works prior to the publications which are included for the method proposed to use the orthogonal sequences for the pilots in case of flat fading channel. The Cramer-Rao Lower bound of the estimators in terms of symbols. The Walsh sequence was used as pilots for the flat fading channel but not suitable for frequency selective fading. An orthogonal m-sequence was used and discussed in Paper V. In FDX operations, the pilots can be used to estimate the SI channel in addition to the communication channel. However, the challenge at the receiver is to distinguish the pilots from the received signal to estimate respective channels such as SI and communication channel. Different approaches enable the receiver to overcome this challenge.

2.1. METHODOLOGY

The conventional approach is different slots (DS) are chosen across the radios for transmitting their respective pilots such that they do not overlap with each other. However, the more efficient approach is to use the same slot (SS) for the pilot transmissions across the radios. This increases the spectral efficiency and also the complexity at the receiver to separate the pilots from different radios. The accuracy of the channel estimation depends on the receiver's ability to distinguish the pilots and estimate their respective channels. Especially in FDX communication link, receivers should be able to distinguish its pilot from others for the estimation of both SI and communication channels. We propose a solution to aid the receiver in distinguishing the pilots from different radios transmitted in a given slot by using orthogonal sequences as pilots.

2.1.1. System Model. In this section, we briefly discuss the proposed method, the system model, and how the orthogonality property was used to separate and estimate the SI and communication channel.

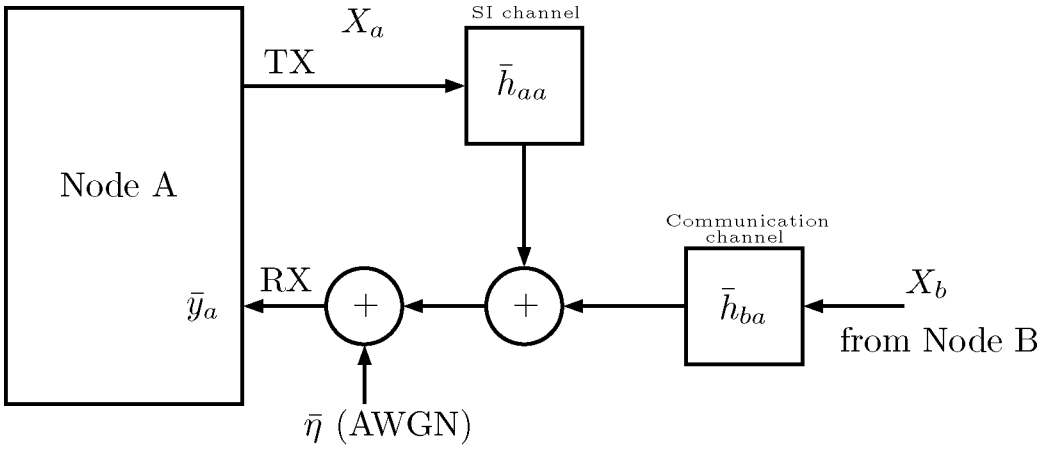

Figure 2.1. Block diagram of FDX system model

Consider a full-duplex system as shown in Figure 2.1, and the received symbol vector of length N for any given slot at node A is given by

$$\bar{y}_a = X_a \bar{h}_{aa} + X_b \bar{h}_{ba} + \bar{\eta}, \tag{2.1}$$

where, X_a is the transmitted symbol matrix containing M columns of the transmitted symbol vector, $\bar{x}_a$ of length N from the node A. Similarly X_b is transmitted symbol matrix containing M columns of the transmitted symbol vector, $\bar{x}_b$ of length N from node B to node A. $\bar{h}_{aa}$ and $\bar{h}_{ba}$ are self-inteference and communication channel coefficient vectors of length M $(N >> M)$ respectively. $\bar{\eta}$ is the AWGN vector of length N. $\bar{\eta} \sim \mathcal{CN}\left(0, \sigma^2\right)$. In this article, to evaluate the proposed method, flat fading channel is considered for both SI and communication channels.

2.1.2. Orthogonal Pilot Sequence. As discussed earlier the known pilot sequences are used to estimate the channel of a communication link. In the proposed method, we use the orthogonal sequences as pilots to separate pilots from different radios by receivers in FDX operation.

The pilot symbols are extracted from the known pilot slots received by the receiver and the property of orthogonality of the pilot symbols is used to separate and estimate the SI channel and the communication channel. Let node A and node B use the orthogonal pilot sequences $\mathbf{x}_{pa}$ and $\mathbf{x}_{pb}$ respectively such that $\mathbf{x}_{pa}^T \cdot \mathbf{x}_{pb} = \mathbf{x}_{pb}^T \cdot \mathbf{x}_{pa} = 0$ and $\mathbf{x}_{pa}^T \cdot \mathbf{x}_{pa} = \mathbf{x}_{pb}^T \cdot \mathbf{x}_{pb} = 1$. Thus, by multiplying transpose of its pilot sequence, the communication channel component from the received symbol can be removed to estimate the SI channel and vice-versa. For a flat fading channel with M taps, multiplying X_{pa}^T on both sides of the system equation (2.1) yields

$$\begin{aligned} X_{pa}^T \bar{y}_a &= X_{pa}^T X_{pa} \bar{h}_{aa} + X_{pa}^T X_{pb} \bar{h}_{ba} + X_{pa}^T \bar{\eta} \\ &= \mathbf{1}_{M\times M}\ \bar{h}_{aa} + \mathbf{0}_{M\times M} + X_{pa}^T \bar{\eta} \\ &= \mathbf{1}_{M\times M}\ \bar{h}_{aa} + X_{pa}^T \bar{\eta}, \end{aligned} \tag{2.2}$$

where, $\mathbf{1}_{M\times M}$ and $\mathbf{0}_{M\times M}$ are all ones and all zeros matrices with dimension $M \times M$ respectively. Similarly, multiplying X_{pb}^T on both sides of the system equation (2.1) yields

$$\begin{aligned} X_{pb}^T \bar{y}_a &= X_{pb}^T X_{pa} \bar{h}_{aa} + X_{pb}^T X_{pb} \bar{h}_{ba} + X_{pb}^T \bar{\eta} \\ &= \mathbf{0}_{M\times M} + \mathbf{1}_{M\times M}\ \bar{h}_{ba} + X_{pb}^T \bar{\eta} \\ &= \mathbf{1}_{M\times M}\ \bar{h}_{ba} + X_{pa}^T \bar{\eta}. \end{aligned} \tag{2.3}$$

Solving the results from Equations (2.2) and (2.3), the SI channel and communication channel coefficients $\hat{h}_{aa}$ and $\hat{h}_{ba}$ can be estimated respectively. Though the nodes A and B are synchronized to establish a reliable communication link, the reflections of node A to

itself likely have an offset. The orthogonal sequence tolerates this offset until the occurrence of a significant ISI which is avoided by considering both the SI and the communication channels being flat fading channels.

The channel coefficients of respective channels for the entire frame can be estimated from the knowledge of the channel coefficients at the pilot locations by using any of the existing interpolation techniques Aghamohammadi *et al.* (1991); Cavers (1991); Sampei *et al.* (1993); Wu *et al.* (2004).

2.2. CRLB FOR THE PROPOSED METHOD

In this section, we derive the Cramer-Rao Lower Bound (CRLB) for the proposed system. In the case of flat fading channel, different reflection arriving at the receiver does not cause inter-symbol interference (ISI) and these reflections sum up to one filter coefficient of the channel. Then, the system equation (2.1) for the k^{th} symbol in a given slot can be written as

$$y_a(k) = x_a(k) h_{aa} + x_b(k) h_{ba} + \eta(k), \tag{2.4}$$

where, h_{aa} and h_{ba} are channel coefficient of the SI and the communication channel and these two parameters are the parameters of interest to be estimated which is indicated by $\bar{\theta} = [h_{aa}\ h_{ba}]^T$.

The probability density function of the received slot with N symbols is given by

$$P\left(\bar{y_a}, \bar{\theta}\right) = \frac{1}{(2\pi\sigma^2)^{\frac{N}{2}}} \cdot exp\left[\frac{-1}{2\sigma^2}\Sigma_{k=0}^{N-1}\left(y_a(k) - x_a(k) h_{aa} - x_b(k) h_{ba}\right)^2\right]. \tag{2.5}$$

To determine the CRLB of the estimator, the Fisher information matrix $I\left(\bar{\theta}\right)$ has to be evaluated which is given by,

$$I\left(\bar{\theta}\right) = \begin{bmatrix} -E\left[\dfrac{\partial^2 \ln P\left(\bar{y_a}, \bar{\theta}\right)}{\partial h_{aa}^2}\right] & -E\left[\dfrac{\partial^2 \ln P\left(\bar{y_a}, \bar{\theta}\right)}{\partial h_{aa} \partial h_{ba}}\right] \\ -E\left[\dfrac{\partial^2 \ln P\left(\bar{y_a}, \bar{\theta}\right)}{\partial h_{ba} \partial h_{aa}}\right] & -E\left[\dfrac{\partial^2 \ln P\left(\bar{y_a}, \bar{\theta}\right)}{\partial h_{ba}^2}\right] \end{bmatrix}. \tag{2.6}$$

Recall that for the estimation of vector parameter, $\bar{\theta} = [\theta_1\ \theta_2\ \ldots\ \theta_n]^T$. If $\hat{\theta}_i$ is an unbiased estimator, then the CRLB of $\hat{\theta}_i$ is ii^{th} element of the inverse of the Fisher information matrix Kay (1993), $I\left(\bar{\theta}\right)$

$$var\left(\hat{\theta}_i\right) \geq \left[I^{-1}\left(\bar{\theta}\right)\right]_{ii}. \tag{2.7}$$

Now, we evaluate the individual elements in the Fisher information matrix. The logarithm of the probability density function and the partial derivatives of the equation.

$$\ln p\left(\bar{y_a}, \bar{\theta}\right) = -\frac{N}{2}\ln\left(2\pi\sigma^2\right) + \frac{1}{2\sigma^2}\Sigma_{k=0}^{N-1}\left(y_a\left(k\right) - x_a\left(k\right)h_{aa} - x_b\left(k\right)h_{ba}\right), \tag{2.8}$$

$$\begin{aligned}
\frac{\partial \ln P\left(\bar{y_a}, \bar{\theta}\right)}{\partial h_{aa}} &= \frac{1}{\sigma^2}\Sigma_{k=0}^{N-1}\left(y_a\left(k\right) - x_a\left(k\right)h_{aa} - x_b\left(k\right)h_{ba}\right)x_a\left(k\right) \\
\frac{\partial \ln P\left(\bar{y_a}, \bar{\theta}\right)}{\partial h_{ba}} &= \frac{1}{\sigma^2}\Sigma_{k=0}^{N-1}\left(y_a\left(k\right) - x_a\left(k\right)h_{aa} - x_b\left(k\right)h_{ba}\right)x_b\left(k\right) \\
\frac{\partial^2 \ln P\left(\bar{y_a}, \bar{\theta}\right)}{\partial h_{aa}^2} &= -\frac{1}{\sigma^2}\Sigma_{k=0}^{N-1}\left(x_a\left(k\right)\right)^2 \qquad (2.9) \\
\frac{\partial^2 \ln P\left(\bar{y_a}, \bar{\theta}\right)}{\partial h_{ba}^2} &= -\frac{1}{\sigma^2}\Sigma_{k=0}^{N-1}\left(x_b\left(k\right)\right)^2 \qquad (2.10) \\
\frac{\partial^2 \ln P\left(\bar{y_a}, \bar{\theta}\right)}{\partial h_{aa}\partial h_{ba}} &= \frac{-1}{\sigma^2}\Sigma_{k=0}^{N-1}\left(x_a\left(k\right)x_b\left(k\right)\right) \qquad (2.11) \\
\frac{\partial^2 \ln P\left(\bar{y_a}, \bar{\theta}\right)}{\partial h_{ba}\partial h_{aa}} &= \frac{-1}{\sigma^2}\Sigma_{k=0}^{N-1}\left(x_b\left(k\right)x_a\left(k\right)\right). \qquad (2.12)
\end{aligned}$$

Since, the Walsh codes are used in the analysis, the results from Equations (2.9), (2.10), (2.11), and (2.12) becomes,

$$\frac{\partial^2 \ln P\left(\bar{y_a}, \bar{\theta}\right)}{\partial h_{aa}^2} = -\frac{N}{\sigma^2} \tag{2.13}$$

$$\frac{\partial^2 \ln P\left(\bar{y_a}, \bar{\theta}\right)}{\partial h_{ba}^2} = -\frac{N}{\sigma^2} \tag{2.14}$$

$$\frac{\partial^2 \ln P\left(\bar{y_a}, \bar{\theta}\right)}{\partial h_{aa} \partial h_{ba}} = 0 \tag{2.15}$$

$$\frac{\partial^2 \ln P\left(\bar{y_a}, \bar{\theta}\right)}{\partial h_{ba} \partial h_{aa}} = 0. \tag{2.16}$$

The expectation of the results from Equations (2.13), (2.14), (2.15), and (2.16) yields

$$E\left[\frac{\partial^2 \ln P\left(\bar{y_a}, \bar{\theta}\right)}{\partial h_{aa}^2}\right] = E\left[\frac{\partial^2 \ln p\left(\bar{y_a}, \bar{\theta}\right)}{\partial h_{ba}^2}\right] = -\frac{N}{\sigma^2} \tag{2.17}$$

$$E\left[\frac{\partial^2 \ln P\left(\bar{y_a}, \bar{\theta}\right)}{\partial h_{aa} \partial h_{ba}}\right] = E\left[\frac{\partial^2 \ln p\left(\bar{y_a}, \bar{\theta}\right)}{\partial h_{ba} \partial h_{aa}}\right] = 0. \tag{2.18}$$

Using the results from Equations (2.17) and (2.18) in (2.6), the Fisher information matrix, $I\left(\bar{\theta}\right)$ can be constructed

$$I\left(\bar{\theta}\right) = \begin{bmatrix} \frac{N}{\sigma^2} & 0 \\ 0 & \frac{N}{\sigma^2} \end{bmatrix} \tag{2.19}$$

$$= \frac{N}{\sigma^2} \begin{bmatrix} 1 & 0 \\ 0 & 1 \end{bmatrix}. \tag{2.20}$$

The variance of the parameters h_{aa} and h_{ba} can be determined using (2.7) and the inverse of the Fisher information matrix $I^{-1}\left(\bar{\theta}\right)$ is

$$I^{-1}\left(\bar{\theta}\right) = \frac{\sigma^2}{N} \begin{bmatrix} 1 & 0 \\ 0 & 1 \end{bmatrix}. \tag{2.21}$$

Therefore, the Cramer-Rao lower bound SI and communication channel estimators are given by

$$var\left(\hat{h}_{aa}\right) \geq \frac{\sigma^2}{N} \tag{2.22}$$

$$var\left(\hat{h}_{ba}\right) \geq \frac{\sigma^2}{N}. \tag{2.23}$$

$$\because \begin{bmatrix} \hat{\theta}_1 = \hat{h}_a a,\ \hat{\theta}_2 = \hat{h}_{ba} \\ I^{-1}\left(\bar{\theta}\right)_{11} = I^{-1}\left(\bar{\theta}\right)_{22} = \frac{\sigma^2}{N} \end{bmatrix}$$

The CRLB of the channel estimator for HDX operations matches while estimating the communication channel. The usage of orthogonal sequences in FDX operations enables the receiver to separate and estimate SI and communication channels.

2.3. SIMULATION ANALYSIS

In this section, we discuss the simulation results illustrating the performance of the estimators using the proposed method in terms of estimation error. The simulation is built using the system model.

The Walsh orthogonal sequences are used as pilot sequences in the simulation. The orthogonality property was tested for different sample offsets within a symbol period. Figure 2.2 shows the sequence product for different sample offsets where samples per symbol is equal to 10. As observed in Figure 2.2, the cross-correlation is almost equal to zero for different sample offsets, whereas the auto-correlation varies over different offsets. The Walsh sequence product yield negative value for odd offset and positive value for even offset and this transition from a positive one to negative one can be observed from Figure 2.2. In FDX operation, the receiver synchronizes with the communication channel and self-

interference shall have sample offset less than one symbol period (flat fading channel), the orthogonality property can be deployed to separate and estimate both the communication and the SI channels.

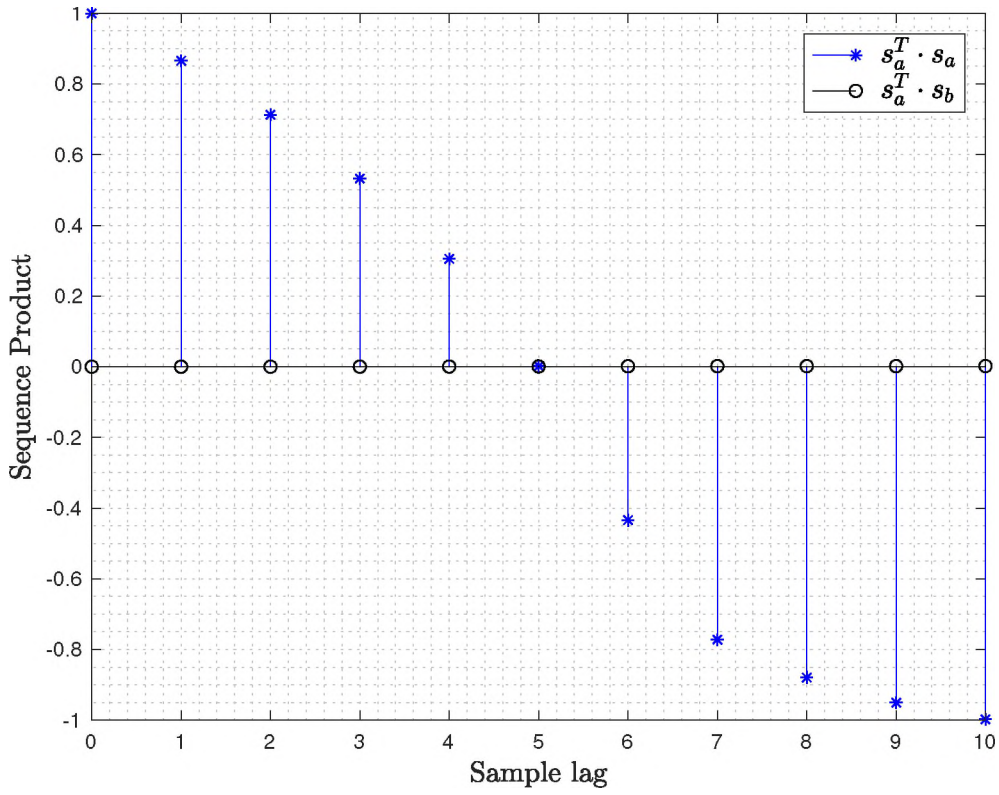

Figure 2.2. Orthogonal sequence product result for different lags across a symbol duration (10 samples/symbol).

The orthogonal pilot sequences of length $N = 1024$ are spread across different slots in a frame in the simulation. The channel coefficients are generated using improved Jake's model Xiao *et al.* (2006). Due to a lack of actual model representing the self-interference available in the literature, we used the channel model used for the communication channel with different parameter. Both the channels are flat fading and the Doppler frequency of the SI channel was set higher than the communication channel. The average error of the estimators of both the channels is evaluated from 100 000 frames in the simulation over different noise levels in the communication link.

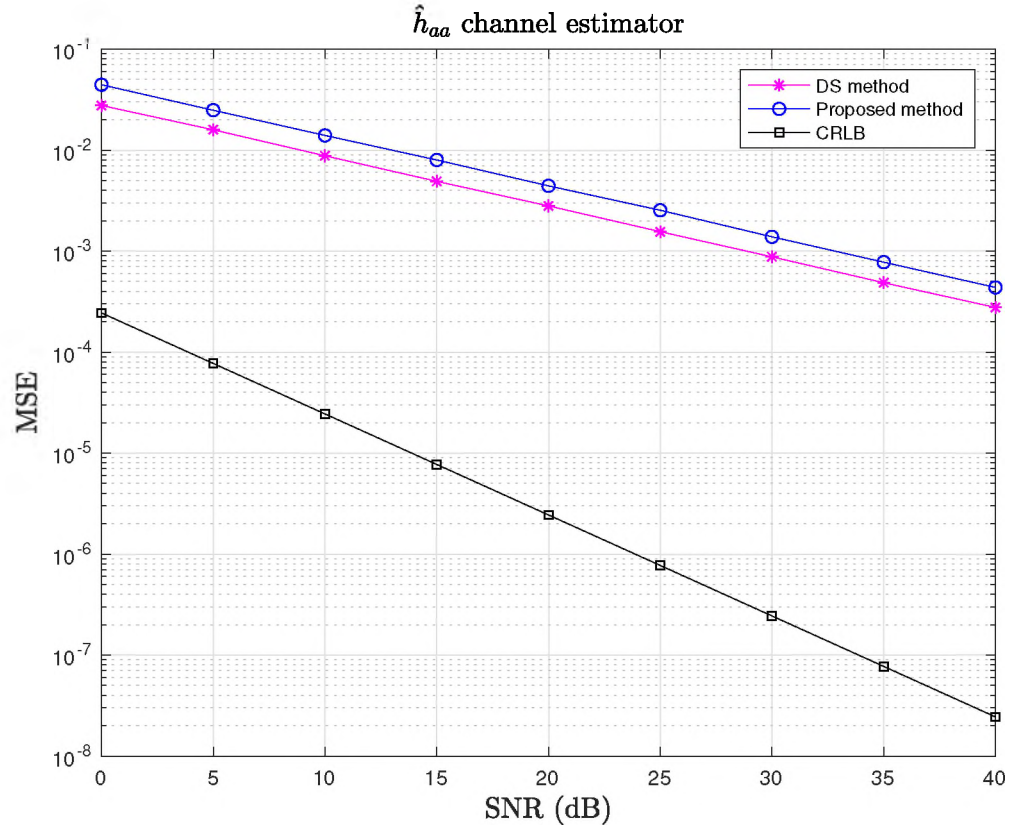

Figure 2.3. Cramer-Rao lower bound of $\hat{h}_{aa}$ and the estimation error using MLE for different methods.

The three cases discussed are simulated and their respective performance is compared using MSE curves. In the DS method, the pilots from different radios are transmitted in different slots, whereas in the SS method, the pilots from different nodes are transmitted in the same slot. In the SS method, offline training was performed to estimate the SI channel in the absence of other signals. The offline SI channel estimation is used in addition to the knowledge of pilots from both the nodes to separate the channels and performed channel estimation of the communication channel. In the proposed method, the orthogonal pilots are transmitted by radios in the same slot. Using the property of orthogonality, the channels are separated and performed the channel estimation of both SI and communication chan-

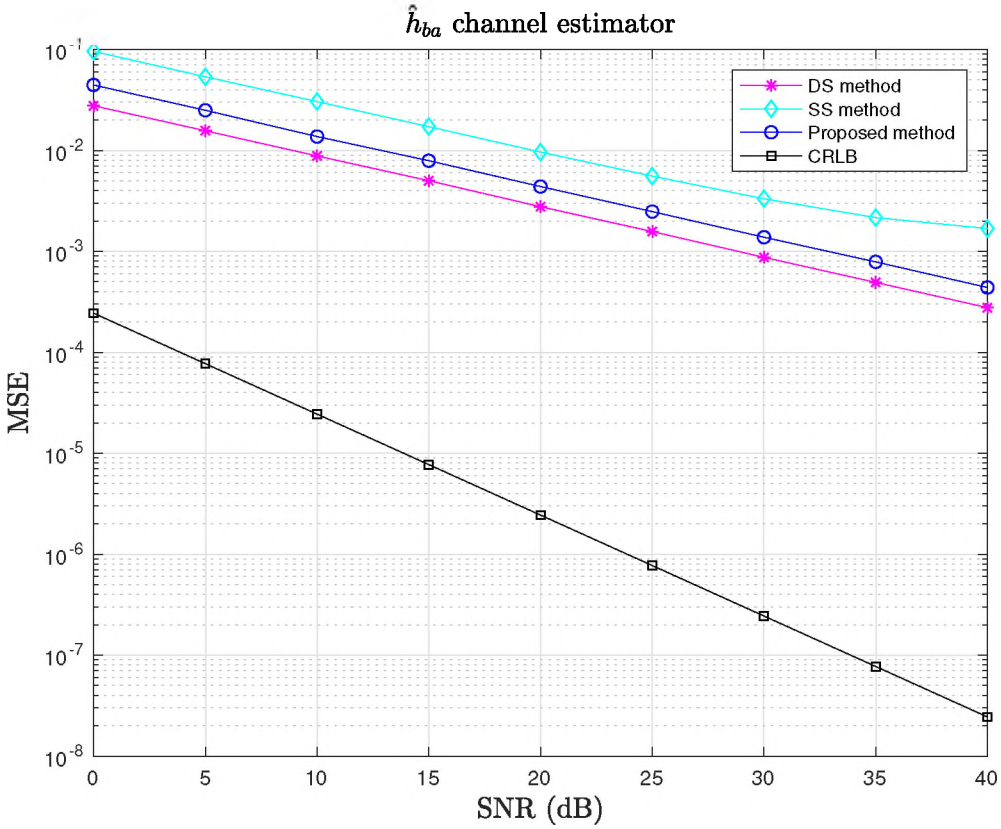

Figure 2.4. Cramer-Rao lower bound of $\hat{h}_{ba}$ and the estimation error using MLE for different methods.

nels. The simulation results illustrating the performance of the estimators to estimate SI and communication channels in addition to their respective CRLB are shown in Figures 2.3 and 2.4 respectively.

We showed that the proposed method using orthogonal sequences as pilots can successfully separate and estimate both SI and communication channel. The proposed method yields around 6 dB on average compared to the SS method. When applied to Wi-Fi operated in full-duplex, there is $\approx 10\%$ increase in peak throughput because of lower pilot overhead than DS method. We derived and showed the CRLB of the proposed method and it matches with the estimator when performed separately. Thus, the use of orthogonal

sequences as pilots in FDX operation reduce the pilot overhead and improve the spectral efficiency. The proposed method can benefit the upcoming next-generation 5G mobile communication where full-duplex operation considered to play a vital role.

3. MISSING DATA NOT AT RANDOM: CHARACTERIZATION OF TARGETED INTERFERENCE IN WIRELESS NETWORKS

Communication systems include data collection and estimation during their operations. At the receiver, the data can be missed due to various reasons such as channel conditions, malicious attack, failure at the receiver. Some of these conditions occur at random, but sometimes, their occurrences are not random. These occurrences can be due to the precise placement of interference to impede communication between the devices. There are different mechanisms proposed in the literature to address this data loss, by requesting retransmission, spreading the signal, etc. A different approach from the statistical analysis used in processing data from the survey, to estimate the data which are missed not at random. In the statistical study, data that are missed not at random manifest during data collection when one or more subjects involved in the survey skip their responses for one or more data fields due to social, economic and health reasons. These missed responses are filled by imputation from the responses collected from other subjects. Similarly, in a wireless network, data lost from a particular node that is under attack can be considered as data missed not at random and can be estimated from the data collected from the surrounding nodes.

3.1. MOTIVATION

One of the challenges in wireless networks that gets the least attention is the occurrence of the data miss for various reasons such as the condition of the channel, nearby interference, malicious attack on the targeted nodes, etc. This data loss is generally ignored since there are back up mechanisms with requesting multiple retransmissions to retrieve the missed data. When focused on these missed data, they can provide insight into the prevailing conditions of the communication link and potential issues with it such as the

rapid fluctuation in the channel, external interference. This improves the estimation of the channel by reducing any bias in the data processing, thus enhance the performance of data decoding at the receiver. The missed data due to these conditions in the communication link can be classified into two groups from a statistical perspective that is missed data at random (MAR), and missed data not at random (MNAR). This classification is used in the statistical analysis of data processing when one or more fields of data collection go missing.

During data collection, MAR occurs when the probability of missing does not depend on the observed data, whereas MNAR occurs when the probability of missing depends on the value itself. Most of the works in the literature consider the data missing at random. This assumption has shown a less impact on the parameter estimates Collins *et al.* (2001). Earlier the missed data in statistical analysis are dealt with by two methods such as listwise deletion and pairwise deletion. Listwise deletion completely drops the entire data set when one or more fields are missing data, whereas pairwise deletion reduces the dropping of the data set and attempts to maximize the use of data for the analysis. In both methods, the estimation tends to have a bias on the estimation by overestimation or underestimation Dong and Peng (2013).

The data missing in the statistical analysis directly relates to the statistical interference occurring during data collection which can be translated to data missing at the reception of the communication link.

3.2. METHODOLOGY

The pattern of the missing data is classified into univariate, monotone and arbitrary. While considering the pattern of the missing data at the reception of a communication link is considered as univariate for a single receiver stream and monotone for multiple receiver streams. We start with a univariate pattern of the current discussion and explore monotone in the future study. We propose to use imputation in the process of replacing data

missed by more probable value using the information from the observed values. Imputation is employed in data mining using machine learning while analyzing incomplete data set Chhabra *et al.* (2019).

Two methods used while imputing missing values with a univariate pattern, the regression method Rubin (1987) and the predictive mean matching method Heitjan and Little (1991); Schenker and Taylor (1996). In our discussion, the regression method is used and common approaches deployed for the regression model are linear regression Healy and Westmacott (1956), non-parametric kernel regression Cheng (1994); Wang and Rao (2002), and semi-parametric regression Wang and Sun (2007).

Considering n nodes in a given network and dataset of the individual reception denoted as X_1, X_2, $\cdots$, X_n. Assuming i_{th} reception in missing the data, then one can construct a regression model from the observed data and given by:

$$X_i = \beta_0 + \beta_1 X_1 + \cdots + \beta_{i-1} X_{i-1} \qquad 1 \leq i \leq n. \tag{3.1}$$

where $\boldsymbol{\beta}$ are the regression coefficients estimated which is estimated using the model. From the resulting coefficient set $\hat{\boldsymbol{\beta}}$, the values of the missing data can be imputed.

Using formulation defined in Bindele and Adekpedjou (2018); Kim and Yu (2011), (3.1) can be rewritten as two random vectors with one x being fully observable and other y subject to missing data not at random. These two vectors are related in a regression model as

$$y_i = g\left(x_i, \boldsymbol{\beta}_0\right) + \zeta_i, \qquad 1 \leq i \leq n. \tag{3.2}$$

The estimation of regression parameters can be performed using the method of moments, least squares, least absolute deviation, maximum likelihood, and rank-based. The model should relate the missed observation as the function of the other observations

taking into account the model error, ζ. For the MNAR the observation of interest can be written as a convex combination of estimation for observation response missed and not missed.

Consider a communication system, whose received signal at the reception written as,

$$y_i = h.x_i + \eta_i \tag{3.3}$$

where, (x_i, y_i) are the transmitted and received signal over n time instance. h is the channel coefficient and η_i is the AWGN $\sim \left(0, \sigma^2\right)$. Assuming (x_i, y_i) over random sample of size n of the random vectors (X, Y) with distribution $F(x_i, y_i)$ where x_i is always observed and y_i observation subject to missingness. The missingness in the observation is assumed to be MNAR considering a targeted interference where the missing observation depends on the y_i value.

Let δ_i is missingness indicator for y_i, where

$$\delta_i = \begin{cases} 0, & \text{if } y_i \text{ is missing,} \\ 1, & \text{if } y_i \text{ is observed,} \end{cases}$$

and response of the missingness indication follows Bernoulli distribution with probability of observation π which depend on the value of y_i (MNAR), $\delta \sim Bernoulli(\pi)$. The missingness indicator is indepedent across all instances, δ_i is independent or δ_j, $\forall i \neq j$.

For the missing and observed instances of y_i,

$$P(y_i|x_i, \delta_i = 0) \qquad \text{for } y_i \text{ missing}$$

$$P(y_i|x_i, \delta_i = 1) \qquad \text{for } y_i \text{ observed}$$

The estimator under the MNAR condition can be obtained by

$$E(Y) = \frac{1}{n}\Sigma_{i=1}^{n}\{\delta_i y_i + (1-\delta_i)\,\hat{m}_0(x_i)\} \tag{3.4}$$

where $\hat{m}_0(x_i)$ is a consistent estimator of $m_0(x_i) = E\{yi|xi, \delta_i = 0\}$. $m_1(x_i)$ can be estimated using the observation, where as it is difficult to estimate with no (missed) observations.

To determine the conditional distribution for the missed observation, the following relationship is used:

$$P(y_i|x_i, \delta_i = 0) = P(y_i|x_i, \delta_i = 1) \cdot \frac{P(\delta_i = 0|x_i, y_i)/P(\delta_i = 1|x_i, y_i)}{P(\delta_i = 0|x_i)/P(\delta_i = 1|x_i)} \tag{3.5}$$

Assuming logistic regression model, Kim and Yu (2011)

$$P(\delta_i = 1|x_i, y_i) = \frac{exp\{g(x_i) + \phi y_i\}}{1 + exp\{g(x_i) + \phi y_i\}} \tag{3.6}$$

for some function $g(\cdot)$ and parameter ϕ.

Using 3.6, the conditional distribution of the missing observation can be written as

$$P(y_i|x_i, \delta_i = 0) = P(y_i|x_i, \delta_i = 1) \cdot \frac{exp(\gamma y_i)}{E\{exp(\gamma y_i)\,|x_i, \delta_i = 1\}} \tag{3.7}$$

$$f_0(y_i|x_i) = f_1(y_i|x_i) \cdot \frac{exp(\gamma y_i)}{E\{exp(\gamma y_i)\,|x_i, \delta_i = 1\}} \tag{3.8}$$

where $\gamma = -\phi$, and $f_0(y_i|x_i), f_1(y_i|x_i)$ are the probability density function of y_i given $x_i, \delta_i = 0$ and 1 respectively.

3.3. RESULTS

In this section, we discussing preliminary results analyzing MNAR in communication system.

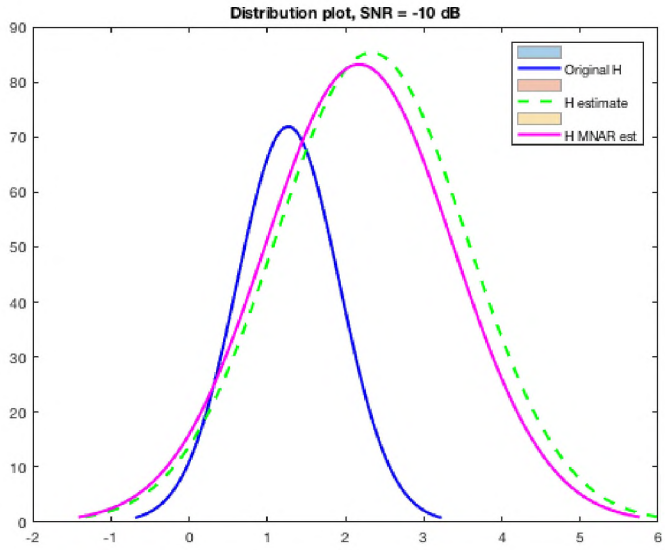

Figure 3.1. Comparison of MNAR and noise interference impact (SNR = -10 dB).

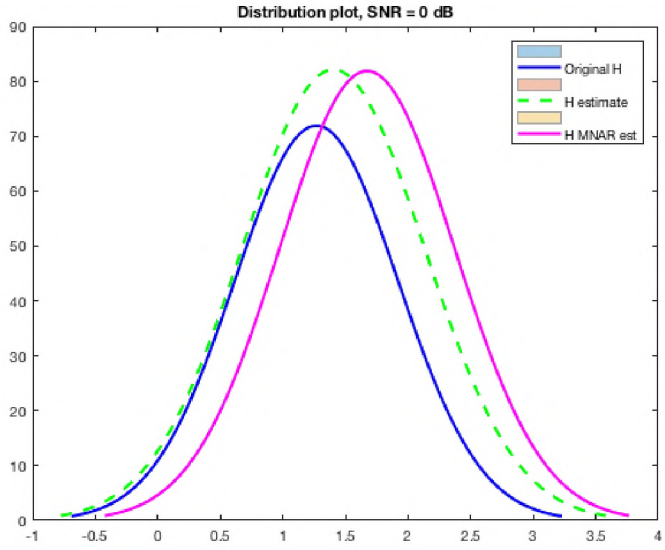

Figure 3.2. Comparison of MNAR and noise interference impact (SNR = 0 dB).

The distribution of the estimation channel coefficients was compared with the true value and the estimation of same the channel coefficients while suffering MNAR. Figures 3.1 to 3.3 show the distribution of the estimated channel coefficients approaches the MNAR

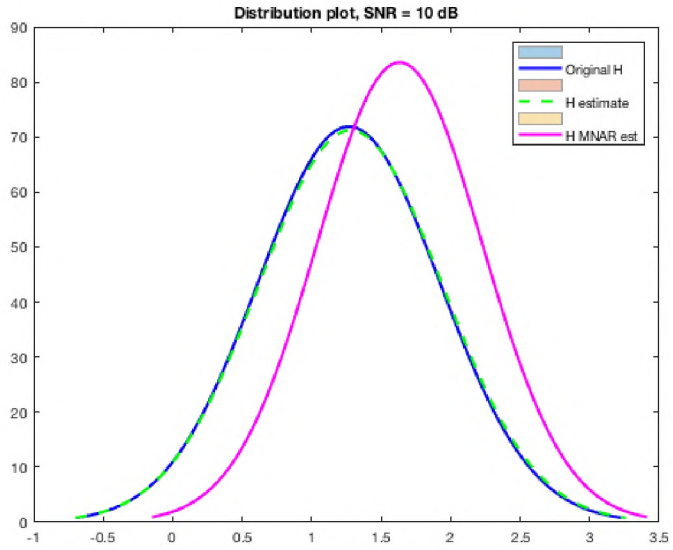

Figure 3.3. Comparison of MNAR and noise interference impact (SNR = 10 dB).

model with the increase in noise interference and provides a motivation towards correlating targeted interference to the response for missing observation occuring not at random (MNAR).

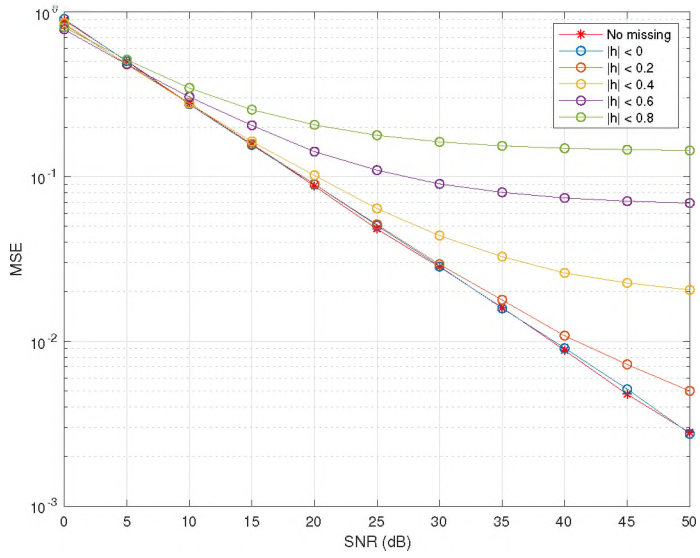

Figure 3.4. Degradation of channel estimate for different levels of interference.

The bias in the estimation with MNAR prevailing negatively impacts the performance of the estimator and cannot be ignored rather as to be mitigated.Figure 3.4 shows the degredation of the channel estimation as the threshold of the missingness increases and potentially affects the decoding of the data if the missingness ignored.

In the current work, the data missed during communication due to an external targeted interference to impede the communication can be treated as missing data not at random. The statistical tools used in statistical analysis responding to missing data not at random is proposed to estimate the lost data or extract information about the interference.

4. UPDATES

In this chapter, the updates beyond the publications to compare with other existing works. The updates include both for the presented heterogeneous mesh network and the proposed full-duplex methodology using orthogonal pilot sequences.

4.1. HETEROGENEOUS MESH NETWORK

The HetMeshNet Al-Saadi *et al.* (2016) comprises of Wi-Fi and LTE networks with cognitive framework employing cognitive heterogeneous routing (CHR) to forward the traffic from one congested cell to other noncongested cells to work as a single network. The routing protocol based on Q-learning dynamically selects the transmission interface (LTE, Wi-Fi) to increase and enhance the average throughput. Both the networks form a grid and distances are equivalent when scaled considering the coverage area of the nodes. The learning rate and discount value estimate the best action in the selection of interfaces for HetMeshNet. In addition to routing the HetMeshNet utilizes the unlicensed Wi-Fi frequencies.

The simulation results for 19 nodes in 4×5 grid with five LTE base stations with one at the center and four distributed around the grid. The simulation results of the average throughput of the network are compared excluding the utilization of unlicensed Wi-Fi frequencies by LTE. The results are tabulated and compared in Table 1.

The average throughput of the CHR with 50 RB (resource blocks) achieved is about 1.7 Mbps compared to the LTE network with 50 RB achieves 1.3 Mbps Al-Saadi *et al.* (2016). An improvement of about 26% whereas the proposed work without a routing algorithm achieves 23%. The results show the presented work with Wi-Fi and Bluetooth

Table 4.1. Comparison of the parameters and results of the presented network.

Parameter	HetMeshNet	Presented network
Number of hops	2 to 5	5
Maximum throughput	5 Mbps (LTE 50)	5.5 Mbps (Wi-Fi 802.11a)
Homogeneous avg. throughput	1.3 Mbps (LTE 50)	1.24 Mbps (Wi-Fi 802.11a)
Heterogeneous avg. throughput	1.7 Mbps (LTE 50 + Wi-Fi 802.11a + CHR)	1.53 Mbps (Wi-Fi 802.11a + Bluetooth + no routing)
% improvement	26%	23%

in smartphones achieves almost the same performance of HetMeshNet with fast LTE links. The Bluetooth links in the presented network present bottlenecks due to the lower capacity than that of Wi-Fi links.

4.2. FULL-DUPLEX COMMUNICATION

The frequency-domain least squares (FD-LS) estimator Shu *et al.* (2017) estimates both communication and self-interference (SI) channels and an estimator based on the expectation-maximization algorithm for relay systems Xiong *et al.* (2016). The results from the initial work using ML estimator Masmoudi and Le-Ngoc (2016) was also used to compare its performance with frequency selective fading channel.

Figure 4.1 shows the results of different methods with the proposed method. The proposed method and FD-LS estimator Shu *et al.* (2017) uses the orthogonal frequency division multiplexing (OFDM) system and exploits the time-domain property of the channel. It can be observed that the proposed method better with lower SNR, and both the methods converge as that SNR increases. The FD-LS estimator performs better for higher SNR due to increase channel information optimizing its pilot matrix. The result from the EM estimator Xiong *et al.* (2016) does not perform well compared to the proposed and FD-LS

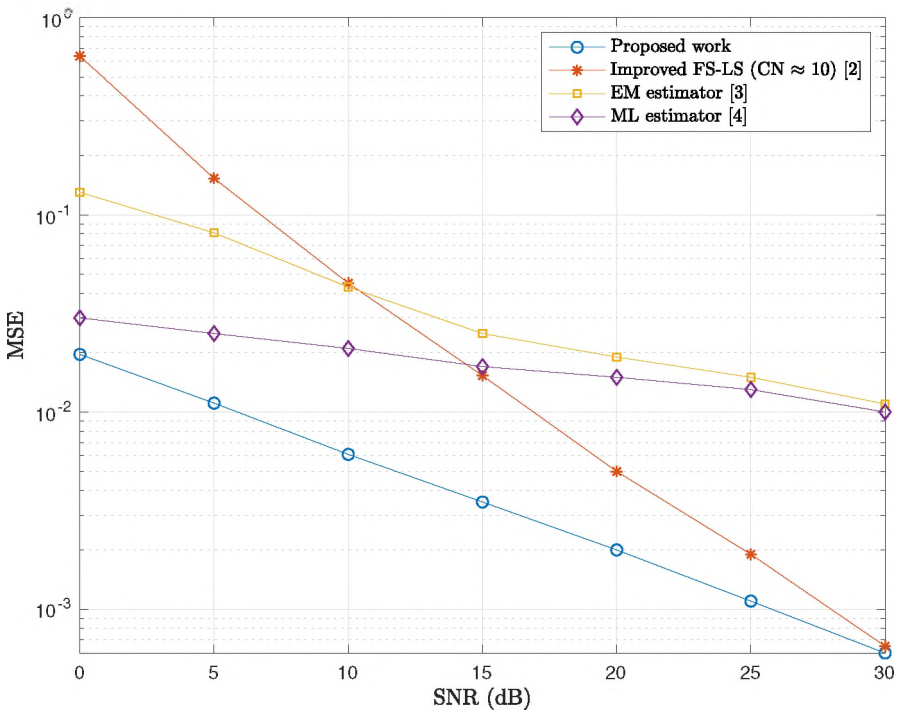

Figure 4.1. MSE of the channel estimates with different existing works.

estimator since it performs time-domain processing with time division duplexing (TDD). In addition, the results from the initial version for the proposed methodology is also presented for the same channel condition performed in time-domain.

The time-domain processing of a multitap channel are complex and it gets simple when performed in the frequency domain. The usage of OFDM, in particular, mitigates the multitap channel as a set of the flat-fading channel across each subcarrier. The orthogonal sequence is the key to the proposed method such that both self-interference and communication channels can be separated and estimated independently.

The results from Figure 4.1 also indicates the performance of the estimators depend on the channel model where the deployment of targeted learning to choose appropriate channel model that fits the data will improve the performance of the channel estimators.

The improvement of the full-duplex communication is illustrated using a Wi-Fi network as an example. The maximum peak throughput achieved for a Wi-Fi system operated in SISO 64 QAM with code rate 5/6 in half duplex is 55.6 Mbps whereas in full-duplex it is 118.1 Mbps. The maximum throughput achieved by full-duplex is nearly twice that of half-duplex. Though full-duplex communication resolves collision, still it suffers suffer self-interference and depends on the methodology to mitigate self-interference Song *et al.* (2017).

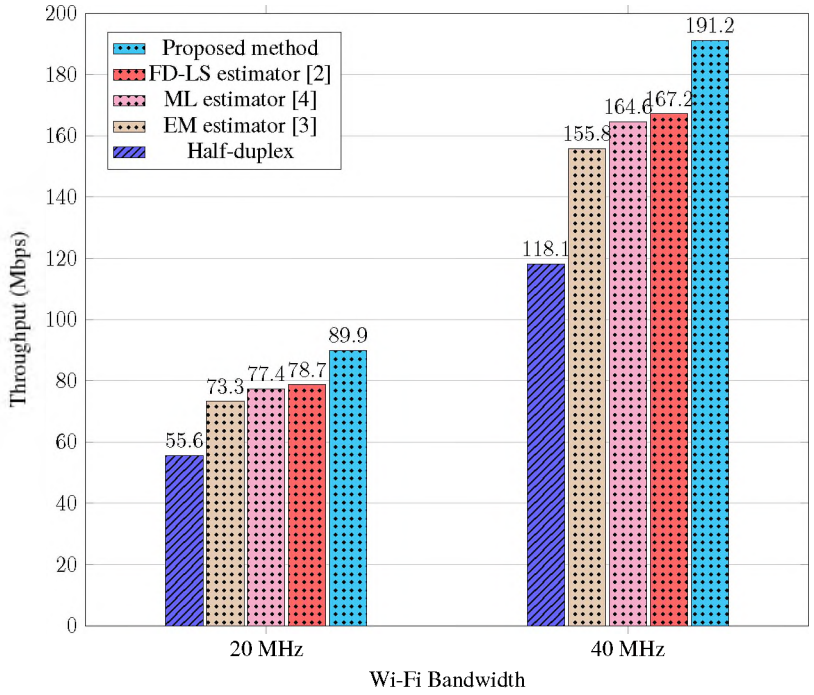

Figure 4.2. Throughput comparison of the different methods (SNR = 15 dB).

Figure 4.2 illustrates the throughput estimated using the channel estimation performance Li *et al.* (2018); Proakis (2008) of different channel estimators for fixed power constraint, SNR (15 dB), modulation, and fading environment (frequency selective channel).

The nodes in half-duplex operation take turns to communicate and wait for feedback from the neighboring nodes results in one-way data traffic. However, full-duplex operation allows simultaneous two-way data traffic where the nodes receives feedback while transmitting the data. In addition to two-way traffic, it mitigates the interference between the nodes in the network. The heterogeneous networks already shows the benefits of decoupling the channels minimizing the bandwidth split among the surrounding nodes. The full-duplex operation adds additional bandwidth to each of the link in the heterogeneous network improves the overall performance of the network. The proposed full-duplex methodology contribute 18% more bandwidth compared to the other listed methods and 62% more bandwidth compared to maximum throughput achieved by half-duplex operation for individual links with 15 dB SNR.

5. SUMMARY AND CONCLUSIONS

The presented research work aimed to build a wireless network that is well-connected covers a large area, easily scalable, and accommodate the growing number of users. Based on the analysis performed, a mesh network in full-duplex communication supported by the target learner in sync with the channel yields a desired wireless network. Each system contributes to the features of the envisioned wireless network. A heterogeneous mesh network can connect more devices with different interfaces compared to the homogeneous mesh network, and convergence devices are at the keys component of the network. The limitation of bandwidth resulting due to the increase in devices and the number of hops can be addressed by the full-duplex communication. The full-duplex doubles the spectral efficiency and potentially address interference among the nodes in the network. The existing platform such as USRPs can be used with the knowledge of their internal leakage provides a potential operation in full-duplex mode. The results from the proposed full-duplex model show the self-interference and communication channels can be estimated and can be used in the mitigation of self-interference. Finally, the channel model plays a critical role in determining the performance of the proposed full-duplex model which can be addressed using the target learner which identifies the best channel model from the pool of channel models.

The results show heterogeneous mesh network is more suitable for connecting more devices and extend the coverage over multiple hops whereas homogeneous mesh network is more suitable for a localized network such as a home network. The identification of bottlenecks in a heterogeneous mesh is very critical and might degrade the performance of the network. The increase in the number of devices with diverse interfaces increases the robustness of a heterogeneous mesh network which allows multiple contingency routes for a dynamic network.

The measurement results of the USRP family of devices shows the operating frequency range in which USRPs can be potentially deployed to operate in full-duplex mode. The limited range can be achieved without any additional schemes. The adaptive filtering shows promising results in mitigation of internal self-interference but more analysis to be performed to evaluate with both internal and external self-interference. The proposed use of the orthogonal pilot sequence enables both the separation and estimation of self-interference and communication channels. The performance of the channel estimator depends not only on the orthogonality of the sequences used but also on their correlation properties.

The preliminary analysis compares the performance of different channel models for different channel conditions. Based on the results of the parameters such as variance, bit-error rate can be used to evaluate the risk by the target learner. Also, the initial results show the correlation between the targeted interference with the response to the missing data not at random.

5.1. CONTRIBUTIONS

The contributions of the presented research work are as follows:

- The integration of different wireless interface/technologies resulting in convergence devices. This is achieved by the development of an Android application enabling the smartphone devices to become convergence devices. Then, a heterogeneous mesh network was built using these convergence devices.
- Characterized the internal self-interference suffered by family of USRP devices across their operating frequencies. Performed full-duplex operation and analyzed the impact of the internal self-interference on the performance of data decoding at the reception.
- Proposed a pilot-based channel estimation method using orthogonal sequences to separate and estimate the self-interference channel and the communication channel in a full-duplex communication.

- Derived the Cramer-Rao Lower Bound of the full-duplex channel estimators of the proposed method.
- Deployment of Targeted learning to identify and select the channel model from a set of methodologies that fits the current state of the channel.

5.2. FUTURE WORKS

In each section of the present research work, there is room for improvement in achieving the most desired wireless network. The addition of routing protocol to the current implementation of a heterogeneous mesh network enables to identify bottleneck links and have multiple contingency routes addressing route failure due to mobility. The implementation extended to multiple platforms such as iOS, Windows, Linux expanding the scope to include more devices to build a robust network. Next, is the implementation of the proposed full-duplex model in hardware platform using USRPs to evaluate the full-duplex operation. The formulation of the target learner with the identified parameters and also exploring other parameters for risk assessment to identify with the channel model best suited for the current channel condition. The evaluation of the proposed missing data not at random in response to the targeted interference and evaluation of the different estimators. Finally, integrating all the individual components, aiding each other to build the envisioned wireless network.

REFERENCES

'Stanford Information Networks Group Full-Duplex Wireless Design,' http://sing.stanford.edu/fullduplex, 2010.

'USRP inserts a peak in the carrier frequency,' https://www.ruby-forum.com/topic/4019305, 2012.

'WBX daughter card schematics,' https://files.ettus.com/schematics/wbx/WBX.pdf, 2012.

'Adaptive Noise Cancellation Using RLS Adaptive Filtering,' http://www.mathworks.com/help/dsp/examples/adaptive-noise-cancellation-using-rls-adaptive-filtering.html, 2013.

'Ettus Research, a National Instruments Company,' https://kb.ettus.com/Knowledge_Base, 2018.

'GNURadio,' https://wiki.gnuradio.org/index.php/Main_Page, 2018.

802.11s, 'IEEE Standard for Information Technology–Telecommunications and information exchange between systems–Local and metropolitan area networks–Specific requirements Part 11: Wireless LAN Medium Access Control (MAC) and Physical Layer (PHY) specifications Amendment 10: Mesh Networking,' 2011 pp. 1–372, doi:10.1109/IEEESTD.2011.6018236.

Abdelhalem, S., Gudem, P., and Larson, L., 'Hybrid Transformer-Based Tunable Differential Duplexer in a 90-nm CMOS Process,' Microwave Theory and Techniques, IEEE Transactions on, 2013, **61**, pp. 1316–1326, doi:10.1109/TMTT.2013.2243748.

Aghamohammadi, A., Meyr, H., and Ascheid, G., 'A New Method for Phase Synchronization and Automatic Gain Control of Linearly Modulated Signals on Frequency-Flat Fading Channels,' IEEE Transactions on Communications, 1991, **39**(1), pp. 25–29, ISSN 00906778, doi:10.1109/26.68273.

Al-Saadi, A., Setchi, R., Hicks, Y., and Allen, S. M., 'Routing protocol for heterogeneous wireless mesh networks,' IEEE Transactions on Vehicular Technology, 2016, **65**(12), pp. 9773–9786, ISSN 00189545, doi:10.1109/TVT.2016.2518931.

Alam, M. N., Jntti, R., Kneckt, J., and Nieminen, J., 'Performance Study of IEEE 802.11s PSM in FTP-TCP,' in '2012 IEEE Vehicular Technology Conference (VTC Fall),' 2012 pp. 1–5, doi:10.1109/VTCFall.2012.6398931.

Alexandris, K., Balatsoukas-Stimming, A., and Burg, A., 'Measurement-based characterization of residual self-interference on a full-duplex MIMO testbed,' in '2014 IEEE 8th Sensor Array and Multichannel Signal Processing Workshop (SAM),' ISSN 1551-2282, 2014 pp. 329–332, doi:10.1109/SAM.2014.6882408.

AmpliSine Labs LLC, 'NEED Help website,' http://amplisinelabs.com/, 2018.

B210-RFswitch, 'SKY13335-381LF: 0.1-6GHz GaAs SPDT Switch,' https://www.skyworksinc.com/-/media/SkyWorks/Documents/Products/301-400/SKY13335_381LF_201093D.pdf, 2014.

BATMAN, 'Better approach to mobile ad-hoc networking,' https://www.open-mesh.org/projects/open-mesh/wiki, 2017.

Beamforming, S.-i. C., Dastjerdi, M. B., Reiskarimian, N., Chen, T., Zussman, G., and Krishnaswamy, H., 'Full Duplex Circulator-Receiver Phased Array Employing,' i, IEEE, ISBN 9781538645451, 2018 pp. 108–111.

Beasley, P. D. L., Stove, A. G., Reits, B. J., and As, B., 'Solving the problems of a single antenna frequency modulated CW radar,' in 'IEEE International Conference on Radar,' 1990 pp. 391–395.

Bharadia, D., McMilin, E., and Katti, S., 'Full duplex radios,' ACM SIGCOMM Computer Communication Review, 2013, **43**(4), pp. 375–375–386–386, ISSN 0146-4833, doi:10.1145/2534169.2486033.

Bickel, P., Klaassen, C., and Ritov, J., Y.and Wellner, *Efficient and Adaptive Estimation for Semiparametric Models*, Springer-Verlag New York, 1998, ISBN 978-0-387-98473-5.

Bindele, H. F. and Adekpedjou, A., 'Rank-based inference with responses missing not at random,' Canadian Journal of Statistics, 2018, **46**(3), pp. 501–528, ISSN 1708945X, doi:10.1002/cjs.11466.

Bojja Venkatakrishnan, S., Alwan, E. A., and Volakis, J. L., 'Wideband rf self-interference cancellation circuit for phased array simultaneous transmit and receive systems,' IEEE Access, 2018, **6**, pp. 3425–3432, ISSN 2169-3536, doi:10.1109/ACCESS.2017.2788179.

Buračas, G. T. and Boynton, G. M., 'Efficient design of event-related fMRI experiments using m-sequences,' NeuroImage, 2002, **16**(3 I), pp. 801–813, ISSN 10538119, doi:10.1006/nimg.2002.1116.

Cao, L., Chen, C. W., Orlik, P., Zhang, J., and Gu, D., 'A trellis-based technique for blind channel estimation and equalization,' Journal of Communications and Networks, 2004, **6**(1), pp. 19–25, ISSN 1229-2370, doi:10.1109/JCN.2004.6596983.

Carrano, R. C., Magalhaes, L. C. S., Saade, D. C. M., and Albuquerque, C. V. N., 'IEEE 802.11s Multihop MAC: A Tutorial,' volume 13, ISSN 1553-877X, 2011 pp. 52–67, doi:10.1109/SURV.2011.040210.00037.

Cavers, J. K., 'An Analysis of Pilot Symbol Assisted Modulation for Rayleigh Fading Channels,' IEEE Transactions on Vehicular Technology, 1991, **40**(4), pp. 686–693, ISSN 0018-9545, doi:10.1109/25.108378.

Chandran, A. M. M. and Zawodniok, M., 'Transmitter leakage analysis when operating USRP (N210) in duplex mode,' in '2015 IEEE International Instrumentation and Measurement Technology Conference (I2MTC) Proceedings,' ISSN 1091-5281, 2015 pp. 340–345, doi:10.1109/I2MTC.2015.7151291.

Cheng, P. E., 'Nonparametric estimation of mean functionals with data missing at random,' Journal of the American Statistical Association, 1994, **89**(425), pp. 81–87, ISSN 01621459.

Chhabra, G., Vashisht, V., and Ranjan, J., 'A classifier ensemble machine learning approach to improve efficiency for missing value imputation,' 2018 International Conference on Computing, Power and Communication Technologies, GUCON 2018, 2019, pp. 23–27, doi:10.1109/GUCON.2018.8674904.

Choi, J. I., Jain, M., Srinivasan, K., Levis, P., and Katti, S., 'Achieving Single Channel, Full Duplex Wireless Communication,' in 'Proceedings of the Sixteenth Annual International Conference on Mobile Computing and Networking,' MobiCom '10, ACM, New York, NY, USA, ISBN 978-1-4503-0181-7, 2010 pp. 1–12, doi:10.1145/1859995.1859997.

Chu, T. M. C. and Zepernick, H. J., 'Performance of a Non-Orthogonal Multiple Access System with Full-Duplex Relaying,' IEEE Communications Letters, 2018, **22**(10), pp. 2084–2087, ISSN 15582558, doi:10.1109/LCOMM.2018.2852308.

Collins, L. M., Schafer, J. L., and Kam, C.-M., 'A comparison of inclusive and restrictive strategies in modern missing data procedures.' 2001, doi:10.1037/1082-989X.6.4.330.

Deng, S., Samimi, M. K., and Rappaport, T. S., '28 GHz and 73 GHz millimeter-wave indoor propagation measurements and path loss models,' in '2015 IEEE International Conference on Communication Workshop (ICCW),' 2015 pp. 1244–1250, doi:10.1109/ICCW.2015.7247348.

Dey, S., Kamal, M. N., Dutta, S., Tiwari, A., Ray, S., Moatasimbillah, M. J., Saha, N., Adhikary, N., Mukherjee, D., Nayak, S., Dey, R., and Saha, S., 'Ad-hoc networked UAVs as Aerial Mesh Network for disaster management application and remote sensing: An approach,' in '2017 8th IEEE Annual Information Technology, Electronics and Mobile Communication Conference (IEMCON),' 2017 pp. 301–304, doi:10.1109/IEMCON.2017.8117231.

Ding, Z., Fan, P., and Poor, H. V., 'On the coexistence between full-duplex and NOMA,' IEEE Wireless Communications Letters, 2018, **7**(5), pp. 692–695, ISSN 21622345, doi:10.1109/LWC.2018.2811492.

Dobre, E. I., Marţian, A., and Vlădeanu, C., 'USRP-based experimental platform for energy detection in cognitive radio systems,' in '2016 International Conference on Communications (COMM),' 2016 pp. 185–188, doi:10.1109/ICComm.2016.7528275.

Dominicis, C. M. D., Ferrari, P., Sisinni, E., Flammini, A., Pivato, P., and Macii, D., 'Timestamping performance analysis of ieee 802.15.4a systems based on sdr platforms,' in '2012 IEEE International Instrumentation and Measurement Technology Conference Proceedings,' ISSN 1091-5281, 2012 pp. 2034–2039, doi: 10.1109/I2MTC.2012.6229356.

Dong, Y. and Peng, C. Y. J., 'Principled missing data methods for researchers,' SpringerPlus, 2013, **2**(1), pp. 1–17, ISSN 21931801, doi:10.1186/2193-1801-2-222.

Duarte, M., Dick, C., and Sabharwal, A., 'Experiment-driven characterization of full-duplex wireless systems,' IEEE Transactions on Wireless Communications, 2012, **11**(12), pp. 4296–4307, ISSN 15361276, doi:10.1109/TWC.2012.102612.111278.

Duarte, M. and Sabharwal, A., 'Full-duplex wireless communications using off-the-shelf radios: Feasibility and first results,' in '2010 Conference Record of the Forty Fourth Asilomar Conference on Signals, Systems and Computers,' 2010 pp. 1558–1562.

E310-RFswitch, 'SKY13373-460LF: 0.1-6GHz SP3T Switch,' https://www.skyworksinc.com/-/media/SkyWorks/Documents/Products/601-700/SKY13373_460LF_201264N.pdf, 2016.

Elahi, E., Qayyum, A., and Naz, S., 'The effect of payload length on QoS in IEEE 802.11s Wireless Mesh Networks,' in '2012 18th IEEE International Conference on Networks (ICON),' 2012 pp. 70–73, doi:10.1109/ICON.2012.6506536.

Ferranti, L., D'Oro, S., Bonati, L., Demirors, E., Cuomo, F., and Melodia, T., 'Hiro-net: Self-organized robotic mesh networking for internet sharing in disaster scenarios,' in '2019 IEEE 20th International Symposium on "A World of Wireless, Mobile and Multimedia Networks" (WoWMoM),' 2019 pp. 1–9, doi:10.1109/WoWMoM.2019.8793029.

Figwer, J., Michalczyk, M., and Główka, T., 'Accelerating the rate of convergence for LMS-like on-line identification and adaptation algorithms. Part 1: Basic ideas,' 2017 22nd International Conference on Methods and Models in Automation and Robotics, MMAR 2017, 2017, **0**(1), pp. 347–350, doi:10.1109/MMAR.2017.8046851.

Frotzscher, A. and Fettweis, G., 'Baseband analysis of TX leakage in WCDMA Zero-IF-receivers,' in '2008 3rd International Symposium on Communications, Control and Signal Processing,' 2008 pp. 129–134.

Frotzscher, A. and Fettweis, G., 'Digital compensation of transmitter leakage in FDD zero-IF receivers,' European Transactions on Telecommunications, 2012, **23**, pp. 105–120, doi:10.1002/ett.1514.

Gaeddert, J. and Annamalai, A., 'New estimators for the weibull fading parameters,' in 'VTC-2005-Fall. 2005 IEEE 62nd Vehicular Technology Conference, 2005.', volume 2, ISSN 1090-3038, 2005 pp. 1367–1371, doi:10.1109/VETECF.2005.1558150.

Ghannouchi, F. M. and Kwan, A. K., 'Software defined radio subsampling receiver for wireless monitoring and sensing medical applications,' in '2015 IEEE International Conference on Ubiquitous Wireless Broadband (ICUWB),' ISSN 2162-6588, 2015 pp. 1–5, doi:10.1109/ICUWB.2015.7324513.

Ghavami, K. and Naraghi-Pour, M., 'Blind Channel Estimation and Symbol Detection for Multi-Cell Massive MIMO Systems by Expectation Propagation,' IEEE Transactions on Wireless Communications, 2018, **17**(2), pp. 943–954, ISSN 1536-1276, doi:10.1109/TWC.2017.2772837.

goTennaMESH, 'Gotennamesh,' https://gotennamesh.com/, 2008.

Guo, H., Xu, J., Zhu, S., and Wu, S., 'Realtime Software Defined Self-Interference Cancellation Based on Machine Learning for In-Band Full Duplex Wireless Communications,' in '2018 International Conference on Computing, Networking and Communications (ICNC),' 2018 pp. 779–783, doi:10.1109/ICCNC.2018.8390351.

Healy, M. and Westmacott, M., 'Missing values in experiments analysed on automatic computers,' Journal of the Royal Statistical Society. Series C (Applied Statistics), 1956, **5**(3), pp. 203–206, ISSN 00359254, 14679876.

Heitjan, D. F. and Little, R. J. A., 'Multiple imputation for the fatal accident reporting system,' Journal of the Royal Statistical Society. Series C (Applied Statistics), 1991, **40**(1), pp. 13–29, ISSN 00359254, 14679876.

Hemadeh, I. A., Satyanarayana, K., El-Hajjar, M., and Hanzo, L., 'Millimeter-Wave Communications: Physical Channel Models, Design Considerations, Antenna Constructions, and Link-Budget,' IEEE Communications Surveys and Tutorials, 2018, **20**(2), pp. 870–913, ISSN 1553877X, doi:10.1109/COMST.2017.2783541.

Hou, X., Gao, C., Zhu, Y., and Yang, S., 'Detection of active attacks based on random orthogonal pilots,' ISBN 9781509028603, 2016 doi:10.1109/WCSP.2016.7752543.

Hua, Y. K. and Chang, W., 'Time Shifted Pilots Scheme for Full-Duplex Massive MIMO Systems,' IEEE Transactions on Vehicular Technology, 2019, **68**(3), pp. 3022–3026, ISSN 00189545, doi:10.1109/TVT.2019.2893547.

Hussain, N., Ziri-Castro, K., Jayalath, D., and Arafah, M., 'Experimental Evaluation of DCOOP Protocol Using USRP-RIO Based Testbed at 5.8 GHz,' in '2016 IEEE 84th Vehicular Technology Conference (VTC-Fall),' 2016 pp. 1–6, doi:10.1109/VTCFall.2016.7881005.

Imboden, T., Akkaya, K., and Moore, Z., 'Performance evaluation of wireless mesh networks using IEEE 802.11s and IEEE 802.11n,' in '2012 IEEE International Conference on Communications (ICC),' 2012 pp. 5675–5679, doi:10.1109/ICC.2012.6364932.

Jain, M., Choi, J. I., Kim, T., Bharadia, D., Seth, S., Srinivasan, K., Levis, P., Katti, S., and Sinha, P., 'Practical, real-time, full duplex wireless,' in 'Proceedings of the 17th annual international conference on Mobile computing and networking - MobiCom '11,' ACM Press, New York, New York, USA, ISBN 9781450304924, 2011 p. 301, doi:10.1145/2030613.2030647.

Jiang, Z., He, Z., Chen, S., Molisch, A. F., Zhou, S., and Niu, Z., 'Inferring Remote Channel State Information: Crame r-Rae Lower Bound and Deep Learning Implementation,' 2018 IEEE Global Communications Conference, GLOBECOM 2018 - Proceedings, 2019, pp. 1–7, doi:10.1109/GLOCOM.2018.8648140.

Joo, J., Park, M. C., Han, D. S., and Pejovic, V., 'Deep Learning-Based Channel Prediction in Realistic Vehicular Communications,' IEEE Access, 2019, **7**, pp. 27846–27858, ISSN 21693536, doi:10.1109/ACCESS.2019.2901710.

Jung, J., Roh, H., Kim, J., Kwak, H., Jeong, M. S., and Park, J., 'TX Leakage Cancellation via a Micro Controller and High TX-to-RX Isolations Covering an UHF RFID Frequency Band of 908–914 MHz,' IEEE Microwave and Wireless Components Letters, 2008, **18**(10), pp. 710–712.

Kawadia, V., Zhang, Y., and Gupta, B., 'System services for implementing ad-hoc routing protocols,' in 'Proceedings. International Conference on Parallel Processing Workshop,' 2002 pp. 135–142, doi:10.1109/ICPPW.2002.1039723.

Kay, S. M., 'Fundamentals of statistical signal processing,' Prentice Hall Signal Processing Series, 1993, ISSN 00401706, doi:10.2307/1269750.

Keating, R., Ratasuk, R., and Ghosh, A., 'Performance analysis of full duplex in cellular systems,' IEEE Vehicular Technology Conference, 2016, **2016-July**(5GArch), ISSN 15502252, doi:10.1109/VTCSpring.2016.7504406.

Khaledian, S., Farzami, F., Smida, B., and Erricolo, D., 'Inherent self-interference cancellation at 900 MHz for in-band full-duplex applications,' 2018 IEEE 19th Wireless and Microwave Technology Conference, WAMICON 2018, 2018, pp. 1–4, ISSN 00189480, doi:10.1109/WAMICON.2018.8363897.

Kiayani, A., Anttila, L., and Valkama, M., 'Modeling and dynamic cancellation of TX-RX leakage in FDD transceivers,' in '2013 IEEE 56th International Midwest Symposium on Circuits and Systems (MWSCAS),' 2013 pp. 1089–1094.

Kim, D., Ju, H., Park, S., and Hong, D., 'Effects of channel estimation error on full-duplex two-way networks,' IEEE Transactions on Vehicular Technology, 2013, **62**(9), pp. 4666–4672, ISSN 00189545, doi:10.1109/TVT.2013.2265407.

Kim, H., Woo, S., Jung, S., and Lee, K., 'A CMOS Transmitter Leakage Canceller for WCDMA Applications,' IEEE Transactions on Microwave Theory and Techniques, 2013, **61**(9), pp. 3373–3380.

Kim, J. K. and Yu, C. L., 'A semiparametric estimation of mean functionals with nonignorable missing data,' Journal of the American Statistical Association, 2011, **106**(493), pp. 157–165, ISSN 01621459, doi:10.1198/jasa.2011.tm10104.

Korpi, D., Aghababaeetafreshi, M., Piilila, M., Anttila, L., and Valkama, M., 'Advanced architectures for self-interference cancellation in full-duplex radios: Algorithms and measurements,' i, ISBN 9781538639542, ISSN 10586393, 2017 pp. 1553–1557, doi:10.1109/ACSSC.2016.7869639.

Korpi, D., Anttila, L., and Valkama, M., 'Reference receiver based digital self-interference cancellation in MIMO full-duplex transceivers,' 2014 IEEE Globecom Workshops, GC Wkshps 2014, 2014, pp. 1001–1007, ISSN 16871499, doi:10.1109/GLOCOMW.2014.7063564.

L. Weizheng, T. X., 'Throughput Analysis of Full-Duplex Network Coding in Two-Way Relay Channel,' IEEE International Conference on Communication Technology, 2017, pp. 85–90.

Lahouli, R., Ben-Romdhane, M., Rebai, C., and Dallet, D., 'Towards flexible parallel sigma delta modulator for software defined radio receiver,' in '2014 IEEE International Instrumentation and Measurement Technology Conference (I2MTC) Proceedings,' ISSN 1091-5281, 2014 pp. 1041–1046, doi:10.1109/I2MTC.2014.6860901.

Lee, D. and Byung-Wook, '2X2 MIMO in-band full-duplex radio front-end with 50 dB self-interference cancellation in 90 MHz bandwidt,' IEEE MTT-S International Microwave Symposium Digest, 2017, pp. 670–672, ISSN 0149645X, doi:10.1109/MWSYM.2017.8058658.

Li, C., Xia, B., Jiang, Q., Yao, Y., and Yang, G., 'Achievable rate of the multiuser two-way full-duplex relay system,' IEEE Transactions on Vehicular Technology, 2018, **67**(5), pp. 4650–4654.

Li, S. and Murch, R. D., 'Full-Duplex Wireless Communication Using Transmitter Output Based Echo Cancellation,' in '2011 IEEE Global Telecommunications Conference - GLOBECOM 2011,' 2011 pp. 1–5.

Li, Y., Sun, L., Zhao, C., and Huang, L., 'A Digital Self-interference Cancellation algorithm based on Spectral Estimation in Co-time Co- frequency Full Duplex System,' 2015 10th International Conference on Computer Science & Education (ICCSE), 2015, **1**(Iccse), pp. 412–415, doi:10.1109/ICCSE.2015.7250280.

Liu, D., Shen, Y., Shao, S., Tang, Y., and Gong, Y., 'On the Analog Self-Interference Cancellation for Full-Duplex Communications with Imperfect Channel State Information,' IEEE Access, 2017, **5**, pp. 9277–9290, ISSN 21693536, doi:10.1109/ACCESS.2017.2702713.

Liu, J., Mei, K., Zhang, X., Ma, D., and Wei, J., 'Online Extreme Learning Machine-based Channel Estimation and Equalization for OFDM Systems,' IEEE Communications Letters, 2019, **PP**(X), pp. 1–1, ISSN 1089-7798, doi:10.1109/lcomm.2019.2916797.

Loon LLC., 'Project loon,' https://loon.com/technology/, 2017.

Luan, Z., Qu, H., Zhao, J., and Chen, B., 'Robust digital non-linear self-interference cancellation in full duplex radios with maximum correntropy criterion,' China Communications, 2016, **13**(9), pp. 53–59, ISSN 16735447, doi:10.1109/CC.2016.7582296.

Mahmood, S. H., Salih, A. M., and Khalil, M. I., 'Broadband services on power line communication systems: A review,' in '2019 22nd International Conference on Control Systems and Computer Science (CSCS),' ISSN 2379-0482, 2019 pp. 465–470, doi:10.1109/CSCS.2019.00085.

Makled, E. A., Yadav, A., Dobre, O. A., and Haynes, R. D., 'Hierarchical Full-Duplex Underwater Acoustic Network: A NOMA Approach,' OCEANS 2018 MTS/IEEE Charleston, OCEAN 2018, 2019, pp. 1–6, doi:10.1109/OCEANS.2018.8604904.

Mark Zuckerberg, 'The technology behind aquila,' https://www.facebook.com/notes/mark-zuckerberg/the-technology-behind-aquila/10153916136506634/, 2016.

Masmoudi, A. and Le-Ngoc, T., 'A Maximum-Likelihood Channel Estimator for Self-Interference Cancelation in Full-Duplex Systems,' IEEE Transactions on Vehicular Technology, 2016, **65**(7), pp. 5122–5132, ISSN 00189545, doi:10.1109/TVT.2015.2461006.

Miura, R., Inoue, M., Owada, Y., Takizawa, K., Ono, F., Suzuki, M., Tsuji, H., and Hamaguchi, K., 'Disaster-resilient wireless mesh network - experimental test-bed and demonstration,' in '2013 16th International Symposium on Wireless Personal Multimedia Communications (WPMC),' 2013 pp. 1–4.

Mohammadi, M., Shi, X., Chalise, B. K., Ding, Z., Suraweera, H. A., Zhong, C., and Thompson, J. S., 'Full-Duplex Non-Orthogonal Multiple Access for Next Generation Wireless Systems,' IEEE Communications Magazine, 2019, **57**(5), pp. 110–116, ISSN 15581896, doi:10.1109/MCOM.2019.1800578.

Muradi, V. S., Paithane, R. K., Ahmed, A., and Pawar, A., 'Spectrum sensing in cognitive radio using Labview and NI USRP,' in '2018 2nd International Conference on Inventive Systems and Control (ICISC),' ISSN null, 2018 pp. 1316–1319, doi:10.1109/ICISC.2018.8399019.

N210-RFswitch, 'HMC174MS8/174MS8E,' http://www.analog.com/media/en/technical-documentation/data-sheets/hmc174.pdf, 2012, rev. 04.0109.

Necker, M. C. and Stuber, G. L., 'Totally blind channel estimation for OFDM on fast varying mobile radio channels,' IEEE Transactions on Wireless Communications, 2004, **3**(5), pp. 1514–1525, ISSN 1536-1276, doi:10.1109/TWC.2004.833508.

Ngo, T., Nishiyama, H., Kato, N., Shimizu, Y., Mizuno, K., and Kumagai, T., 'On the throughput evaluation of wireless mesh network deployed in disaster areas,' in '2013 International Conference on Computing, Networking and Communications (ICNC),' 2013 pp. 413–417, doi:10.1109/ICCNC.2013.6504119.

Price, N. D. and Chandran, A. M. M., 'Performance of ieee 802.11s for wireless mesh telemetry networks,' 2017.

Proakis, J., *Digital Communications*, 5th edition, 2008, ISBN 978-0072957167.

Rethfeldt, M., Danielis, P., Beichler, B., Konieczek, B., Uster, F., and Timmermann, D., 'Evaluating Cross-Layer Cooperation of Congestion and Flow Control in IEEE 802.11s Networks,' in '2016 IEEE 30th International Conference on Advanced Information Networking and Applications (AINA),' 2016 pp. 181–188, doi:10.1109/AINA.2016.12.

RFC3561, 'Ad hoc On-Demand Distance Vector (AODV) Routing,' https://datatracker.ietf.org/doc/rfc3561/, 2017.

RFC3626, 'Optimized Link State Routing Protocol (OLSR),' https://datatracker.ietf.org/doc/rfc3626/, 2017.

RFC4728, 'The Dynamic Source Routing Protocol (DSR) for Mobile Ad Hoc Networks for IPv4,' https://datatracker.ietf.org/doc/rfc4728/, 2017.

Ridwan, M. A., Radzi, N. A. M., Abdullah, F., Din, N. M., and Al-Mansoori, M. H., 'Fiber wireless testbed using universal software radio peripheral (usrp),' in '2016 IEEE Region 10 Conference (TENCON),' 2016 pp. 3601–3604, doi:10.1109/TENCON.2016.7848729.

Rowell, D., 'Introduction to Recursive-Least-Squares(RLS) Adaptive Filters,' 2008.

Rubin, D. B., 'Inference and missing data,' Biometrika, 1976, **63**(3), pp. 581–592, ISSN 0006-3444, doi:10.1093/biomet/63.3.581, with comments by R. J. A. Little and a reply by the author.

Rubin, D. B., *Multiple Imputation for Nonresponse in Surveys*, John Wiley, 1987.

Saafan, A. M. and El-Badawy, H. M., 'Automated testbed for spectrum allocation in hostile environment based on usrp cognitive radio system,' in '2017 34th National Radio Science Conference (NRSC),' 2017 pp. 178–185, doi:10.1109/NRSC.2017.7893502.

Saci, A., Al-Dweik, A., Shami, A., and Iraqi, Y., 'One-Shot Blind Channel Estimation for OFDM Systems Over Frequency-Selective Fading Channels,' IEEE Transactions on Communications, 2017, **65**(12), pp. 5445–5458, ISSN 0090-6778, doi:10.1109/TCOMM.2017.2740925.

Samimi, M. K., MacCartney, G. R., Sun, S., and Rappaport, T. S., '28 GHz Millimeter-Wave Ultrawideband Small-Scale Fading Models in Wireless Channels,' in '2016 IEEE 83rd Vehicular Technology Conference (VTC Spring),' 2016 pp. 1–6, doi: 10.1109/VTCSpring.2016.7503970.

Samimi, M. K. and Rappaport, T. S., 'Local multipath model parameters for generating 5G millimeter-wave 3GPP-like channel impulse response,' in '2016 10th European Conference on Antennas and Propagation (EuCAP),' 2016 pp. 1–5, doi:10.1109/EuCAP.2016.7481410.

Sampei, S., Sunaga, T., and Introduction, I., 'In Land Mobile Radio Communications,' IEEE Transactions on Vehicular Technology, 1993, **42**(2).

Sarangapani, J., *Wireless Ad Hoc and Sensor Networks: Protocols, Performance, and Control*, Control Engineering Series, CRC Press Taylor & Francis Group, LLC, Boca Raton, FL, 2007, ISBN 0-8247-2675-8.

Schenker, N. and Taylor, J. M., 'Partially parametric techniques for multiple imputation,' Computational Statistics and Data Analysis, 1996, **22**(4), pp. 425 – 446, ISSN 0167-9473, doi:https://doi.org/10.1016/0167-9473(95)00057-7.

Senol, H., Li, X., and Tepedelenlioglu, C., 'Rapidly time-varying channel estimation for full-duplex amplify-and-forward one-way relay networks,' IEEE Transactions on Signal Processing, 2018, **66**(11), pp. 3056–3069, ISSN 1053587X, doi:10.1109/TSP.2018.2824254.

Shahin, N., LaSorte, N. J., Rajab, S. A., and Refai, H. H., '802.11g channel characterization utilizing labview and NI-USRP,' in '2013 IEEE International Instrumentation and Measurement Technology Conference (I2MTC),' ISSN 1091-5281, 2013 pp. 753–756, doi:10.1109/I2MTC.2013.6555516.

Shammaa, M., Vogt, H., El-Mahdy, A., and Sezgin, A., 'Adaptive Self-Interference Cancellation for Full Duplex Systems with Auxiliary Receiver,' 2019 International Conference on Advanced Communication Technologies and Networking (CommNet), 2019, pp. 1–8, doi:10.1109/commnet.2019.8742358.

Shu, F., Wang, J., Li, J., Chen, R., and Chen, W., 'Pilot Optimization, Channel Estimation, and Optimal Detection for Full-Duplex OFDM Systems with IQ Imbalances,' IEEE Transactions on Vehicular Technology, 2017, **66**(8), pp. 6993–7009, ISSN 00189545, doi:10.1109/TVT.2017.2667686.

Song, L., Liao, Y., and Song, L., 'Handbook of Cognitive Radio,' Handbook of Cognitive Radio, 2017, pp. 1–27, doi:10.1007/978-981-10-1389-8.

Sugita, M., Matsue, H., Yamaguchi, K., Shimodaira, T., Shirotori, M., and Nanamatsu, S., 'Development strategy of disaster-resistant wifi mesh networks and the disaster monitoring and reporting system in a local area,' in '2015 International Conference on Information Networking (ICOIN),' 2015 pp. 139–144, doi:10.1109/ICOIN.2015.7057871.

The Weather Company - IBM, 'A new era of alerting,' https://weather.com/apps/ibm/meshnetworkalerts, 2017.

Tian, L., Wang, S., Cheng, Z., and Bu, X., 'All-digital self-interference cancellation in zero-IF full-duplex transceivers,' China Communications, 2016, **13**(11), pp. 27–34, ISSN 16735447, doi:10.1109/CC.2016.7781715.

Tong, Z., Russ, C., Vanka, S., and Haenggi, M., 'Prototype of Virtual Full Duplex via Rapid On-Off-Division Duplex,' IEEE Transactions on Communications, 2015, **63**(10), pp. 3829–3841, doi:10.1109/TCOMM.2015.2465958.

Tzeremes, G. and Christodoulou, C. G., 'Use of weibull distribution for describing outdoor multipath fading,' in 'IEEE Antennas and Propagation Society International Symposium (IEEE Cat. No.02CH37313),' volume 1, 2002 pp. 232–235 vol.1, doi:10.1109/APS.2002.1016291.

van der Laan, M. J., 'Targeted maximum likelihood based causal inference. I,' Int. J. Biostat., 2010a, **6**(2), pp. Art. 2, 44, ISSN 1557-4679.

van der Laan, M. J., 'Targeted maximum likelihood based causal inference. II,' Int. J. Biostat., 2010b, **6**(2), pp. Art. 3, 33, ISSN 1557-4679.

van der Laan, M. J. and Rose, S., *Targeted Learning - Causal Inference for Observational and Experimental Data*, Springer, 2010, ISBN 9780387775005, doi:10.1007/978-0-387-98135-2.

van der Laan, M. J. and Rose, S., *Targeted Learning in Data Science - Causal Inference for Complex Longitudinal Studies*, Springer, 2018, ISBN 978-3-319-65303-7, doi:10.1007/978-3-319-65304-4.

van der Laan, M. J. and Rubin, D., 'Targeted maximum likelihood learning,' Int. J. Biostat., 2006, **2**, pp. Art. 11, 40, ISSN 1557-4679, doi:10.2202/1557-4679.1043.

Voet, K. and Moer, W. V., 'Design of a software-defined radio for use in the IEEE L- and S-band,' in '2011 IEEE International Instrumentation and Measurement Technology Conference,' ISSN 1091-5281, 2011 pp. 1–4, doi:10.1109/IMTC.2011.5944002.

Wang, H., Huang, Y., Jin, S., Du, Y., and Yang, L., 'Pilot contamination reduction in multi-cell TDD systems with very large MIMO arrays,' Wireless Personal Communications, 2017, **96**(4), pp. 5785–5808, ISSN 1572-834X, doi:10.1007/s11277-017-4447-1.

Wang, J. C. P., Hagelstein, B., and Abolhasan, M., 'Experimental evaluation of IEEE 802.11s path selection protocols in a mesh testbed,' in '2010 4th International Conference on Signal Processing and Communication Systems,' 2010 pp. 1–3, doi:10.1109/ICSPCS.2010.5709664.

Wang, Q. and Rao, J. N. K., 'Empirical likelihood-based inference under imputation for missing response data,' The Annals of Statistics, 2002, **30**(3), pp. 896–924, ISSN 00905364.

Wang, Q. and Sun, Z., 'Estimation in partially linear models with missing responses at random,' J. Multivar. Anal., 2007, **98**(7), p. 1470–1493, ISSN 0047-259X, doi: 10.1016/j.jmva.2006.10.003.

Wu, J., Xiao, C., and Olivier, J. C., 'Time-varying and frequency-selective channel estimation with unequally spaced pilot symbols,' International Journal of Wireless Information Networks, 2004, **11**(2), pp. 93–104, ISSN 10689605, doi: 10.1023/B:IJWI.0000034541.89020.70.

Wu, Y., Liu, T., Cao, M., Li, L., and Xu, W., 'Pilot contamination reduction in massive MIMO systems based on pilot scheduling,' EURASIP Journal on Wireless Communications and Networking, 2018, **2018**(1), p. 21, ISSN 1687-1499, doi: 10.1186/s13638-018-1029-1.

Xiang, W., Zheng, K., and Shen, X. S., *5G mobile communications*, Springer, 2016, ISBN 9783319342085, doi:10.1007/978-3-319-34208-5.

Xiao, C., Member, S., Zheng, Y. R., and Beaulieu, N. C., 'Novel Sum-of-Sinusoids Simulation Models for Rayleigh and Rician Fading Channels,' IEEE Transactions on Wireless Communications, 2006, **5**(12).

Xing, H., Wei, D., and Yin, F., 'Channel estimation using orthogonal superimposed pilot for MIMO systems,' ICSPS 2010 - Proceedings of the 2010 2nd International Conference on Signal Processing Systems, 2010, **2**, pp. 625–628, doi:10.1109/ICSPS.2010.5555739.

Xiong, X., Wang, X., Riihonen, T., and You, X., 'Channel Estimation for Full-Duplex Relay Systems With Large-Scale Antenna Arrays,' IEEE Transactions on Wireless Communications, 2016, **15**(10), pp. 6925–6938, ISSN 15361276, doi:10.1109/TWC.2016.2593729.

Ye, H., Li, G. Y., and Juang, B. H., 'Power of Deep Learning for Channel Estimation and Signal Detection in OFDM Systems,' IEEE Wireless Communications Letters, 2018, **7**(1), pp. 114–117, ISSN 21622345, doi:10.1109/LWC.2017.2757490.

Yoon, H., Park, J.-S., and Jang, B.-J., 'Testbed for analyzing performance degradation of MIMO-OFDM WLAN due to WPAN interferer using USRP,' in '2016 Eighth International Conference on Ubiquitous and Future Networks (ICUFN),' 2016 pp. 487–489, doi:10.1109/ICUFN.2016.7537079.

Yu, J.-L., Zhang, B., and Chen, P.-T., 'Blind and semi-blind channel estimation with fast convergence for MIMO-OFDM systems,' Signal Processing, 2014, **95**, pp. 1–9, ISSN 0165-1684, doi:10.1016/j.sigpro.2013.08.006.

Zhang, W., Gao, F., and Yin, Q., 'Blind Channel Estimation for MIMO-OFDM Systems With Low Order Signal Constellation,' IEEE Communications Letters, 2015, **19**(3), pp. 499–502, ISSN 1089-7798, doi:10.1109/LCOMM.2015.2393889.

Zheng, B., Chen, F., Wen, M., Li, Q., Liu, Y., and Ji, F., 'Secure NOMA Based Cooperative Networks with Rate-Splitting Source and Full-Duplex Relay,' Proceedings of the International Symposium on Wireless Communication Systems, 2018, **2018-August**, pp. 1–5, ISSN 21540225, doi:10.1109/ISWCS.2018.8491208.

Zitouni, R., Ataman, S., Mathian, M., and George, L., 'Radio frequency measurements on a SBX daughter board using GNU Radio and USRP N-210,' in '2015 IEEE International Workshop on Measurements Networking (M N),' 2015 pp. 1–5, doi: 10.1109/IWMN.2015.7322969.

VITA

Arul Mathi Maran Chandran received his B.Tech. degree in Electronics and Communication Engineering from Pondicherry University, India in 2008. He graduated from Missouri University of Science and Technology with the M.S. degree in Electrical Engineering in May, 2015. He received his Ph.D. degree in Electrical Engineering from Missouri University of Science and Technology in August, 2020. He worked as graduate research assistant under Dr. Maciej Zawodniok and graduate teaching assistant for multiple lab courses. In addition to being a graduate research assistant, he also supervised undergraduate senior design groups and graduate course final projects.

In 2008, he joined MBIT Wireless, Chennai, India where he worked on ASIC front-end design and development of WiMAX and LTE. In 2013, he joined Qualcomm, Chennai, India where he worked on different verification efforts for USB3 development. His research interests included communication systems, wireless networks, software-defined radios, embedded systems, and machine learning.

He held officer positions in different student organizations at Missouri S&T such as President (2017 - 2018), Vice President (2016 - 2017) of Missouri S&T Astronomical Research Society (STARS), Graduate Coordinator (2019) of Tau Beta Pi (The Missouri Beta Chapter).

He became a member of Eta Kappa Nu (The Gamma Theta Chapter) and Tau Beta Pi (The Missouri Beta Chapter) honor societies. He got licensed as an amateur radio operator and volunteer examiner (VE) with extra-class license (call sign: KEØMLK) from Federal Communications Commission (FCC).